The determination of the fundamental resonant frequency of a substrate-mounted open cylindrical dielectric resonator

Lewis, A. P.

Award date:
1986

Awarding institution:
University of Bath

THE DETERMINATION OF THE FUNDAMENTAL RESONANT FREQUENCY OF A SUBSTRATE-MOUNTED OPEN CYLINDRICAL DIELECTRIC RESONATOR

submitted by

A.P. LEWIS

for the degree of PhD

of the University of Bath

1986

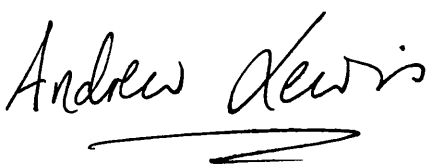

ProQuest LLC
789 East Eisenhower Parkway
P.O. Box 1346
Ann Arbor, MI 48106-1346

To my fiancée

Helen

SYNOPSIS

In recent years, the cylindrical dielectric resonator has found many practical applications in microwave systems. In order to utilise this resonator, the microwave designer needs to be able to easily calculate its fundamental resonant frequency, and several methods have been developed for this purpose in both the isolated and enclosed situations. However, in the important case of the substrate-mounted open dielectric resonator, simple, accurate calculations of the fundamental resonant frequency have not been possible.

This particular situation for the dielectric resonator is examined in this thesis, and, after a review of previous methods used to model the dielectric resonator in the three physical situations, an integral equation is developed that describes the substrate-mounted resonator. Since the solution of this integral equation is very difficult, several approximate numerical solution techniques are considered. However, these are rejected in favour of a quasi-analytical iterative method, which is then demonstrated for the case of a monomode dielectric substrate, and the theoretical results are shown to be in very good agreement with experimental values for the fundamental resonant frequency. Extension of this iterative technique to include the continuous modes of the dielectric substrate is then considered and shown to be possible.

ACKNOWLEDGEMENTS

I wish to express my sincere thanks to my supervisor, Professor J.P. McGeehan, and to Professor T.E. Rozzi, for the support they have shown, and the guidance they have given, throughout this work. I also wish to thank those within Bath University who have been prepared to give encouragement, and I particularly wish to thank Bernard Wickenden of Plessey Materials Ltd., Towcester, for his help in offering the facilities of his test department in order to enable me to carry out vital measurements. Finally, I am most grateful to the UK Science and Engineering Research Council for the award of a research studentship.

CONTENTS

ABBREVIATIONS

OCB open circuit boundary

TE transverse electric to the y-direction

TM transverse magnetic to the y-direction

SUBSCRIPTS

The abbreviations TE and TM have subscripts 1, m, n when referring to the independent resonant modes of the cylindrical pillbox dielectric resonator. These subscripts indicate, respectively, the number of field maxima in the azimuthal, radial and longitudinal directions. The subscript n takes the value δ for certain resonances, where δ represents a field variation of a fraction of a half-wavelength.

LIST OF SYMBOLS

$\underline{A}$	an arbitrary vector
A,B	constants
$\underline{B}$	magnetic flux density
$B_o(z)$	linear combination of cylindrical Bessel functions, of order zero and argument z
$B_n(z)$	arbitrary cylindrical Bessel function, of order n and argument z
C	constant
C_g	coefficient in the Green's function $G(\underline{x},\underline{x}')$
$\underline{C}$	matrix eigenvector
$\underline{D}$	electric flux density
$\underline{E}$	electric field
$G(\underline{x},\underline{x}')$	Green's function
$\hat{G}$	Green's function operator
$\underline{H}$	magnetic field
$H_n^{(2)}(z)$	Hankel function of the second kind, of order n and argument z
$\underline{I}$	the identity matrix
I_{rad}, I_ρ	integrals in the radial direction
I_θ, I_y	integrals in the azimuthal and longitudinal directions, respectively
$J_n(z)$	cylindrical Bessel function of the first kind, of order n and argument z
K(u,v)	kernel of an integral equation
$\underline{K}$	kernel matrix
K	kernel operator
$K_n(z)$	modified Hankel function, of order n and argument z
$L(\theta)$	aximuthal component of the potential function Φ
M,N	upper limits of series expansions

$N_n(z)$	cylindrical Bessel function of the second kind (Neumann function), of order n and argument z
P_n, Q_n	coefficients of the radial series expansion in the trial function
Q	quality factor
R	radius of the cylindrical dielectric resonator
$R(\rho)$	radial component of the potential function $\Phi(y)$
S	surface of a dielectric interface
$S(\rho), S(y)$	summations in the radial and longitudinal directions respectively
V	volume
X_ρ, X_y	linear multipliers in the radial and longitudinal directions, respectively
$Y(X,y)$	y-directed eigenfunction of the continuous modes of the dielectric slab waveguide
$Y_n(y)$	y-directed eigenfunction of the discrete bound modes of the dielectric slab waveguide
$Z_n(z)$	arbitrary cylindrical Bessel function of order n and argument z
a,b	arbitrary scalars
c_n	series expansion coefficient
c	speed of light in vacuo
d	height of the dielectric substrate
f(u)	function of the variable u
f_{res}	fundamental resonant frequency
g	two-dimensional Green's function, transverse to the y-axis
h	height of the cylindrical dielectric resonator
i	index

j	index or $\sqrt{-1}$ (depending on situation)
k_o	wavenumber of free space
k_{bn}, k_{bc}	y-directed wavenumbers for the discrete and continuous modes, respectively
k_y	y-directed wavenumber
k_ρ	radial wavenumber
$\underline{n}$	outward normal to a surface S
$p(u)$	function of the variable u
q	azimuthal wavenumber
$r(f,u)$	residual of the homogeneous Fredholm equation of the second kind
s,t	indexes
u,v	variables
$w(y)$	weight function
$\underline{x}$	position vector (ρ,θ,y) of a point in observation space
$\underline{x}'$	position vector (ρ',θ',y') of a point in source space
y	axial (longitudinal) direction in the cylindrical coordinate system
$\hat{y}$	unit vector in the axial direction
z	variable
Γ	surface boundary
Δ,Λ	constants
$\underline{\Pi}$	y-directed vector potential
Υ	constant
Φ	y-directed scalar potential function
$\Psi(y)$	y-directed eigenfunction
α,β	constants
β_n	radial wavenumber of the trial function
γ	y-directed wavenumber, in the air region, of the discrete slab modes

δ_{nm}	delta symbol, defined as $\begin{cases} 1 & n = m \\ 0 & n \neq m \end{cases}$
$\delta(\underline{x}-\underline{x}')$	Dirac delta function
ε	permittivity (dielectric constant) of a material
ε_o	permittivity of free space
$\varepsilon_{rel}, \varepsilon_b$	relative permittivity
η	normalisation coefficient
θ	azimuthal direction in the cylindrical coordinate system
$\hat{\theta}$	unit vector in the azimuthal direction
λ	eigenvalue
κ	λ^{-1}
μ	permeability
μ_o	permeability of free space
μ_{rel}	relative permeability
ξ	y-directed wavenumber in the dielectric substrate
ρ	radial direction in the cylindrical coordinate system
$\hat{\rho}$	unit vector in the radial direction
σ	y-directed continuum wavenumber in the dielectric slab
σ_s	summation
τ, ϕ	arbitrary scalars
χ	y-directed continuum wavenumber in the air region
ψ	scalar potential function
ω	angular frequency
∇	vector operator, nabla
∇^2	Laplacian operator
∇_t^2	part of the Laplacian transverse to the y-direction
∇_o	nabla operating on the source coordinates $\underline{x}'$
(ψ, ϕ)	the inner product of the functions ψ and ϕ

Subscripts

a	air region
b	represents either a, r or s
c	continuum
e	refers to electric potential
h	refers to magnetic potential
i	image case
im	imaginary component of a complex quantity
m,n	indexes of the discrete modes
r	resonator region
re	real component of a complex quantity
s	substrate region
t	index
y	longitudinal direction
θ	azimuthal direction
ρ	radial direction

Superscripts

$\sim$	approximate value
$-$	complex conjugate
'	the prime is used in two separate ways, always clearly distinguished in the thesis. If the prime is the superscript on a variable (e.g. $\underline{x}'$), then that variable is in source space. However, if the prime is the superscript on a function (e.g. $J_o'(\beta_n\rho)$), then it indicates the first derivative, with respect to the argument, of the function. A double prime always indicates the second derivative with respect to the argument.

CHAPTER 1

INTRODUCTION

In 1939 Richtmyer [1] proposed the concept of the dielectric resonator, although it was not until 1968 that the first major application for dielectric resonators was developed. In that year, Cohn [2] published a paper giving theoretical formulae for the coupling coefficient between adjacent magnetic-dipole cylindrical pillbox dielectric resonators, for both transverse and axial orientation within a metal waveguide. He further showed that these formulae enabled waveguide bandpass filters to be designed, where the inclusion of dielectric resonators gave rise to a typical reduction in size of 95% when compared to conventional waveguide filters. However, Cohn also included the caveat that the use of dielectric resonators was hindered by the large variation of the relative permittivity with temperature that was a feature of the dielectric materials at that time, and he predicted that this disadvantage would be overcome if materials having a temperature coefficient, $\Delta\varepsilon_r/\varepsilon_r$, of less than 50 ppm/^{o}C were developed.

In the early 1970's, such materials were first produced, and, by 1979, ceramics were commercially available with temperature coefficients in the range -4 to +12 ppm/^{o}C [3]. During the same period, the expansion of the communications industry led to the overcrowding of the frequency spectrum below 10 GHz, and thus the millimetre-wave region became the subject of much interest as a possible communications band. At such frequencies, the conventional metal waveguiding techniques become prohibitively expensive, since the small dimensions require extremely tight machining tolerance, and thus new waveguiding mechanisms, such as microstrip [4], image guide and insulated image guide [5,6] have received much investigation. Moreover, the development of these

new technologies was hastened by the commercial desire for the production of microwave integrated circuits, and, within these new structures, which are all constructed using dielectric materials and metal planes, the dielectric resonator finds a ready home. For these reasons, and particularly due to the advent of temperature-stable ceramics, dielectric resonators are now widely used in many different microwave applications.

One of the fundamental building blocks of any communications system is the filter, and in this regard the dielectric resonator proves very useful. As Cohn showed [2], the size of standard waveguide filters can be dramatically reduced through the use of dielectric resonators, and Fiedziuszko [7] produced a dual-mode C-band filter, using cylindrical dielectric resonators, mounted in metal waveguide, that met the typical requirements for satellite use, and yet was only 8% of the volume of a comparable metal cavity filter. However, the applicability of dielectric resonators is not limited to conventional waveguide filter design, and Majewski [8] developed a directional filter using a resonator suspended between two microstrip lines, as shown in Figure 1.1, which provided band-reject and band-pass characteristics.

Another major use for dielectric resonators is in the stabilisation of microwave oscillators and Podcameni and Bermudez [9] describe one particular configuration, shown in Figure 1.2, that can be used to control the output frequency of an FET oscillator, while ceramic dielectric resonators provide the stability of a Gunn diode in a planned microwave radio system to work at 29 GHz [10]. Further applications for dielectric resonators are found in slow-wave structures [11], up- and downconverters [12], and they may also be used as miniature replacements for cavity resonators, although very high Q-factors cannot be achieved due to the open nature of the resonator surface.

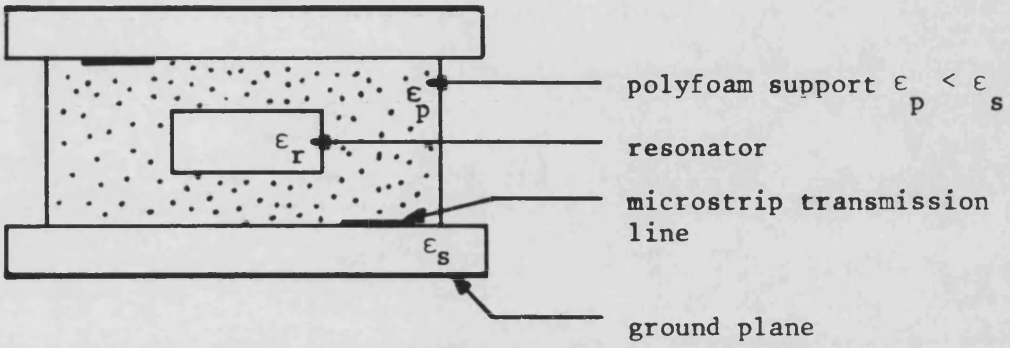

Figure 1.1 Directional filter constructed from a dielectric resonator suspended between two microstrip lines

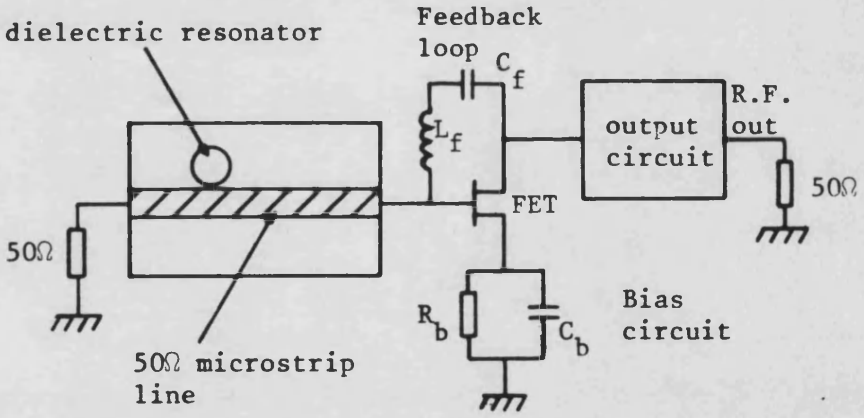

Figure 1.2 Schematic layout of an FET oscillator showing the stabilising input dielectric resonator

An obvious consequence of this sudden growth in the practical use of the dielectric resonator is that there has been a great need for an accurate theoretical model of the resonator, so that design procedures may be simplified and standardised. The basic needs of the microwave designer using dielectric resonators are to be able to accurately predict the fundamental resonant frequency, quality factor, and the coupling coefficient of the cylindrical dielectric resonator in different circumstances. However, unlike the metal cavity resonator, which has a precisely defined modal structure due to its conducting walls, the dielectric resonator is an open structure, and its resonances are produced by the sudden change in relative permittivity at its surface, which has the effect of partially confining the electromagnetic energy. It is therefore apparent that the electromagnetic fields within the resonator are linked with those outside, and, due to the physical shape of the cylindrical pillbox, this has provided great difficulties in formulating a theoretical analysis.

In fact, over the past twenty years, much research effort has been exercised on the problem of the dielectric resonator, and has concentrated upon three main configurations for the cylindrical pillbox. These are the isolated resonator, the substrate-mounted open resonator, and the enclosed resonator. The first situation of the isolated resonator has received the most attention, and, recently, some accurate theoretical models have been developed [13-15]. However, the isolated resonator has no practical applications, and so the situation of the enclosed resonator, which has a structure similar to that of shielded microstrip and thus is much more useful, has been the subject of several studies. Once again, in recent years, accurate solutions have proved possible if the resonator is enclosed in a metal

waveguide below cut-off [16,17].

However, the remaining structure, where the dielectric resonator is placed upon a grounded dielectric substrate, and thus matches the physical structures of open microstrip and insulated image guide, has received little study. This particular structure, along with having numerous practical applications, is also arguably the most interesting theoretically, since the propagating modes of the dielectric slab waveguide also have to be taken into account. In addition to supporting surface waves where the energy is mainly contained within the dielectric material, it is well known [18,19] that such a waveguide supports a continuous spectrum that represents both radiation modes and evanescent waves. However, the inclusion of these continuous modes presents serious difficulties, and, although they play only a very minor role in the determination of the fundamental resonant frequency of the resonator, they are probably the reason why so little research has been undertaken on the substrate-mounted resonator. In fact, only one research group [20] has provided a working model, and this was very complex and involved a very lengthy numerical solution.

In an attempt to remedy this situation, and also due to the strong interest into open guiding structures prevailing at the time [5,6], it was decided to attempt to formulate an analytical model of the substrate-mounted cylindrical pillbox dielectric resonator that was both simple to solve, and yet able to provide an accurate prediction for the fundamental resonant frequency. The method developed is based upon the transformation of the differential equation that applies within the resonator volume into an integral equation by using the method of Green's functions. In fact, although the theory is demonstrated for the specific case of the substrate-mounted resonator, the actual method is equally applicable to either of the other two resonator configurations

mentioned above through a judicious choice of the particular Green's function employed.

The thesis begins, in chapter 2, with a brief survey of the previous techniques used to model the dielectric resonator. In chapter 3, the integral equation appropriate for the fundamental resonant mode is derived, and in chapter 4 a survey of possible techniques for the solution of this equation is given. This leads to the development of a quasi-analytical iterative procedure which is eminently suited to numerical solution on a computer, and which is presented in chapter 5 for the case of a dielectric substrate excited into monomode operation.

In chapter 6, the theoretical results obtained for the fundamental resonant frequency are analysed, and are compared both with experimental values, and also with results obtained from the extension of a previously developed theoretical model. Since, as was mentioned above, the complete description of the substrate-mounted resonator cannot be achieved without considering the continuous spectrum of modes (although, as is shown in chapter 6, their inclusion only provides a minor contribution to the solution) chapter 7 is devoted to a study of the practical details arising from the nature of the continuous spectrum.

In conclusion, chapter 8 summarises the success of this integral equation model and of the iterative method employed to solve for the fundamental resonant frequency, and also outlines several directions in which further work could proceed.

REFERENCES

[1] R.D. Richtmyer, "Dielectric resonators", J. Appl. Phys., Vol.10, pp.391-398, June 1939.

[2] S.B. Cohn, "Microwave bandpass filters containing high-Q dielectric resonators", IEEE Trans. Microwave Theory Tech., Vol.MTT-16, pp.218-227, April 1968.

[3] M.R. Stiglitz, "Dielectric resonators: past, present and future", Microwave Journal, Vol.22, pp.19-36, July 1981.

[4] T.C. Edwards, "*Foundations for Microstrip Circuit Design*". New York: Wiley, 1981.

[5] S-T. Peng and A.A. Oliner, "Guidance and leakage properties of a class of open dielectric waveguides: part I - mathematical formulations", IEEE Trans. Microwave Theory Tech., Vol.MTT-29, pp.843-854, September 1981.

[6] T. Itoh, "Open guiding structures for mmW integrated circuits", Microwave Journal, Vol.23, pp.113-126, September 1982.

[7] S.J. Fiedziuszko, "Dual-mode dielectric resonator loaded cavity filters", IEEE Trans. Microwave Theory Tech., Vol.MTT-30, pp.1311-1316, September 1982.

[8] M.L. Majewski, "Microwave directional filter using suspended dielectric resonators", in Proc. 11th European Microwave Conf., pp.158-163 (Amsterdam, The Netherlands, September 1981).

[9] A. Podcameni and L.A. Bermudez, "Large signal design of GaAs FET oscillators using input dielectric resonators", IEEE Trans Microwave Theory Tech., Vol.MTT-31, pp.358-361, April 1983.

[10] B.C. Barnes, B.L. Clark and W. Thorpe, "Technology for a 29 GHz local distribution radio", in Proc. 11th European Microwave Conf., pp.119-125, (Amsterdam, The Netherlands, September 1981).

[11] A. Karp, H.J. Shaw and D.K. Winslow, "Circuit properties of microwave dielectric resonators", IEEE Trans. Microwave Theory Tech., Vol.MTT-16, pp.818-828, October 1968.

[12] J.R. Mahieu, "Low conversion loss up and downconverters using dielectric resonators for applications with millimetric communication systems", in Proc. 6th European Microwave Conf., pp.664-668, (Rome, Italy, September 1976).

[13] M. Tsuji, H. Shigesawa and K. Takiyama, "Analytical and experimental investigations on several resonant modes in open dielectric resonators", IEEE Trans. Microwave Theory Tech., Vol.MTT-32, pp.628-633, June 1984.

[14] R. de Smedt, "Correction due to a finite permittivity for a ring resonator in free space", IEEE Trans. Microwave Theory Tech., Vol.MTT-32, pp.1288-1293, October 1984.

[15] A.W. Glisson, D. Kajfez and J. James, "Evaluation of modes in in dielectric resonators using a surface integral formulation". IEEE Trans. Microwave Theory Tech., Vol.MTT-31, pp.1023-1029, December 1983.

[16] M. Jaworski and M. Pospieszalski, "An accurate solution of the cylindrical dielectric resonator problem", IEEE Trans. Microwave Theory Tech., Vol.MTT-27, pp.639-643, July 1979.

[17] J. Krupka, "Computations of frequencies and intrinsic Q factors of TE_{onm} modes of dielectric resonators", IEEE Trans. Microwave Theory Tech., Vol.MTT-33, pp.274-277, March 1985.

[18] R.E. Collin, "*Field Theory of Guided Waves*". New York: McGraw-Hill, 1960, Chapter 11.

[19] V.V. Shevchenko, "*Continuous Transitions in Open Waveguides*". Boulder, Colorado: The Golem Press, 1971, pp.94-116.

[20] P. Gelin, S. Toutain, P. Kennis and J. Citerne, "Scattering of the TE_{01} and TM_{01} modes on transverse discontinuities in a rod dielectric waveguide-application to the dielectric resonators", IEEE Trans. Microwave Theory Tech., Vol.MTT-29, pp.712-719, July 1981.

CHAPTER 2

HISTORICAL REVIEW OF PREVIOUS WORK

The dielectric resonator was first proposed in 1939 by Richtmyer [1], who suggested that a suitably shaped dielectric object could function as an electrical resonator at microwave frequencies. He performed his research on resonators positioned in free space, and was able to show that such a resonator must radiate a proportion of its energy.

Owing to the simplicity of its structure, Richtmyer first analysed the spherical dielectric resonator, and he determined its resonant frequency by matching expressions obtained for the internal and external electric fields at the surface of the sphere. Secondly he studied a toroidal dielectric resonator by considering it as a length of cylindrical dielectric rod waveguide bent to form a closed ring. Consequently, he used the above principle of field matching on the external surface, coupled with the condition of phase equality at the two ends of the rod, to calculate the resonant frequencies of the structure.

In practice, Richtmyer's results are of limited use in microwave systems, since the spherical and toroidal resonators do not allow easy integration into planar structures. In fact, the cylindrical pillbox, shown in Figure 2.1, is the most commonly used shape for a dielectric resonator, since its flat end faces allow straightforward integration into planar systems (e.g. microstrip). Furthermore, its structure allows the presence of θ-independent modes such that the resonator supports independent transverse electric (TE) and transverse magnetic (TM) modes with respect to the cylindrical axis y. Consequently,

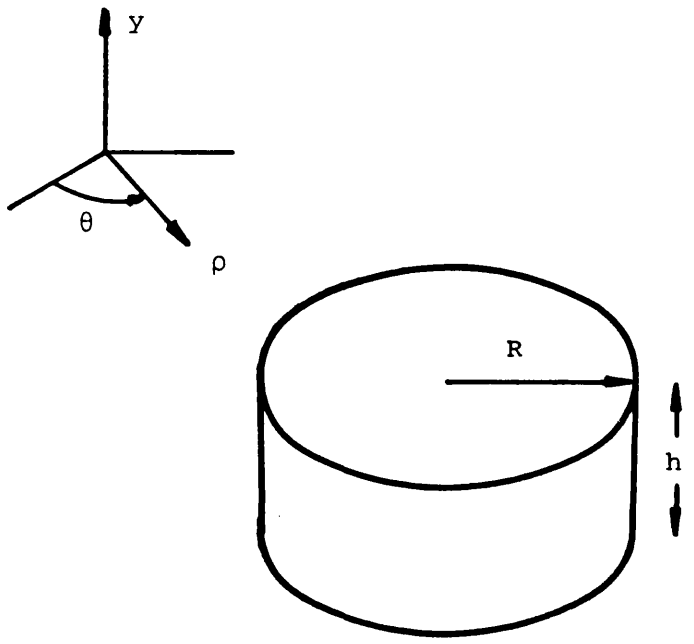

Figure 2.1 The cylindrical pillbox dielectric resonator

the remainder of this review will be concerned with research carried out upon the cylindrical pillbox resonator, and in particular the techniques employed to calculate its fundamental resonant frequency.

Although the cylindrical pillbox resonator is convenient practically, this is not the case theoretically, since the boundary does not coincide with a separable geometry. Thus, early researchers [2,3] implemented the open-circuit boundary (OCB) method in order to provide approximate calculations of the resonant frequency and quality factor (Q) of different resonator modes. This technique, devised by Yee [2], used the fact that a surface between air and an imaginary magnetic conductor of infinite magnetic conductivity is an open circuit (analogous to a short circuit at a perfect electrical conductor). Thus, at such a surface, the tangential magnetic and normal electric fields are zero.

A resonator made of material with infinite relative dielectric constant, ε_r, will satisfy the OCB condition for the electric field and thus a resonator of high ε_r may be modelled approximately by the OCB technique. However, in order to increase the accuracy of the theoretical results, Yee found that it was necessary to modify the method. Consequently, dependent upon the mode being analysed, either the cylindrical or the end surfaces were considered as satisfying the magnetic wall conditions, and on the remaining surface boundary the tangential fields were matched.

Owing to the nature of the OCB method, Yee analysed dielectric resonators situated in free space and made several important discoveries relating to the nature of the resonance. Firstly, he found that the calculated resonant frequency was complex, indicating that the resonator supports damped oscillations, which agrees with

Richtmyer's theory that the resonator must radiate some of its energy. Secondly, he deduced that the introduction of a metallic surface close to the resonator will alter the values of its resonant frequencies, and this effect is now widely employed to provide fine tuning of dielectric resonators in microwave devices (e.g. filters and sources). Yee also calculated that, for a cylindrical pillbox resonator, the fundamental mode is determined by the resonator dimensions, and that, if the ratio of the diameter to the height is greater than unity, the lowest resonant frequency is provided by the $TE_{01\delta}$ mode. The subscripts represent the number of field maxima in the circumferential, radial, and longitudinal directions respectively, and the symbol δ indicates that in the y-direction the field varies by a fraction of a half wavelength. The theoretical results obtained by Yee agree reasonably well with his experimental results, which were found by examining resonators placed within metal waveguide, and show that the OCB method of analysis gives an approximate solution to the determination of the resonant frequency of a cylindrical pillbox resonator of high permittivity.

In 1966, Chow [4] presented a method of analysis where he solved the problem in two stages. First he calculated, by matching the fields on the cylindrical surface, the longitudinal propagation constant of a dielectric rod waveguide. Then he considered the resonator as a length of dielectric-filled magnetic wall waveguide with a cut-off air-filled guide attached to both ends, and, using the value for the propagation constant of the rod guide, he constructed expressions for the impedances looking either side of the boundary between air and dielectric. Resolution of these expressions, under the condition that they must be complex conjugates at resonance, led to a trans-

cendental equation. The solution of this equation provided the resonant frequencies of the $TE_{01\delta+1}$ mode of rutile resonators ($\varepsilon_r \simeq 100$) that were accurate to within about 2% of the measured values.

The next major advance in the theoretical treatment of the dielectric resonator was made by Van Bladel [5], who expanded the electric and magnetic fields in increasing powers of $1/\sqrt{\varepsilon_r}$. In the limit as $\varepsilon_r \to \infty$, it was found that only first order terms in the expansion were necessary to satisfy the boundary conditions, and that, for infinite permittivity, the magnetic wall condition was satisfied by the TM_{omn} modes, where m and n are integers.

Verplanken and Van Bladel [6] proceeded to calculate the TM_{011} resonant mode of an isolated high permittivity cylindrical ring resonator (which allows the cylindrical pillbox as a special case). Unfortunately, they presented no experimental results to substantiate their work. However, it is known that in practice a resonator does not have infinite permittivity, and also that the TM_{omn} modes have an azimuthal magnetic field, so that, in general, these modes have a finite tangential magnetic field at the surface of the resonator. Thus the magnetic wall condition does not hold, and so the results must be inaccurate.

In 1976, Konishi, Hoshino and Utsumi [7] presented a variational method for obtaining the resonant frequency of a dielectric pillbox in free space. Starting from the magnetic wall solution, an expression for the resonant frequency was obtained by variating the surface impedance from infinity. The method was applied to the $TE_{01\delta}$ modes of the pillbox resonator and comparison with experimental results shows that this technique has an error of about 1%, whereas the magnetic wall model results are shown to deviate from actual values by about 10%.

Prior to 1977, all analysis of dielectric resonators had been carried out assuming that the resonator was isolated in free space. However, such a resonator has no practical use, and thus Itoh and Rudokas [8] developed their technique for a pillbox resonator situated on a grounded dielectric substrate of relative dielectric constant much less than that of the resonator. They used the method first developed by Marcatili [9] in order to match the electromagnetic field at the resonator surfaces, ignoring both the edge effects and the matching between regions of space external to the resonator. This matching procedure, based on an assumed exponential field decay outside the pillbox, produced two coupled eigenvalue equations, which, for the $TE_{01\delta}$ mode of an isolated resonator (a special case of the substrate mounted resonator), are easily solved.

The $TE_{01\delta}$ resonant frequencies thus obtained agree to within 2% of the measured values for high permittivity isolated pillboxes, but for lower values of ε_r the method becomes increasingly inaccurate as the resonator no longer gives good field confinement. For the higher modes, and for the practical resonator on a grounded dielectric slab waveguide, the coupled equation system becomes rather involved and requires extensive computation, and Itoh presents no results for such cases.

The method proposed by Guillon and Garault [10] started from the magnetic wall model, but, since it is known that this gives only an approximate result, they set out to improve the accuracy of the results by including field matching on the resonator surfaces. They devised a technique that involved a series of calculations on the dielectric resonator assuming both perfect and imperfect magnetic walls, and they showed that, for the TE_{01n} modes of an isolated cylindrical pillbox,

the method agreed to within 1% of their experimental results. However, the technique entailed solving five sets of coupled characteristic equations, with each solution being used to set parameters for the next set, and thus it was a lengthy and complex procedure.

Guillon and Garault also showed that their method could be adapted to solve the shielded resonator problem, as shown in Figure 2.2, which is a situation more akin to that found in microstrip circuits. Consequently, several researchers [11]-[14] concentrated on discovering methods that produced accurate solutions for the resonant frequency of the enclosed cylindrical dielectric resonator.

Pospieszalski [11] proposed a technique where a resonator between two metal plates was treated as a length of lossless dielectric rod waveguide excited in the TE_{01} mode surrounded by parallel-plate waveguide perpendicular to the rod axis. In this axial direction, the magnetic field was described by a sinh dependence, and its cross-sectional distribution was taken to be that of the TE_{01} mode at the cut-off frequency of the dielectric rod. These assumptions led to theoretical $TE_{01\delta}$ resonant frequencies that differed from experimental values by less than 3.5%, and, for a dielectric pillbox that is in contact with the metal plates, the method provided the exact solution.

In 1983, Maystre, Vincent and Mage [12] used a similar procedure to Pospieszalski [11], but applied more accurate modal expansions for the $TE_{01\delta}$ electric field, and the results they obtained agree to within 1% of the experimental values.

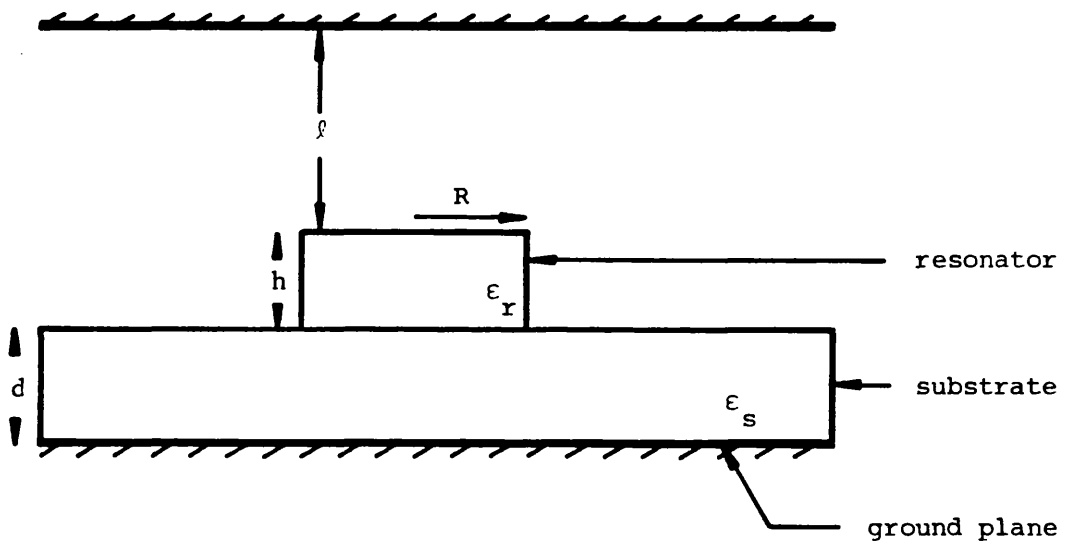

Figure 2.2 The shielded cylindrical dielectric resonator

A variational approach was used to calculate the $TE_{01\delta}$ resonant frequency by Jaworski and Pospieszalski [13]. Green's function equations were set up relating the electric field (in the two regions internal and external to the extended cylindrical surface of the enclosed resonator) to an unknown longitudinal magnetic field at the surface of the pillbox, which was expressed as a sum of the complete set of functions satisfying the boundary conditions of the parallel-plate waveguide. Matching of the electric field at the boundary between the two regions, together with the inclusion of a set of trial functions, led to a determinantal equation which was solved to give results for the resonant frequency with an error of less than 0.75%. The accuracy of the result depended upon the number of terms taken in the series approximations for the magnetic field and the trial function, and, in fact, the computed value converged to the exact solution for the fundamental resonant frequency of the dielectric resonator.

It is to be expected that very accurate solutions for the shielded resonator can be obtained, since, for a parallel-plate waveguide there are no radiation modes. Thus, the resonator problem may be entirely described by a complete set of bound modes, and Krupka [14] used such a set to solve the problem using the Rayleigh-Ritz variational procedure. This gave answers as accurate as those obtained by Jaworski [13] and Maystre [12], but with greater ease of computation.

Whilst the research described above was being conducted on the enclosed dielectric resonator, many workers continued to examine the more complex situation of the open resonator, which, due to its radiative nature, cannot be accurately modelled by a complete set of bound modes within the resonator. The method applied by Verplanken and Van Bladel [15] was based upon the latter's original work [5],

which was extended in order to analyse the TE_{01n} modes of an isolated dielectric ring resonator, as shown in Figure 2.3. Field equations were set up for an unknown function proportional to the azimuthal electric field, and the method of finite elements was applied to the solution of these equations.

The cylindrical pillbox resonator is seen to be a special case of the ring resonator, and the results presented for the pillbox were shown to be correct, to within the limits of experimental accuracy, for high values of ε_r, but as the permittivity decreases the error in the results increases and, for a pillbox with $\varepsilon_r = 35$, the difference between experimental and theoretical values reaches 7%. The explanation of this behaviour is found in the fact that, as in [5], a series expansion in increasing powers of $1/\sqrt{\varepsilon_r}$ was used to define the boundary conditions, and thus the results are valid in the limit as $\varepsilon_r \to \infty$. A further reason for the inaccuracy is that, in order to solve the problem, the authors imposed a condition on the far-field behaviour that excluded analysis of the radiation field.

A useful by-product of Verplanken and Van Bladel's approach was that they were able to determine the $TE_{01\delta}$ field pattern for the isolated dielectric pillbox resonator. Consequently, they showed very clearly that the electric and magnetic fields are not confined to the resonator volume, but in fact penetrate into all regions of space in the vicinity of the pillbox.

A new approach was provided by Gelin, Toutain, Kennis, and Citerne [16] in which they considered the dielectric pillbox resonator to be a length of dielectric rod waveguide sandwiched between two discontinuities. In this way they were able to analyse both the isolated resonator and the substrate-mounted resonator by simply

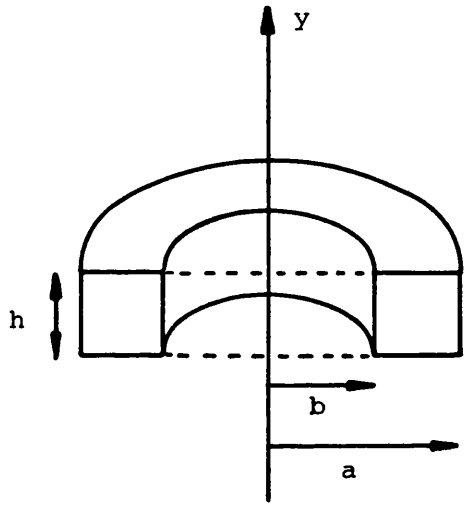

Figure 2.3 Cross-section of the isolated dielectric ring resonator

varying one of the discontinuity conditions. The first step was to analyse each interface by transforming (using orthogonality properties) the relations obtained from field matching into coupled singular integral equations. The resonator problem was then solved by studying the interaction between two such discontinuities.

However, the full rigorous solution would have necessitated excessive computation time due to the excitation of continuous modes at each discontinuity. Thus, on the basis of results from the previous analyses of the individual interfaces, it was judged that little error would be introduced by neglecting the coupling from the continuum to the reflected guided mode at the discontinuities.

The results thus obtained for the $TE_{01\delta}$ resonant frequency of the isolated resonator agreed well with those given by Guillon and Garault [10], particularly when the permittivity is high. It was also shown that the error between experimental and theoretical values was less than 3% for both isolated and substrate-mounted resonators excited in the $TE_{01\delta}$ mode. The method is equally applicable to the $TM_{01\delta}$ mode and some unsubstantiated theoretical results for the isolated pillbox were presented. For the TM excitation, however, it was shown that, near the cut-off frequency of the rod, a significant amount of the guided mode energy is coupled to the radiation modes at an interface. Consequently, the lowest transverse magnetic mode ($TM_{01\delta}$) has a low value of Q, and calculation of its resonant frequency will be inaccurate if the continuum modes are ignored.

In 1982, Tsuji, Shigesawa, Aoki and Takiyama [17] described a method of analysis for the substrate-mounted resonator. Since the cylindrical pillbox does not coincide with a separable geometry, it

was decided to divide the problem into two separate regions, with the boundary being the extended cylindrical surface of the resonator. The two regions were then treated as independent multi-layer dielectric slab radial waveguides. The field components were expressed in terms of the TE and TM propagating surface wave modes of the individual slab waveguides, and these fields were matched at the interfaces between the dielectric layers, and the resulting system of equations was solved by matching the fields on the cylindrical surface. However, the contributions due to the radiation modes were neglected in the field equations, which were, necessarily, truncated infinite expansions, and so the continuity relations could never be satisfied. Therefore, the resonant frequency was calculated by minimising the mean of the square of the consequent error.

Tsuji et al. investigated experimentally the resonances of polyethylene disc resonators. The relative permittivity of polyethylene is about 2.28, and, consequently, such resonators only provide very weak field confinement if they resonate in the lower modes (i.e. TE_{omn}, TM_{omn}). Accordingly, thin cylindrical discs of large radii (35-90 mm) were excited so that there were many field maxima in the azimuthal direction. Such modes are inevitably hybrid and results for the $HE_{11\nu}$ modes ($\nu > 49$) were presented, and very good agreement between theory and practice was demonstrated.

A few months later, another paper was published by Tsuji, Shigesawa and Takiyama [18] where a similar method was employed to investigate the θ-independent modes of cylindrical pillbox resonators. This time, however, an isolated resonator was studied using the spherical co-ordinate system. The problem was divided into two regions, interior and exterior to the resonator, and the fields in each area were

expanded in terms of solutions to Helmholtz's equation. As before, the boundary conditions on the resonator surface could not be satisfied by the chosen field expansions, and so the resonant frequency was determined by minimising the mean-square error.

Theoretical results were presented for both the $TE_{01\delta}$ and $TM_{01\delta}$ modes of an isolated dielectric resonator. The $TE_{01\delta}$ mode results were demonstrated to be in very good agreement with those presented by Konishi [7], and the TM excitation results were shown to agree with those of Gelin et al. [16] and also with results obtained using Van Bladel's model [5]. A further paper [19] was published by Tsuji et al. in which experimental results were compared with the theoretical results obtained by the method of [18]. Agreement for the $TE_{01\delta}$ mode was better than 0.5%, but it was not possible to measure the $TM_{01\delta}$ resonance since this mode has a very low Q-factor ($Q \simeq 8$). Experimental and theoretical results were also compared for a number of hybrid modes, and again agreement was very good (< 1% error).

The method proposed by Van Bladel [5], [6], [15] suffered from the major drawback that it is only valid in the limit as $\varepsilon_r \to \infty$. In 1984 De Smedt [20] managed to extend the limit of applicability of this perturbational approach by including higher order terms in the series expansion of the fields in terms of $1/\sqrt{\varepsilon_r}$. The work was carried out for an isolated resonator, and results were compared with those given by Tsuji et al. [18] for a cylindrical pillbox, and, for $\varepsilon_r > 25$, the difference in the $TE_{01\delta}$ resonant frequency was claimed to be less than 0.1%.

The most recent approach used to solve the problem of the isolated dielectric resonator was derived by Glisson, Kajfez, and James [21],[22]. The electromagnetic fields were expressed in terms

of surface electric and magnetic currents and coupled integral equations were then derived by imposing the condition of continuity of the tangential fields at the resonator surface. Application of the method of moments to the two coupled equations led to a set of simultaneous equations, the solution of which provided the resonant frequency. Results were given for the two lowest θ-independent modes and for three hybrid modes. Comparison with experimental results for an isolated cylindrical pillbox made of material with a relative permittivity of 38 showed that the technique provides very accurate values for the resonant frequency, the least accurate being the $TM_{01\delta}$ mode with an error of 1%.

In conclusion, it has been shown that, over the past twenty years, much research effort has been exercised in order to obtain an accurate theoretical model of the cylindrical pillbox dielectric resonator. In two physical situations, namely the enclosed resonator and the isolated resonator, this research has met with great success, and several techniques exist for accurate calculation of the fundamental resonant frequency [12-14,19-21].

However, the more general case of the dielectric resonator situated upon a dielectric substrate (which requires consideration of the radiation modes, and allows the isolated resonator as a special case) has largely been ignored. To date, only two analytical methods [8,16] have been developed for this resonator, and, in fact, only Gelin et al.[16] actually present any theoretical results. These results were obtained by a long and complex procedure, and, for the two situations considered, were accurate to within 3% of the experimental values. Consequently, the research presented in this thesis addressed itself to the general case of the substrate-mounted cylindrical dielectric resonator, with the aim of producing a simple, yet accurate, theoretical model.

REFERENCES

[1] R.D. Richtmyer, "Dielectric resonators", J. Appl. Phys., Vol.10, pp.391-398, June 1939.

[2] H.Y. Yee, "An investigation of microwave dielectric resonators", Microwave Lab. Rep. 1065, Stanford University, Stanford, CA, July 1963.

[3] J.C. Sethares and S.J. Naumann, "Design of microwave dielectric resonators", IEEE Trans. Microwave Theory Tech., Vol.MTT-14, pp.2-7, January 1966.

[4] K.K. Chow, "On the solution and field pattern of cylindrical dielectric resonators", IEEE Trans. Microwave Theory Tech., Vol.MTT-14, p.439, September 1966.

[5] J. Van Bladel, "On the resonances of a dielectric resonator of very high permittivity", IEEE Trans. Microwave Theory Tech., Vol.MTT-23, pp.199-208, February 1975.

[6] M. Verplanken and J. Van Bladel, "The electric-dipole resonances of ring resonators of very high permittivity", IEEE Trans. Microwave Theory Tech., Vol.MTT-24, pp.108-112, February 1976.

[7] Y. Koshini, N. Hoshino and Y. Utsumi, "The resonant frequency of a $TE^{o}_{01\delta}$ dielectric resonator", IEEE Trans. Microwave Theory Tech., Vol.MTT-24, pp.112-114, February 1976.

[8] T. Itoh and R.S. Rudokas, "New method for computing the resonant frequencies of dielectric resonators", IEEE Trans. Microwave Theory Tech., Vol.MTT-25, pp.52-54, January 1977.

[9] E.A.J. Marcatili, "Dielectric rectangular waveguide and directional coupler for integrated optics", Bell Syst. Tech. J., Vol.48, pp.2071-2102, September 1969.

[10] P. Guillon and Y. Garault, "Accurate resonant frequencies of dielectric resonators", IEEE Trans. Microwave Theory Tech., Vol.MTT-25, pp.916-922, November 1977.

[11] M. Pospieszalski, "Cylindrical dielectric resonators and their applications in TEM line microwave circuits", IEEE Trans. Microwave Theory Tech., Vol.MTT-27, pp.233-238, March 1979.

[12] D. Maystre, P. Vincent and J.C. Mage, "Theoretical and experimental study of the resonant frequency of a cylindrical dielectric resonator", IEEE Trans. Microwave Theory Tech., Vol.MTT-31, pp.844-848, October 1983.

[13] M. Jaworski and M. Pospieszalski, "An accurate solution of the cylindrical dielectric resonator problem", IEEE Trans. Microwave Theory Tech., Vol.MTT-27, pp.639-643, July 1979.

[14] J. Krupka, "Computations of frequencies and intrinsic Q factors of TE_{onm} modes of dielectric resonators", IEEE Trans. Microwave Theory Tech., Vol.MTT-33, pp.274-277, March 1985.

[15] M. Verplanken and J. Van Bladel, "The magnetic-dipole resonances of ring resonators of very high permittivity", IEEE Trans. Microwave Theory Tech., Vol.MTT-27, pp.328-333, April 1979.

[16] P. Gelin, S. Toutain, P. Kennis and J. Citerne, "Scattering of the TE_{01} and TM_{01} modes on transverse discontinuities in a rod dielectric waveguide - application to the dielectric resonators", IEEE Trans. Microwave Theory Tech., Vol.MTT-29, pp.712-719, July 1981.

[17] M. Tsuji, H. Shigesawa, H. Aoki and K. Takiyama, "Analytical and experimental considerations on the resonant frequency and the quality factor of dielectric resonators", IEEE Trans. Microwave Theory Tech., Vol.MTT-30, pp.1952-1957, Nov. 1982.

[18] M. Tsuji, H. Shigesawa and K. Takiyama, "On the complex resonant frequency of open dielectric resonators", IEEE Trans. Microwave Theory Tech., Vol.MTT-31, pp.392-396, May 1983.

[19] M. Tsuji, H. Shigesawa and K. Takiyama, "Analytical and experimental investigations on several resonant modes in open dielectric resonators", IEEE Trans. Microwave Theory Tech., Vol.MTT-32, pp.628-633, June 1984.

[20] R. De Smedt, "Correction due to a finite permittivity for a ring resonator in free space", IEEE Trans. Microwave Theory Tech., Vol.MTT-32, pp.1288-1293, October 1984.

[21] A.W. Glisson, D. Kajfez and J. James, "Evaluation of modes in dielectric resonators using a surface integral equation formulation", IEEE Trans. Microwave Theory Tech., Vol.MTT-31, pp.1023-1029, December 1983.

[22] D. Kajfez, A.W. Glisson and J. James, "Computed modal field distributions for isolated dielectric resonators", IEEE Trans. Microwave Theory Tech., Vol.MTT-32, pp.1609-1616, December 1984.

CHAPTER 3

THE FORMULATION OF AN INTEGRAL EQUATION FOR THE DIELECTRIC RESONATOR

This thesis is concerned with the study of the cylindrical pill-box dielectric resonator mounted on a grounded dielectric substrate, as shown in Figure 3.1, and in particular with the determination of the fundamental resonant frequency of such a structure, which is dependent upon the constituent materials and their dimensions. In order to solve this problem, it is necessary to analyse the nature of the various dielectric materials, and, specifically, the effects caused by the dielectric interfaces, which serve to determine the electromagnetic field structure.

In this chapter, this analysis is carried out in terms of two unknown independent scalar potential functions, and the work begins by deriving equations for the electric and magnetic fields in terms of these potentials. Then, for each potential function, the resulting three differential equations, which are linked through the boundary conditions, are transformed, using a Green's function approach, into an integral equation. Finally, the appropriate Green's function for the grounded dielectric slab waveguide is derived.

3.1 The Derivation of the Electromagnetic Field Equations

3.1.1 Maxwell's equations

In a source-free, uniform region of space, the electric and magnetic fields, given by $\underline{E}$ and $\underline{H}$ respectively, must satisfy Maxwell's equations,

$$\nabla \times \underline{E} = -\frac{\partial \underline{B}}{\partial t} \qquad (3.1a)$$

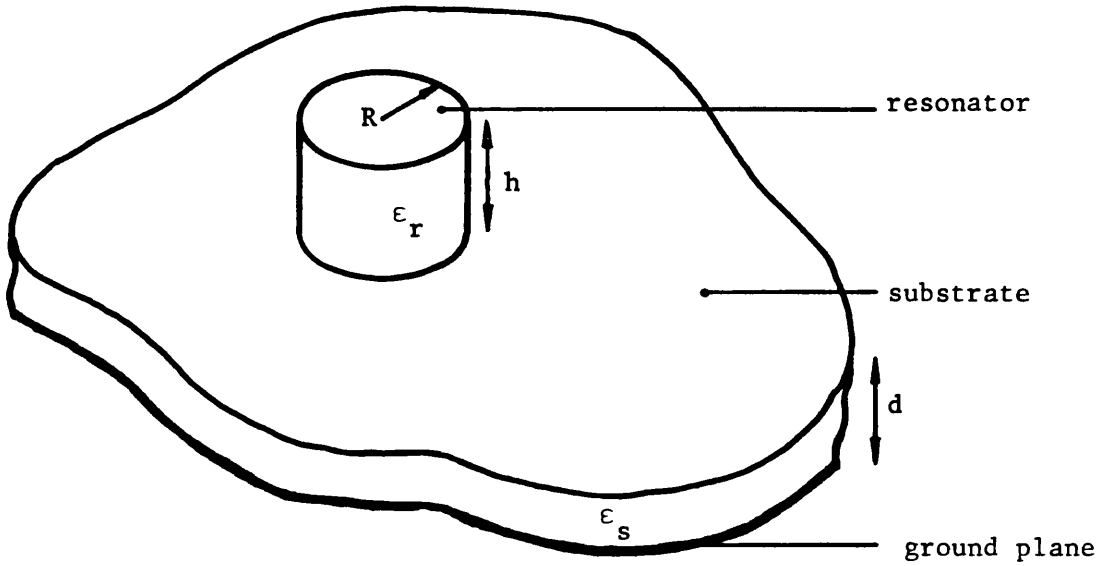

Figure 3.1 The cylindrical pillbox dielectric resonator mounted upon a grounded dielectric substrate

$$\nabla \times \underline{H} = \frac{\partial \underline{D}}{\partial t} \qquad (3.1b)$$

$$\nabla \cdot \underline{D} = 0 \qquad (3.1c)$$

$$\nabla \cdot \underline{B} = 0 \qquad (3.1d)$$

where the electric flux density, $\underline{D}$, and the magnetic flux density, $\underline{B}$, are defined by the constitutive relations

$$\underline{D} = \varepsilon \underline{E} \qquad (3.2a)$$

$$\underline{B} = \mu \underline{H} \qquad (3.2b)$$

The parameters ε and μ are known respectively as the permittivity and permeability of the region, and are defined as

$$\varepsilon = \varepsilon_{rel} \varepsilon_o \qquad (3.3a)$$

$$\mu = \mu_{rel} \mu_o \qquad (3.3b)$$

where ε_o, μ_o are constants known respectively as the permittivity and permeability of free space. The relative permittivity, ε_{rel}, and the relative permeability, μ_{rel}, take values dependent upon the constituent material of the region under consideration, and, for all the dielectric materials considered in this thesis, μ_{rel} is always unity, and the symbol is therefore not included in the subsequent analysis.

Without loss of generality, it is convenient to assume a time dependence of the form $\exp(j\omega t)$ for the electromagnetic fields (which, henceforward, will be suppressed for brevity) and thus equations (3.1) become

$$\nabla \times \underline{E} = - j\omega\mu_o \underline{H} \qquad (3.4a)$$

$$\nabla \times \underline{H} = j\omega\varepsilon \underline{E} \qquad (3.4b)$$

$$\nabla \cdot \underline{E} = 0 \qquad (3.4c)$$

$$\nabla \cdot \underline{H} = 0 \qquad (3.4d)$$

where use of equations (3.2) and (3.3) has been made, and ω is the angular frequency.

The reduced Maxwell's equations (3.4) are independent of the choice of co-ordinate system. However, consideration of the physical shape of the substrate-mounted dielectric resonator (shown in Figure 3.1) indicates that solution in cylindrical co-ordinate geometry would be prudent, and the relevant properties of the operator ∇ in this system are given in Appendix A, together with a summary of some of the important vector identities involving ∇.

3.1.2 The vector and scalar potentials

It is well known [1-3] that the cylindrical dielectric pillbox resonator supports independent transverse electric and transverse magnetic field structures with respect to the axial direction, y. It is therefore desirable to be able to formulate the following theory in such a manner that these independent modes may be analysed separately, and this may be achieved by introducing two unknown, independent vector potential functions.

The vector identity given in equation (A.12) states that the divergence of the curl of any vector is identically zero. Consequently, defining the electric and magnetic fields as

$$\underline{E} = \nabla \times \underline{\Pi}_h \qquad (3.5a)$$

$$\underline{H} = \nabla \times \underline{\Pi}_e \qquad (3.5b)$$

where $\underline{\Pi}_e$, $\underline{\Pi}_h$ are known as the electric and magnetic vector potentials respectively, satisfies the equations (3.4c) and (3.4d). Furthermore, it is found that the desired independent modes are provided by choosing the vector potentials to be polarised in the axial direction, so that

$$\underline{\Pi}_e = \hat{y}\,\psi_e \qquad (3.6a)$$

$$\underline{\Pi}_h = \hat{y}\,\psi_h \qquad (3.6b)$$

where $\hat{y}$ is a unit vector in the y-direction, and ψ_e and ψ_h are electric and magnetic scalar potentials, respectively.

It is important to note that the introduction of these unknown vector potentials is a mathematical device employed both to simplify the theoretical analysis, and to generate separate solutions for the two independent families of transverse modes. Substitution of equations (3.5) in the reduced Maxwell's equations (3.4) leads to two differential equations that must be solved for the scalar potentials ψ_e and ψ_h, and, once these have been determined, the electromagnetic fields are easily found.

3.1.3 The transverse electric field

Considering only the magnetic vector potential, $\underline{\Pi}_h$, the electric field within a uniform region of space is given by equation (3.5a)

$$\underline{E} = \nabla \times \underline{\Pi}_h \qquad (3.7)$$

and thus equation (3.4b) may be written as

$$\nabla \times \underline{H} = j\omega\varepsilon\,(\nabla \times \underline{\Pi}_h) \qquad (3.8)$$

Recognising that ε is constant in a uniform region of space, the vector identities (A.13) and (A.8) enable equation (3.8) to be re-arranged, to give

$$\nabla \times (\underline{H} - j\omega\varepsilon\underline{\Pi}_h) = 0 \qquad (3.9)$$

and equation (A.11) states that the curl of the gradient of any scalar is identically equal to zero, so that it is possible to write

$$\underline{H} - j\omega\varepsilon\underline{\Pi}_h = -\nabla\tau \qquad (3.10)$$

where τ is an arbitrary scalar. The magnetic field is therefore given by

$$\underline{H} = j\omega\varepsilon\underline{\Pi}_h - \nabla\tau \qquad (3.11)$$

It is clear that the expressions (3.7) and (3.11), for the electric and magnetic fields respectively, have now been obtained in terms of an unknown magnetic vector potential, $\underline{\Pi}_h$, and an arbitrary scalar, τ. Substitution of these relations in the hitherto unused equation (3.4a) leads to the relationship

$$\nabla \times \nabla \times \underline{\Pi}_h = - j\omega\mu_o (j\omega\varepsilon\underline{\Pi}_h - \nabla\tau) \qquad (3.12)$$

which may be expanded to give

$$\nabla \times \nabla \times \underline{\Pi}_h = \varepsilon_{rel} k_o^2 \underline{\Pi}_h + j\omega\mu_o \nabla\tau \qquad (3.13)$$

where the wavenumber of free space, k_o, is defined as

$$k_o = \sqrt{\varepsilon_o \mu_o}\,\omega \qquad (3.14)$$

and ω is the angular frequency. The vector identity (A.10) states that, for any vector $\underline{A}$,

$$\nabla \times \nabla \times \underline{A} = \nabla(\nabla.\underline{A}) - \nabla^2\underline{A} \qquad (3.15)$$

and thus equation (3.13) becomes

$$\nabla(\nabla.\underline{\Pi}_h) - \nabla^2\underline{\Pi}_h = \varepsilon_{rel} k_o^2 \underline{\Pi}_h + j\omega\mu_o \nabla\tau \qquad (3.16)$$

The introduction of the magnetic vector potential, $\underline{\Pi}_h$, in equation (3.5a) was in terms of its curl alone, and so it is now possible to define its divergence as

$$\nabla . \underline{\Pi}_h = j\omega\mu_o\tau \qquad (3.17)$$

and, since $j\omega\mu_o$ is constant, equation (3.16) becomes

$$\nabla^2 \underline{\Pi}_h + \varepsilon_{rel} k_o^2 \underline{\Pi}_h = 0 \qquad (3.18)$$

and the magnetic field is now given by

$$\underline{H} = j\omega\varepsilon \underline{\Pi}_h - \frac{1}{j\omega\mu_o} \nabla(\nabla . \underline{\Pi}_h) \qquad (3.19)$$

Substitution of equation (3.6b) into equation (3.18) yields the magnetic scalar potential differential equation

$$\nabla^2 \psi_h + \varepsilon_{rel} k_o^2 \psi_h = 0 \qquad (3.20)$$

and use of equation (3.6b) in equations (3.7) and (3.19), combined with expansion of the divergence and curl operations in cylindrical co-ordinates, gives the relations

$$\underline{E} = \hat{\rho} \left[\frac{1}{\rho} \cdot \frac{\partial \psi_h}{\partial \theta} \right] + \hat{\theta} \left[- \frac{\partial \psi_h}{\partial \rho} \right] \qquad (3.21)$$

$$\underline{H} = \frac{-1}{j\omega\mu_o} \left\{ \hat{\rho} \left[\frac{\partial^2 \psi_h}{\partial \rho \partial y} \right] + \hat{\theta} \left[\frac{1}{\rho} \cdot \frac{\partial^2 \psi_h}{\partial \theta \partial y} \right] + \hat{y} \left[\frac{\partial^2 \psi_h}{\partial y^2} + \varepsilon_{rel} k_o^2 \psi_h \right] \right\} \qquad (3.22)$$

where $\hat{\rho}$, $\hat{\theta}$, $\hat{y}$ are unit vectors in the radial, azimuthal and axial directions respectively.

Examination of equation (3.21) shows that there is no electric field component in the axial direction, and thus the magnetic vector potential has produced a field transverse electric to the y-direction.

3.1.4 The transverse magnetic field

In order to derive the transverse magnetic field components, it is necessary to consider the electric vector potential, $\underline{\Pi}_e$, and thus, within a uniform region of space, the magnetic field is given by equation (3.5b)

$$\underline{H} = \nabla \times \underline{\Pi}_e \qquad (3.23)$$

and equation (3.4a) may now be written as

$$\nabla \times \underline{E} = - j\omega\mu_o \nabla \times \underline{\Pi}_e \tag{3.24}$$

which is rearranged to give

$$\nabla \times (\underline{E} + j\omega\mu_o \underline{\Pi}_e) = 0 \tag{3.25}$$

Following a similar procedure to that used in obtaining the TE field, the electric field is written, in terms of the electric vector potential and an arbitrary scalar ϕ, as

$$\underline{E} = - j\omega\mu_o \underline{\Pi}_e + \nabla\phi \tag{3.26}$$

Substitution of equations (3.23) and (3.26) into equation (3.4b) yields

$$\nabla \times \nabla \times \underline{\Pi}_e = j\omega\varepsilon(- j\omega\mu_o \underline{\Pi}_e + \nabla\phi) \tag{3.27}$$

which, after defining the divergence of the electric vector potential as

$$\nabla \cdot \underline{\Pi}_e = j\omega\varepsilon\phi \tag{3.28}$$

becomes

$$\nabla^2 \underline{\Pi}_e + \varepsilon_{rel} k_o^2 \underline{\Pi}_e = 0 \tag{3.29}$$

and the electric field is now given by the relationship

$$\underline{E} = - j\omega\mu_o \underline{\Pi}_e + \frac{1}{j\omega\varepsilon} \nabla(\nabla \cdot \underline{\Pi}_e) \tag{3.30}$$

Expansion of the vector potential, $\underline{\Pi}_e$, in terms of the electric scalar potential gives the differential equation

$$\nabla^2\psi_e + \varepsilon_{rel}k_o^2\psi_e = 0 \qquad (3.31)$$

and the electromagnetic fields satisfy the following relations,

$$\underline{E} = \frac{1}{j\omega\varepsilon}\left\{\hat{\rho}\left[\frac{\partial^2\psi_e}{\partial\rho\partial y}\right] + \hat{\theta}\left[\frac{1}{\rho}\cdot\frac{\partial^2\psi_e}{\partial\theta\partial y}\right] + \hat{y}\left[\frac{\partial^2\psi_e}{\partial y^2} + \varepsilon_{rel}k_o^2\psi_e\right]\right\} \qquad (3.32)$$

$$\underline{H} = \hat{\rho}\left[\frac{1}{\rho}\cdot\frac{\partial\psi_e}{\partial\theta}\right] + \hat{\theta}\left[-\frac{\partial\psi_e}{\partial\rho}\right] \qquad (3.33)$$

and it is clear from equation (3.33) that there is no magnetic field in the axial direction, and thus the electric vector potential, $\underline{\Pi}_e$, has produced a TM field structure.

3.1.5 The total field equations

In practice, many resonator modes do not have a transverse polarisation, but actually have six field components. However, it is known [4] that any arbitrary field in a homogeneous, source-free region can be expressed as the sum of a TE and a TM field. Consequently, the general field components in cylindrical co-ordinates are given by,

$$E_\rho = \frac{1}{\rho}\cdot\frac{\partial\psi_h}{\partial\theta} + \frac{1}{j\omega\varepsilon}\cdot\frac{\partial^2\psi_e}{\partial\rho\partial y} \qquad (3.34a)$$

$$E_\theta = -\frac{\partial\psi_h}{\partial\rho} + \frac{1}{j\omega\varepsilon}\cdot\frac{1}{\rho}\cdot\frac{\partial^2\psi_e}{\partial\theta\partial y} \qquad (3.34b)$$

$$E_y = \frac{1}{j\omega\varepsilon}\left[\frac{\partial^2\psi_e}{\partial y^2} + \varepsilon_{rel}k_o^2\psi_e\right] \qquad (3.34c)$$

$$H_\rho = \frac{-1}{j\omega\mu_o} \cdot \frac{\partial^2 \psi_h}{\partial \rho \partial y} + \frac{1}{\rho} \cdot \frac{\partial \psi_e}{\partial \theta} \qquad (3.34d)$$

$$H_\theta = \frac{-1}{j\omega\mu_o} \cdot \frac{1}{\rho} \cdot \frac{\partial^2 \psi_h}{\partial \theta \partial y} - \frac{\partial \psi_e}{\partial \rho} \qquad (3.34e)$$

$$H_y = \frac{-1}{j\omega\mu_o} \left[\frac{\partial^2 \psi_h}{\partial y^2} + \varepsilon_{rel} k_o^2 \psi_h \right] \qquad (3.34f)$$

where the electric and magnetic potentials both satisfy the differential equation

$$\nabla^2 \psi_{e,h} + \varepsilon_{rel} k_o^2 \psi_{e,h} = 0 \qquad (3.35)$$

and inspection of equation (3.34c) shows that the reason for calling $\underline{\Pi}_e$ the electric vector potential is because any axial electric field is derived solely from it. Similarly, any axial magnetic field is derived solely from the magnetic vector potential.

3.2 Independent and Hybrid Resonant Modes

The work detailed previously in this chapter applies to any uniform, source-free spatial domain, and it has been shown that the electromagnetic field components may be obtained by solving the differential scalar potential equation (3.35). Examination of the configuration of the substrate-mounted cylindrical pillbox dielectric resonator, shown in Figure 3.1, shows that the structure consists of a resonator, of relative permittivity ε_r, placed upon a grounded dielectric substrate, of relative permittivity ε_s, surrounded by air. Thus, in the half-space above the metal boundary, there are three uniform regions, which are linked by the following conditions

of field continuity at their interfaces,

$$\underline{n} \times \underline{E}_1 = \underline{n} \times \underline{E}_2 \tag{3.36a}$$

$$\underline{n} \cdot \underline{D}_1 = \underline{n} \cdot \underline{D}_2 \tag{3.36b}$$

$$\underline{n} \times \underline{H}_1 = \underline{n} \times \underline{H}_2 \tag{3.36c}$$

$$\underline{n} \cdot \underline{H}_1 = \underline{n} \cdot \underline{H}_2 \tag{3.36d}$$

where the subscripts 1 and 2 refer to the two regions adjacent to the interface, and $\underline{n}$ is the unit vector normal to this interface. Moreover, on the ground plane, the additional boundary conditions,

$$\underline{n} \times \underline{E} = 0 \tag{3.37a}$$

$$\underline{n} \cdot \underline{H} = 0 \tag{3.37b}$$

must be satisfied.

Thus far in the analysis, the electric and magnetic scalar potentials have only had to satisfy the differential equation (3.35), and, consequently, there has been no visible difference between them. However, the presence of independent transverse electric and transverse magnetic resonator modes, as well as the hybrid modes, is explained by the above boundary conditions. The two scalar potentials may be considered independently, and they generate transverse electric and transverse magnetic field structures, in any region of space, according to the equations (3.34). It is apparent, from these equations, that the scalar potentials produce the electric and magnetic field components in different manners, and, consequently, the boundary conditions (3.36) and (3.37) must be satisfied in

dissimilar fashion, leading to different solutions for the magnetic and electric scalar potentials.

It is found that only certain electromagnetic field structures, known as modes, can satisfy these boundary conditions, and each mode has a particular resonant frequency associated with it. Consequently, the magnetic and electric scalar potentials can each produce many different TE and TM modes, respectively. Within each family of transverse modes, the resonant frequencies must all be different, but there is the possibility that separate TE and TM modes may have identical resonant frequencies. In fact, owing to the cylindrical shape of the dielectric resonator, this is a common situation, and, at such a resonant frequency the resonator supports both a TE and a TM mode. When the boundary conditions can only be satisfied by a combination of both, then a hybrid mode results.

However, there are a number of independent TE and TM modes, and, most importantly, the independent $TE_{01\delta}$ mode has the lowest resonant frequency. In many practical circuits involving dielectric resonators, it is this fundamental $TE_{01\delta}$ mode that is excited, and thus it is necessary to develop an accurate theoretical model in order to predict the resonant frequency of this fundamental mode. Consequently, the research detailed in this thesis has been directed at this particular goal, and the electric and magnetic potentials are treated together until the application of the boundary conditions causes the analysis to concentrate on the magnetic scalar potential alone. However, the solution technique adopted is not confined to the TE modes alone, but can equally well be applied to the TM modes.

3.3 Transformation of the Differential Scalar Potential Equation into an Integral Equation

Within the three uniform regions of the substrate-mounted cylindrical dielectric resonator, the differential equation (3.35) must be satisfied. Thus, the following equations apply,

$$\nabla^2\psi_r(\underline{x}) + \varepsilon_r k_o^2 \psi_r(\underline{x}) = 0 \qquad \text{in the resonator} \qquad (3.38a)$$

$$\nabla^2\psi_a(\underline{x}) + \varepsilon_a k_o^2 \psi_a(\underline{x}) = 0 \qquad \text{in the air} \qquad (3.38b)$$

$$\nabla^2\psi_s(\underline{x}) + \varepsilon_s k_o^2 \psi_s(\underline{x}) = 0 \qquad \text{in the substrate} \qquad (3.38c)$$

where the subscripts r, a, s refer to the resonator, air, and substrate regions, respectively, and the vector $\underline{x}$ represents the point (ρ,θ,y) in cylindrical co-ordinates. In order to simplify the terminology in the subsequent analysis, the subscripts e and h have been omitted from the symbol ψ whilst the theoretical treatment is identical for both potential functions.

The electromagnetic field within the substrate-mounted cylindrical dielectic resonator may be determined by solving equations (3.38) in each of the three regions, and then applying the boundary conditions (3.36) and (3.37) to the resulting potential functions, and this process also determines the resonant frequency of the structure. Unfortunately, it is found in practice that the solution of these boundary conditions presents great difficulty, since the physical structure does not coincide with a separable geometry. However, this dilemma can be overcome by transforming the differential problem into an integral equation , which includes these boundary conditions. Thus, the solution of one equation gives the transverse mode field structure, and also the resonant frequency, of the substrate-mounted cylindrical dielectric resonator.

In order to effect the transformation to an integral equation, it is necessary to add the term $\varepsilon_a k_o^2 \psi_r(\underline{x})$ to both sides of equation (3.38a), yielding the relationship

$$\nabla^2\psi_r(\underline{x}) + \varepsilon_a k_o^2 \psi_r(\underline{x}) = -(\varepsilon_r - \varepsilon_a) k_o^2 \psi_r(\underline{x}) \qquad (3.39)$$

which is valid inside the resonator. Examination of this equation shows that the left hand side is identical in form to equation (3.38b), and so it is seen that equation (3.39) is an inhomogeneous form of the differential scalar potential equation (3.38b) in the air region. It is also noted, from equation (3.39), that the resonator may be considered mathematically as a source, of strength $(\varepsilon_r - \varepsilon_a) k_o^2 \psi_r(\underline{x})$, above a grounded dielectric slab, and this fact suggests that the method of Green's functions [5-7] might prove helpful in determining the resonant frequency and the potential function, ψ_r.

In the Green's function approach, the problem is solved by finding the effect of a unit source at any point, and then the general solution is written as a superposition of such sources representing the actual source function. Considering the homogeneous case of the grounded dielectric slab waveguide, the Green's function, $G(\underline{x},\underline{x}')$, is defined to be the potential function at an observation point, $\underline{x}$, caused by a unit source located at the point $\underline{x}'$. Thus, the Green's function must satisfy the equations (3.38b) and (3.38c) at all points, except at the source point, $\underline{x}'$, where its second derivative is discontinuous by the strength of the unit source. Consequently, the Green's function must satisfy the following relations

$$\nabla^2 G_s(\underline{x},\underline{x}') + \varepsilon_s k_o^2 G_s(\underline{x},\underline{x}') = -\delta(\underline{x} - \underline{x}') \quad \text{in the slab} \qquad (3.40a)$$

$$\nabla^2 G_a(\underline{x},\underline{x}') + \varepsilon_a k_o^2 G_a(\underline{x},\underline{x}') = -\delta(\underline{x} - \underline{x}') \quad \text{in the air} \qquad (3.40b)$$

where the Dirac delta function is defined by the relationship

$$\iiint \delta(\underline{x} - \underline{x}')f(\underline{x})dV = \begin{cases} f(\underline{x}') & \underline{x}' \text{ in region V} \\ 0 & \underline{x}' \text{ not in region V} \end{cases} \tag{3.41}$$

for any function $f(\underline{x})$. Furthermore, the Green's functions $G_s(\underline{x},\underline{x}')$ and $G_a(\underline{x},\underline{x}')$ must also be such that the continuity relations (3.36) and (3.37) are satisfied on the boundaries of the dielectric slab.

The analysis proceeds by multiplying equation (3.39) by $G_a(\underline{x},\underline{x}')$ and equation (3.40b) by $\psi_r(\underline{x})$, which gives the equations

$$G_a(\underline{x},\underline{x}')\nabla^2\psi_r(\underline{x}) + \varepsilon_a k_o^2 G_a(\underline{x},\underline{x}')\psi_r(\underline{x}) = -(\varepsilon_r - \varepsilon_a)k_o^2 G_a(\underline{x},\underline{x}')\psi_r(\underline{x}) \tag{3.42a}$$

and

$$\psi_r(\underline{x})\nabla^2 G_a(\underline{x},\underline{x}') + \varepsilon_a k_o^2 \psi_r(x) G_a(\underline{x},\underline{x}') = -\psi_r(\underline{x})\delta(\underline{x} - \underline{x}') \tag{3.42b}$$

Using the symmetrical nature of the Green's function, the source and observation points are now interchanged, and equation (3.42b) is subtracted from equation (3.42a). The result of this operation is then integrated over the volume of the resonator, with respect to the source co-ordinates, to give the relationship

$$\psi_r(\underline{x}) = (\varepsilon_r - \varepsilon_a)k_o^2 \iiint_{\text{resonator}} G_a(\underline{x},\underline{x}')\psi_r(\underline{x}')dV' + \iiint_{\text{resonator}} [G_a(\underline{x},\underline{x}')\nabla_o^2\psi_r(\underline{x}') - \psi_r(\underline{x}')\nabla_o^2 G_a(\underline{x},\underline{x}')]dV' \tag{3.43}$$

where ∇_o^2 means the Laplacian, ∇^2, operating on the source co-ordinates. The second integral in equation (3.43) may be converted to a surface integral by using Green's second identity, which states that

$$\iiint (a\nabla^2 b - b\nabla^2 a)dV = \iint \left(a\frac{\partial b}{\partial n} - b\frac{\partial a}{\partial n}\right) dS \tag{3.44}$$

where a and b are scalars and n is the outward normal to the surface S enclosing the volume V. Consequently, the integral equation (3.43) becomes

$$\psi_r(\underline{x}) = (\varepsilon_r - \varepsilon_a)k_o^2 \iiint_{\text{resonator}} G_a(\underline{x},\underline{x}')\psi_r(\underline{x}')dV' + \iint_{\substack{\text{resonator}\\ \text{boundary}}} [G_a(\underline{x},\underline{x}') \frac{\partial \psi_r(\underline{x}')}{\partial n_r'} - \psi_r(\underline{x}') \frac{\partial G_a(\underline{x},\underline{x}')}{\partial n_r'}] dS' \tag{3.45}$$

where $\partial/\partial n_r'$ represents the derivative with respect to the normal to the resonator surface, and is to be taken in the source variable, $\underline{x}'$.

In Appendix B, the physical interpretation of the volume and surface integrals is discussed, and it is found that the expected differences between the TE and TM solutions are contained within the surface integral. It is discovered, upon expanding this surface integral, that the electric potential, ψ_e, satisfies a much more complex integral equation than does the magnetic potential, ψ_h, for which case most of the constituent terms of the surface integral vanish. Furthermore, it is shown in Appendix C that the boundary conditions on the resonator cannot be satisfied by a transverse resonant mode, except in the special case of no θ-dependence, and thus, in the general case, six field components are necessary to match the electric and magnetic fields over the boundary, and so the resonant modes are hybrid.

However, the TE_{omn} and TM_{omn} modes are capable of independently satisfying the boundary conditions, which is convenient since this research is directed towards finding the solution for the $TE_{01\delta}$ mode. It is also shown, in Appendix B, that the surface integral accounts for the contribution of charge induced on the dielectric interfaces by the equivalent sources within the resonator. Therefore, the

contribution of the surface integral is second order with respect to the volume integral. This fact, together with the knowledge that the magnetic potential does not have any contributions from some of the dielectric interfaces, suggests that the $TE_{01\delta}$ mode may be solved, without introducing much error, by considering the reduced integral equation

$$\psi_{hr}(\underline{x}) = (\varepsilon_r - \varepsilon_a)k_o^2 \iiint_{\text{resonator}} G_a(\underline{x},\underline{x}')\psi_{hr}(\underline{x}')dV' \qquad (3.46)$$

where the Green's function, $G_a(\underline{x},\underline{x}')$, for the grounded dielectric slab waveguide is derived below in the cylindrical co-ordinate system.

3.4 The Green's Function

It was shown in section 3.3 that the Green's function used to obtain the integral equation (3.46) is the Green's function valid in the air region above a grounded dielectric slab waveguide, as shown in Figure 3.2. It is evident that, as the slab waveguide is only bounded in the y-direction, it is convenient to derive the Green's function by first removing the y-dependence in order to leave a two-dimensional Green's function problem.

The desired Green's function for the dielectric slab waveguide must satisfy equation (3.40)

$$\nabla^2 G_b(\underline{x},\underline{x}') + \varepsilon_b k_o^2 G_b(\underline{x},\underline{x}') = -\delta(\underline{x} - \underline{x}') \qquad (3.47)$$

where the subscript b either takes the value a or s dependent upon the vertical position under consideration. Since the cylindrical co-ordinate system is separable, the three-dimensional delta function may be written as a product of three one-dimensional delta functions, so that equation (3.47) becomes

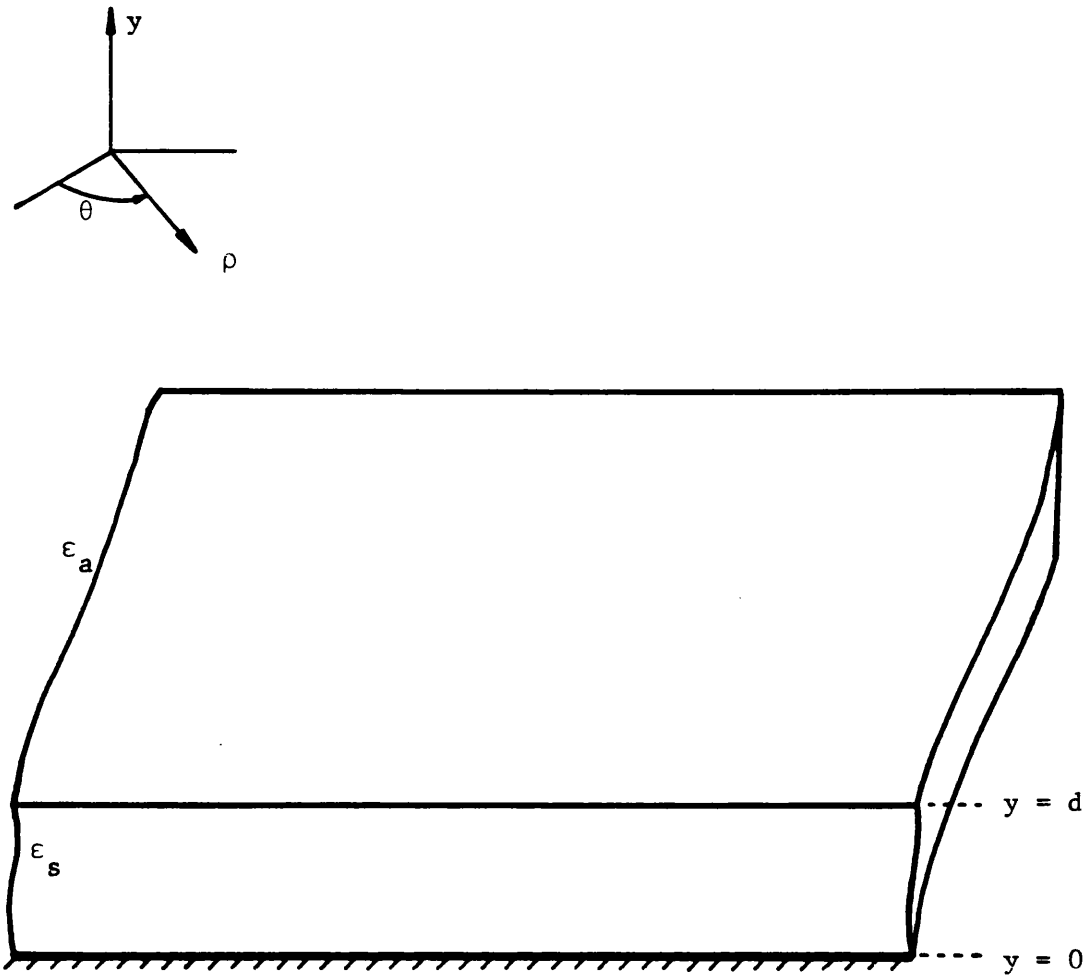

Figure 3.2 The grounded dielectric slab waveguide

$$(\nabla_t^2 + \frac{\partial^2}{\partial y^2} + \varepsilon_b k_o^2) G_b(\underline{x},\underline{x}') = -\frac{1}{\rho}\ \delta(\rho - \rho')\delta(\theta - \theta')\delta(y - y') \tag{3.48}$$

where ∇_t^2 is that part of the Laplacian, ∇^2, transverse to the y-direction.

In order to remove the y-dependence of equation (3.48) it is necessary to use the completeness relationship, which states that a delta function may be expanded in terms of a complete set of orthogonal eigenfunctions in the relevant direction. The y-directed orthonormal eigenfunctions for the dielectric slab waveguide are determined in Appendix D, and consist of both a discrete set of bound modes, $Y_n(y)$, which are known as surface waves since their energy is confined to the vicinity of the slab, and a continuous spectrum of radiation modes, $Y(\chi,y)$, of wavenumber χ, which have no restriction on their energy distribution. The form of these discrete and continuous eigenfunctions, for both TM and TE polarisations, are given in Tables D.1 and D.2, respectively, where the multiplicative constants have been chosen such that the eigenmodes are normalised to unity over the range of y.

The completeness relationship using the above orthonormal functions is derived in Appendix F, and is found to be

$$\delta(y - y') = w_b(y') \left[\sum_n Y_n(y) Y_n(y') + \int_o^\infty Y(\chi,y) Y(\chi,y') d\chi \right] \tag{3.49}$$

where the weight factor w(y') arises from the Sturm-Liouville equation, as shown in Appendix E, and takes the value

$$w_b(y') = \begin{cases} 1 & \text{for TE modes} \\ 1/\varepsilon_b & \text{for TM modes} \end{cases} \tag{3.50}$$

Utilising the separable nature of the Helmholtz equation in cylindrical co-ordinates, the y-directed component of the Green's

function is now written as the expansion of the delta function $\delta(y - y')$, as given in equation (3.49), and tables (D.1) and (D.2) show that equation (3.48) becomes

$$\sum_n w_b(y')Y_n(y)Y_n(y') \left(\nabla_t^2 + \varepsilon_b k_o^2 - k_{bn}^2\right) g_n(\rho,\rho';\theta,\theta') + \int_o^\infty w_b(y')Y(\chi,y)Y(\chi,y') \left(\nabla_t^2 + \varepsilon_b k_o^2 - k_{bc}^2\right) g_c(\rho,\rho';\theta,\theta')d\chi = -\frac{1}{\rho}\delta(\rho - \rho')\delta(\theta - \theta')\delta(y - y') \qquad (3.51)$$

where $g(\rho,\rho';\theta,\theta')$ is the two-dimensional Green's function transverse to the y-direction, and k_{bn} and k_{bc} are the y-directed wavenumbers for the discrete and continuous modes respectively. Substitution of equation (3.49) in the right hand side of equation (3.51), and use of the orthogonality relationships given in Appendix E, gives the results

$$Y_m(y) \left(\nabla_t^2 + k_{\rho m}^2\right) g_m(\rho,\rho';\theta,\theta') = -\frac{1}{\rho}\delta(\rho - \rho')\delta(\theta - \theta') Y_m(y) \qquad (3.52a)$$

$$Y(\chi',y) \left(\nabla_t^2 + k_{\rho c}^2\right) g_c(\rho,\rho';\theta,\theta') = -\frac{1}{\rho}\delta(\rho - \rho')\delta(\theta - \theta') Y(\chi',y) \qquad (3.52b)$$

where

$$k_{\rho m}^2 = \varepsilon_b k_o^2 - k_{bm}^2 \qquad (3.53a)$$

$$k_{\rho c}^2 = \varepsilon_b k_o^2 - k_{bc}^2 \qquad (3.53b)$$

Equating the coefficients of $Y_m(y)$, and of $Y(\chi',y)$, leads to the two-dimensional Green's function equation

$$\left(\nabla_t^2 + k_\rho^2\right)g(\rho,\rho';\theta,\theta') = -\frac{1}{\rho}\delta(\rho - \rho')\delta(\theta - \theta') \qquad (3.54)$$

where the radial wavenumber depends upon the y-directed wavenumber under consideration. Harrington [8] gives the solution for equation (3.54) as

$$g(\rho,\rho';\theta,\theta') = \frac{1}{4j} H_o^{(2)}(k_\rho|\rho - \rho'|) \qquad (3.55)$$

where $H_o^{(2)}(x)$ is the Hankel function of the second kind of order zero and argument x, and which represents outward travelling waves.

The desired Green's function for the dielectric slab waveguide is therefore found to be

$$G_b(\underline{x},\underline{x}') = \frac{w_b(y')}{4j}\left[\sum_n H_o^{(2)}(k_{\rho n}|\rho - \rho'|)Y_n(y)Y_n(y') + \int_o^\infty H_o^{(2)}(k_{\rho c}|\rho - \rho'|)Y(\chi,y)Y(\chi,y')d\chi\right] \qquad (3.56)$$

where $Y_n(y)$ and $Y(\chi,y)$ are given in Tables (D.1) and (D.2) for the TM and TE modes respectively.

REFERENCES

[1] H.Y. Yee, "An investigation of microwave dielectric resonators", Microwave Lab. Rep. 1065, Stanford University, Stanford, CA, July 1963.

[2] S.B. Cohn, "Microwave bandpass filters containing high-Q dielectric resonators", IEEE Trans. Microwave Theory Tech., Vol.MTT-16, pp.218-227, April 1968.

[3] T. Itoh and R.S. Rudokas, "New method for computing the resonant frequencies of dielectric resonators", IEEE Trans. Microwave Theory Tech., Vol.MTT-25, pp.52-54, January 1977.

[4] R.F. Harrington, "*Time-Harmonic Electromagnetic Fields*". New York: McGraw-Hill, 1961, p.131.

[5] P.M. Morse and H. Feshbach, "*Methods of Theoretical Physics - Part 1*". New York: McGraw-Hill, 1953, Chapter 7.

[6] R.E. Collin, "*Field Theory of Guided Waves*". New York: McGraw-Hill, 1960, Chapter 2.

[7] D.C. Stinson, "*Intermediate Mathematics of Electromagnetics*". Englewood Cliffs, N.J.: Prentice-Hall, 1976, Chapter 2.

[8] R.F. Harrington, "*Time-Harmonic Electromagnetic Fields*". New York: McGraw-Hill, 1961, pp.223-225.

CHAPTER 4

DISCUSSION OF TECHNIQUES FOR THE SOLUTION OF THE SCALAR POTENTIAL INTEGRAL EQUATION

The scalar potential integral equation developed in chapter 3, and given by equation (3.46) as

$$\psi_{hr}(\underline{x}) = (\varepsilon_r - \varepsilon_a)k_o^2 \iiint_{\text{resonator}} G_a(\underline{x},\underline{x}')\psi_{hr}(\underline{x}')dV' \qquad (4.1)$$

is a particular type of integral equation known as a homogeneous Fredholm equation of the second kind. This chapter starts with a brief discussion of the properties of this type of equation in one-dimension, followed by a short survey of several numerical methods developed to provide approximate solutions. The application of these techniques to the integral equation (4.1) is then considered, and a further solution, based on a quasi-analytical iterative procedure, is presented.

4.1 The Homogeneous Fredholm Equation of the Second Kind

An equation in which an unknown function appears under an integral sign is known as an integral equation, and the Fredholm equation of the second kind is defined to be an integral equation where the unknown function, represented by f in the following discussion, also appears as the result of the integration. The general form of this type of equation is given by

$$f(u) = p(u) + \kappa \int_a^b K(u,v)f(v)dv \qquad (4.2)$$

where p(u) is a known function, K(u,v) is known as the kernel of the integral equation, and κ is a parameter whose significance will soon become apparent.

If the function p(u) is set to zero, then the homogeneous form of equation (4.2) is obtained,

$$f(u) = \kappa \int_a^b K(u,v)f(v)dv \qquad (4.3)$$

and it is apparent that this equation has the trivial solution f = 0. Obviously, such solutions have no importance, and thus the unknown function, f, is given by the non-trivial solutions to equation (4.3), which may be rewritten, in operator form, as

$$\lambda f = Kf \qquad (4.4)$$

where $\lambda = \kappa^{-1}$ and

$$K = \int_a^b dv\ K(u,v) \qquad (4.5)$$

Equation (4.4) is an eigenvalue equation, and any non-trivial solution, f, is known as an eigenfunction, corresponding to a particular eigenvalue, λ. In general, it is found that these eigenvalues are complex and the eigenvalue with the largest magnitude is known as the dominant eigenvalue.

Since the analytic solution of equation (4.3) is often not easily determined, several numerical techniques have been developed in order to find an approximate value for the dominant eigenvalue and its associated eigenfunction.

4.2 Numerical Approximation Techniques

The numerical methods developed for solving the integral equation (4.3) all involve expanding the unknown function, f, as a finite series approximation, and may be divided broadly into two classifications [1] depending upon the form of the expansion. The first type of numerical solution, which includes both the quadrature and product-integration

methods, removes the difficulties introduced by the integration of f by replacing this integral with the calculation of a finite summation. However, the second category, which includes the collocation and Galerkin methods, uses a different approach where only the unknown function, f, is approximated by a set of pre-selected basis functions.

Despite the apparent differences between these two classes of numerical solution, all of the four methods mentioned above generate matrix eigenvalue equations of the form

$$(\underline{K} - \tilde{\lambda}\underline{I})\underline{\tilde{C}} = 0 \qquad (4.6)$$

where $\underline{I}$ is the identity matrix and the tilde indicates that the unknown eigenvalue, $\tilde{\lambda}$, and eigenvector, $\underline{\tilde{C}}$, will be obtained as approximations to their true values. The differences between these numerical methods are found in the manner in which the matrix $\underline{K}$ is generated from the kernel, K(u,v), of the integral equation, and in the relationship between the unknown function, f, and the eigenvector, $\underline{C}$.

Equation (4.6) is a standard matrix eigenvalue problem which only gives a non-trivial solution if the matrix $(\underline{K} - \tilde{\lambda}\underline{I})$ is singular. Therefore, the approximate eigenvalues, $\tilde{\lambda}$, may be calculated by solving the determinant equation

$$\det(\underline{K} - \tilde{\lambda}\underline{I}) = 0 \qquad (4.7)$$

and the corresponding eigenfunctions, $\underline{\tilde{C}}$, may then be determined by solving the coupled equation set represented by the matrix equation (4.6).

Owing to the nature of these numerical techniques, the solutions obtained for the eigenvalues, and their associated eigenfunctions, of the integral equation (4.3) are necessarily approximate. In each of

the techniques, the unknown function is replaced by an expansion, and therefore it is seen that the accuracy of the approximate solution for f increases if the number of terms, N, in the series expansion is increased. Furthermore, as N is increased, the accuracy of the approximation of the dominant eigenvalue is also increased.

Nevertheless, it is apparent that a major disadvantage of these numerical methods is that any results obtained are only approximations. However, one method of improving the accuracy of the results, without incurring the computational complexities associated with large N, is to use one of the numerical methods mentioned above to provide an approximate solution, and then to use the method of least-squares.

4.2.1 The method of least-squares

This numerical technique can best be explained by considering the residual, r(f,u), which is defined to be

$$r(f,u) = \int_a^b K(u,v)f(v)dv - \lambda f(u) \qquad (4.8)$$

Evidently the integral equation (4.3) is satisfied when r(f,u) is identically equal to zero for all u, and, in order to best approximate this condition, this technique minimises, in the least-squares sense, the value of the residual over the whole range of integration [a,b].

The method of least-squares starts with an approximate eigenfunction, $\tilde{f}(u)$, and proceeds to minimise the inner product,

$$(r,r) = \int_a^b r(\tilde{f},u)\,\overline{r(\tilde{f},u)}\,du = \int_a^b |r(\tilde{f},u)|^2\,du \qquad (4.9)$$

where the bar represents the complex conjugate of the function, in order to obtain an approximate eigenvalue, $\tilde{\lambda}$. Since the residual is the difference of two functions, the inner product is expanded to give

$$(r,r) = (K\tilde{f},K\tilde{f}) - \tilde{\lambda}(\tilde{f},K\tilde{f}) - \overline{\tilde{\lambda}}(K\tilde{f},\tilde{f}) + |\tilde{\lambda}|^2 (\tilde{f},\tilde{f}) \qquad (4.10)$$

where the symbol K represents the integral operator as defined in equation (4.5).

In general, the eigenvalue $\tilde{\lambda}$ is complex, and thus equation (4.10) may be written as

$$(r,r) = (K\tilde{f},K\tilde{f}) - (\alpha + j\beta)(\tilde{f},K\tilde{f}) - (\alpha - j\beta)(K\tilde{f},\tilde{f}) + (\alpha^2 + \beta^2)(\tilde{f},\tilde{f}) \qquad (4.11)$$

where the eigenvalue is defined to be

$$\tilde{\lambda} = \alpha + j\beta \qquad (4.12)$$

In order that the value of $\tilde{\lambda}$ minimises the inner product, (r,r), it is necessary that

$$\frac{\partial}{\partial\alpha}[(r,r)] = \frac{\partial}{\partial\beta}[(r,r)] = 0 \qquad (4.13)$$

and consequently, it is found that

$$\alpha = \frac{1}{2}\left[\frac{(\tilde{f},K\tilde{f}) + (K\tilde{f},\tilde{f})}{(\tilde{f},\tilde{f})}\right] \qquad (4.14a)$$

and

$$\beta = \frac{j}{2}\left[\frac{(\tilde{f},K\tilde{f}) - (K\tilde{f},\tilde{f})}{(\tilde{f},\tilde{f})}\right] \qquad (4.14b)$$

and therefore the value of $\tilde{\lambda}$ is given by

$$\tilde{\lambda} = \frac{(K\tilde{f},\tilde{f})}{(\tilde{f},\tilde{f})} \qquad (4.15)$$

Confirmation that this value of $\tilde{\lambda}$ does indeed minimise (rather than maximise) the residual in the least-squares sense is provided by examining the second differential of the inner product with respect to the eigenvalue, at the value of $\tilde{\lambda}$ given in equation (4.15). It is seen from equation (4.11), that

$$\frac{\partial^2}{\partial\alpha^2}[(r,r)] = \frac{\partial^2}{\partial\beta^2}[(r,r)] = 2(\tilde{f},\tilde{f}) = 2\int_a^b |\tilde{f}(u)|^2\,du \tag{4.16}$$

and since this is always positive, the eigenvalue given by

$$\tilde{\lambda} = \frac{\int_a^b \int_a^b \overline{\tilde{f}(u)}K(u,v)\tilde{f}(v)\,dudv}{\int_a^b |\tilde{f}(u)|^2\,du} \tag{4.17}$$

does minimise the residual in the least-squares sense.

If the kernel, K(u,v), is either complex symmetric or Hermitian, and is square integrable, then it is shown in reference [2] that equation (4.17) is a variational expression, where, for an error $\delta\tilde{f}$ in the approximate solution $\tilde{f}$, the eigenvalue has an error proportional to $|\delta\tilde{f}|^2$. Consequently, if an approximation to the true eigenfunction, f, has been obtained with an error of 10%, then use of equation (4.17) to calculate a value for $\tilde{\lambda}$ will result in an approximation to the true eigenvalue with an error of only 1%.

4.3 Extension of the Numerical Methods to the Three-Dimensional Case

All of the numerical methods covered in the preceding section have been described in connection with the solution of the homogeneous Fredholm equation of the second kind in one dimension, but, in fact, the variables $\underline{x}$ and $\underline{x}'$ in the scalar potential integral equation (4.1) each represent a point in three-dimensional space. Thus, equation (4.1) may be rewritten as

$$\psi_r(\rho,\theta,y) = (\varepsilon_r - \varepsilon_a)k_o^2 \iiint_{\text{resonator}} G_a(\rho,\theta,y;\rho',\theta',y') \cdot \psi_r(\rho',\theta',y')\,\rho'd\rho'd\theta'dy' \tag{4.18}$$

In practice, each of the one-dimensional numerical methods can be extended to cover the three-dimensional case, and it is seen that the calculation of the dominant, or largest, eigenvalue would produce the desired fundamental, or lowest, resonant frequency. However, it is found that the degree of complexity of the approximations rises very rapidly with regard to the number of dimensions.

Although modern computers can handle multi-dimensional matrices and vectors with little difficulty, the combination of expansions required to derive a three-dimensional matrix equation is difficult to physically comprehend. For example, applying three separate quadrature rules to equation (4.18) would lead to a six-dimensional matrix for the Green's function. Furthermore, if an expansion method were employed, the resulting matrix, $\underline{K}$, would require a triple integral, involving the Green's function, to be performed for each of its components.

Owing to the complexity of the implementation of these numerical methods, it was decided to attempt to seek a solution to the integral equation (4.18) by using a more analytical evaluation of the integrals by means of an iterative procedure.

4.4 The Iterative Approach

One of the properties of the homogeneous Fredholm equation of the second kind is that the kernel acts as a smoothing operator, having the effect of smoothing out any discontinuity, or roughness, in the function upon which it operates. A consequence of this effect is that a test function which undergoes the integral operation described by equation (4.18) will emerge as a better representation of the true solution, $\psi_r(\underline{x})$. This principle has been used in several iterative methods [3,4] for solving the one-dimensional Fredholm equation of the

second kind, but these standard techniques suffer from the drawback that the results that are obtained for the eigenfunction contain the eigenvalue as a parameter. Thus, in practice, these methods are employed when the eigenvalue is known, and only the eigenfunction needs to be determined.

A further disadvantage of the above standard iterative techniques is that each successive iteration produces a new approximation in a different analytic form from the previous one. This effect is most pronounced at the start of the iterative procedure, but has less impact as the correct solution is approached. Consequently, these iterative procedures are not well-suited to quasi-analytic implementation on a computer, and need to be implemented either manually or completely numerically. However, it is apparent that a quasi-analytic iterative technique suitable for computer implementation may be devised if it is possible to produce successive trial functions that have the same basic form, and the method described below has this property.

The integral equation (4.18) may rewritten, in iterative format, as

$$[(\varepsilon_r - \varepsilon_a)k_o^2]^{-1}[\psi_r(\underline{x})]_{n+1} = \iiint_{\text{resonator}} G_a(\underline{x},\underline{x}')[\psi_r(\underline{x}')]_n \, dV' \tag{4.19}$$

where the trial function $[\psi_r(\underline{x})]_n$ is constructed from independent sets of orthonormal basis functions in the radial and axial directions. Inspection of equation (4.19) shows that, if $[\psi_r(\underline{x}')]_n$ were the exact scalar potential function, then evaluation of the integral

$$I = \iiint_{\text{resonator}} G_a(\underline{x},\underline{x}')[\psi_r(\underline{x}')]_n dV' \tag{4.20}$$

would produce a linear multiple of the function $[\psi_r(\underline{x}')]$ but transformed from source space into observation space. Furthermore, this linear multiplier is equal to the eigenvalue $[(\varepsilon_r - \varepsilon_a)k_o^2]^{-1}$.

Considering now the original choice of trial function, $[\psi_r(\underline{x}')]_o$, it is clear that performing the integral defined in equation (4.20) will produce a new function that, generally speaking, bears little resemblance to the original. However, using orthogonality principles, this new function may be re-expressed in terms of the original basis functions, but with altered coefficients. After normalising this new trial function, the above process may be iterated until the change in successive trial functions becomes purely linear. At this point, the trial function is a good representation of the desired scalar potential, and, since the Green's function $G_a(\underline{x},\underline{x}')$ is symmetric, it is known [5] that the linear multiplication factor yields the dominant eigenvalue, from which the fundamental resonant frequency may be calculated.

It is seen from the above discussion that a quasi-analytic iterative procedure has been developed to solve equation (4.1) for both the fundamental $TE_{01\delta}$ resonant frequency, and for the associated magnetic scalar potential function. Furthermore, by a process of constructing orthonormal trial functions that are orthogonal to any previously determined eigenfunctions, the higher order TE_{omn} resonant modes may also be determined, as shown in reference [6].

Although this iterative method requires the analytical evaluation of the integral given in equation (4.20), which is by no means simple, the extra work involved in constructing this solution is far outweighed by the subsequent simplicity of the numerical computational procedure required to give the fundamental resonant frequency. Moreover, comparison with the other solution techniques discussed in

this chapter clearly shows the advantages of the iterative approach, in that it provides accurate solutions for the fundamental resonant frequency and is also easily implemented on a numerical computer.

REFERENCES

[1] C.T.H. Baker, "*The Numerical Treatment of Integral Equations*". Oxford: O.U.P., 1977.

[2] J. Schwinger and D.S. Saxon, "*Discontinuities in Waveguides*". New York: Gordon and Breach, 1968.

[3] Ll. G. Chambers, "*Integral Equations: A Short Course*". London: International Textbook Company Ltd., 1976.

[4] B.L. Moiseiwitsch, "*Integral Equations*". London: Longmans, 1977.

[5] R. Courant and D. Hilbert, "*Methods of Mathematical Physics - Volume 1*". New York: Interscience Publishers, 1953, pp.122-125.

[6] *ibid.*, pp.126-128.

CHAPTER 5

THE ITERATIVE SOLUTION

In chapter 3, the magnetic scalar potential function within a cylindrical pillbox dielectric resonator, which is situated upon a grounded dielectric substrate, was found to satisfy the integral equation (3.46)

$$\psi_{hr}(\underline{x}) = (\varepsilon_r - \varepsilon_a)k_o^2 \iiint_{\text{resonator}} G_a(\underline{x},\underline{x}')\psi_{hr}(\underline{x}')dV' \qquad (5.1)$$

In order to solve this equation to give the fundamental resonant frequency of the dielectric resonator, an iterative method was described in chapter 4 which was based upon the analytical evaluation of the integral given in equation (5.1). However, in practice the nature of the Green's function, $G_a(\underline{x},\underline{x}')$, makes this integration over the resonator volume difficult to perform, and many different approaches were considered before the method described below was developed.

This chapter describes the process used to formulate the iterative relationship, and starts with a discussion of the choice of the trial function, followed by the determination of the exact form of the Green's function. Then the major steps undertaken in the analytical evaluation of the integral are given, before detailing the procedure used to re-express the result of this integration back in terms of the original trial function. Finally, the chapter concludes with an explanation of the computational process used to calculate the fundamental resonant frequency.

5.1 The Trial Function

It was shown, in chapter 4, that, if an orthonormal series expansion is used to construct a trial function for the magnetic potential, then repeated application of the integral given in equation (5.1) will eventually transform this trial function into the correct form for ψ_{hr}. This process may therefore be used to determine the magnetic potential function, and hence the electromagnetic field structure within the resonator, but, more importantly, it may be used to determine the fundamental resonant frequency of the dielectric resonator.

In order to produce the desired result, it is evidently appropriate to choose a trial function that is based upon the expected form of the $TE_{01\delta}$ scalar potential function, which has zero variation in the azimuthal direction, a sinusoidal variation in the axial direction, and a distribution in the radial direction based upon the Bessel function of the first kind of order zero. The principle of operation of the iterative procedure is that orthonormal series expansions are constructed in both the radial and axial directions, the coefficients of which are initially set to unity. Evaluation of the integral of equation (5.1) upon this trial function yields new values for these coefficients, which are then normalised, and this process is repeated until only a linear change is detected between two successive trial functions. At this point the correct form of the magnetic scalar potential function has been produced, and the linear multiplier may be used to calculate the resonant frequency.

5.1.1 The radial expansion

Since the expected form of the magnetic scalar potential function in the radial direction is that of a zero order Bessel function, it is prudent to choose an expansion in terms of such Bessel functions. Therefore, the series needs to be constructed from zero order Bessel functions of varying argument, which must be orthogonal over the resonator volume in the manner

$$\int_o^R \rho' \, J_o(\beta_n \rho') J_o(\beta_m \rho') d\rho' = \eta_n^2 \delta_{nm} \quad , \quad \delta_{nm} = \begin{cases} 1 & n = m \\ 0 & n \neq m \end{cases} \tag{5.2}$$

where η_n^2 is the norm of the Bessel function $J_o(\beta_n \rho')$. It is known [1] that any two Bessel functions $Z_p(\alpha x)$ and $B_p(\gamma x)$ satisfy the indefinite integral

$$\int x \, Z_p(\alpha x) B_p(\gamma x) dx = \frac{(\gamma x) Z_p(\alpha x) B_{p-1}(\gamma x) - (\alpha x) Z_{p-1}(\alpha x) B_p(\gamma x)}{(\alpha^2 - \gamma^2)} \tag{5.3}$$

and thus equation (5.2) becomes

$$\frac{(\beta_n R) J_1(\beta_n R) J_o(\beta_m R) - (\beta_m R) J_o(\beta_n R) J_1(\beta_m R)}{(\beta_n^2 - \beta_m^2)} = \eta_n^2 \delta_{nm} \tag{5.4}$$

It is apparent that, if the values of βR are now chosen to be zeros of either $J_o(z)$ or $J_1(z)$, then equation (5.4) is satisfied if $n \neq m$, whilst, if $n = m$, the equation (5.2) becomes

$$\int_o^R \rho' [J_o(\beta_n \rho')]^2 d\rho' = \eta_n^2 \tag{5.5}$$

which gives the norm of $J_o(\beta_n \rho')$ as

$$\eta_n^2 = \frac{R^2}{2} [J_o(\beta_n R)]^2 \tag{5.6}$$

Returning to the choice of the wavenumber, β, it is seen that it is not prudent to set the values of $\beta_n R$ as the zeros of $J_o(z)$, since then the trial function would be forced to zero on the circumference of the resonator, which is known not to be the case for the $TE_{01\delta}$ mode. Consequently, the wavenumbers are chosen to satisfy

$$J_1(\beta_n R) = 0 \tag{5.7}$$

where the index n indicates that the n^{th} zero of $J_1(z)$ is to be taken to calculate β_n, and realising that $J_o(0) = 1$, the series expansion is generalised by the inclusion of a constant by choosing β_o to be zero (which also satisfies equation (5.7), even though $z = 0$ is not normally regarded as one of the zeros of $J_1(z)$).

Therefore the orthonormal trial function in the radial direction is chosen to be

$$\psi_{hr}(\rho') = \sum_{n=0}^{N} \frac{P_n J_o(\beta_n \rho')}{\eta_n} \tag{5.8}$$

where the coefficients, P_n, are initially set at unity.

5.1.2 The axial expansion

In the y-direction, the magnetic potential has a sinusoidal distribution, and orthogonality is necessary over the height of the resonator. Thus, the trial function in the axial direction is chosen to be the Fourier series

$$\psi_{hr}(y') = \frac{A_o}{\sqrt{h}} + \sqrt{\frac{2}{h}} \sum_{m=1}^{M} \left\{ A_m \cos\left[\frac{2m\pi}{h}(y' - d)\right] + B_m \sin\left[\frac{2m\pi}{h}(y' - d)\right] \right\} \tag{5.9}$$

where A_m and B_m are the coefficients, and the multiplying factors $1/\sqrt{h}$ and $\sqrt{2/h}$ arise from the normalisation of the sinusoids over the resonator height.

5.1.3 The complete trial function

In the θ-direction there is no variation in the potential function, and thus the complete trial function is given by multiplying the two expansions (5.8) and (5.9) together, so that

$$\psi_{hr}(\underline{x}') = \sum_{n=0}^{N} \frac{P_n J_o(\beta_n \rho')}{\eta_n} \left\{ \frac{A_o}{\sqrt{h}} + \sqrt{\frac{2}{h}} \sum_{m=1}^{M} \left\{ A_m \cos\left[\frac{2m\pi}{h}(y' - d)\right] + B_m \sin\left[\frac{2m\pi}{h}(y' - d)\right] \right\} \right\} \qquad (5.10)$$

Theoretically, the limits N and M should be infinite, but in practice this is impossible to compute, and thus the series are truncated to a point where the loss of further terms does not significantly affect the computed result.

5.2 The Green's Function

In section 3.4, the Green's function for the air region above a grounded dielectric slab waveguide was derived, and was found to be given by equation (3.56)

$$G_a(\underline{x},\underline{x}') = \frac{1}{4j} \left\{ \sum_n H_o^{(2)}(k_{\rho n}|\rho - \rho'|)\, Y_n(y) Y_n(y') + \int_o^{\infty} H_o^{(2)}(k_{\rho c}|\rho - \rho'|)\, Y(X,y) Y(X,y') dX \right\} \qquad (5.11)$$

where the eigenfunctions $Y_n(y)$ and $Y(X,y)$ are given in Tables D.1 and D.2 of Appendix D for the TM and TE modes, respectively, and the radial wavenumbers are related to those in the axial direction by

$$k_o^2 = k_{\rho n}^2 - \gamma_n^2 = k_{\rho c}^2 + \chi^2 \qquad (5.12)$$

The solution of the integral equation (5.1) with the full Green's function given by equation (5.11) is extremely complicated, and therefore it is advisable to seek a simplified version of this Green's function for an initial attempt at the solution. Considering the two eigenfunctions, $Y_n(y)$ and $Y(\chi,y)$, it is shown in Appendix D that the continuum modes represent the energy that is radiated away from the dielectric slab, while the discrete modes describe most of the energy that remains confined to the dielectric region and its immediate neighbourhood. Consequently, since a dielectric resonator has the property that it stores electromagnetic energy at certain resonant frequencies, it is seen that the discrete modes, $Y_n(y)$, will be much more important than the continuum in the determination of the resonant frequency. This conclusion is also justified by the fact that no previous research has considered these continuum modes, and yet accurate results for the resonant frequency have been obtained. Therefore, as an initial attempt to solve the integral equation (5.1), only the discrete modes will be considered, and the problem of the continuum modes will be returned to in chapter 7.

In Appendix D it is shown that the discrete y-directed wavenumbers satisfy the transcendental equations

$$(k_{yn}d)\tan(k_{yn}d) = \frac{\varepsilon_s}{\varepsilon_a}(\gamma_n d) \qquad \text{TM modes} \qquad (5.13a)$$

$$(k_{yn}d)\cot(k_{yn}d) = -(\gamma_n d) \qquad \text{TE modes} \qquad (5.13b)$$

and are also related by the equation

$$(k_{yn}d)^2 + (\gamma_n d)^2 = (\varepsilon_s - \varepsilon_a)(k_o d)^2 \qquad (5.13c)$$

where k_{yn} is the wavenumber in the slab, and γ_n the wavenumber in the air.

These equations (5.13) are shown graphically in Figure 5.1 for a grounded polystyrene slab ($\varepsilon_{rel} = 2.5$) of thickness 1 mm. The circular loci represent equation (5.13c) for constant values of the free-space wavenumber, k_o, and the number of transcendental curves that are intersected determines the number of TM and TE modes that exist at that frequency. Moreover, the intersection points give the values of k_{yn} and γ_n for each mode. It is therefore clear from Figure 5.1 that only one TM mode exists on the grounded polystyrene slab up to a frequency in excess of 30 GHz. Since the fundamental resonant frequencies of the dielectric resonators to be studied are expected to lie in the X-band (8.0 - 12.5 GHz) region, it is seen that the Green's function can be further simplified, without any reduction in accuracy, by considering this particular polystyrene substrate, so that only the first TM mode needs to be considered. Thus, according to Table D.1, the required Green's function is given by

$$G_a(\underline{x},\underline{x}') = C_g \exp[-\gamma(y - d)]H_o^{(2)}(k_\rho|\rho - \rho'|)\exp[-\gamma(y' - d)] \tag{5.14}$$

where C_g is given by

$$C_g = -\frac{j}{2} \frac{\cos^2(k_y d)}{\left\{\left(\frac{d}{\varepsilon_s}\right) + \left(\frac{\varepsilon_a}{\gamma}\right)\left[\frac{k_y^2 + \gamma^2}{\varepsilon_a^2 k_y^2 + \varepsilon_s^2 \gamma^2}\right]\right\}} \tag{5.15}$$

and γ and k_y are determined by the frequency under consideration, through equations (5.13a and c).

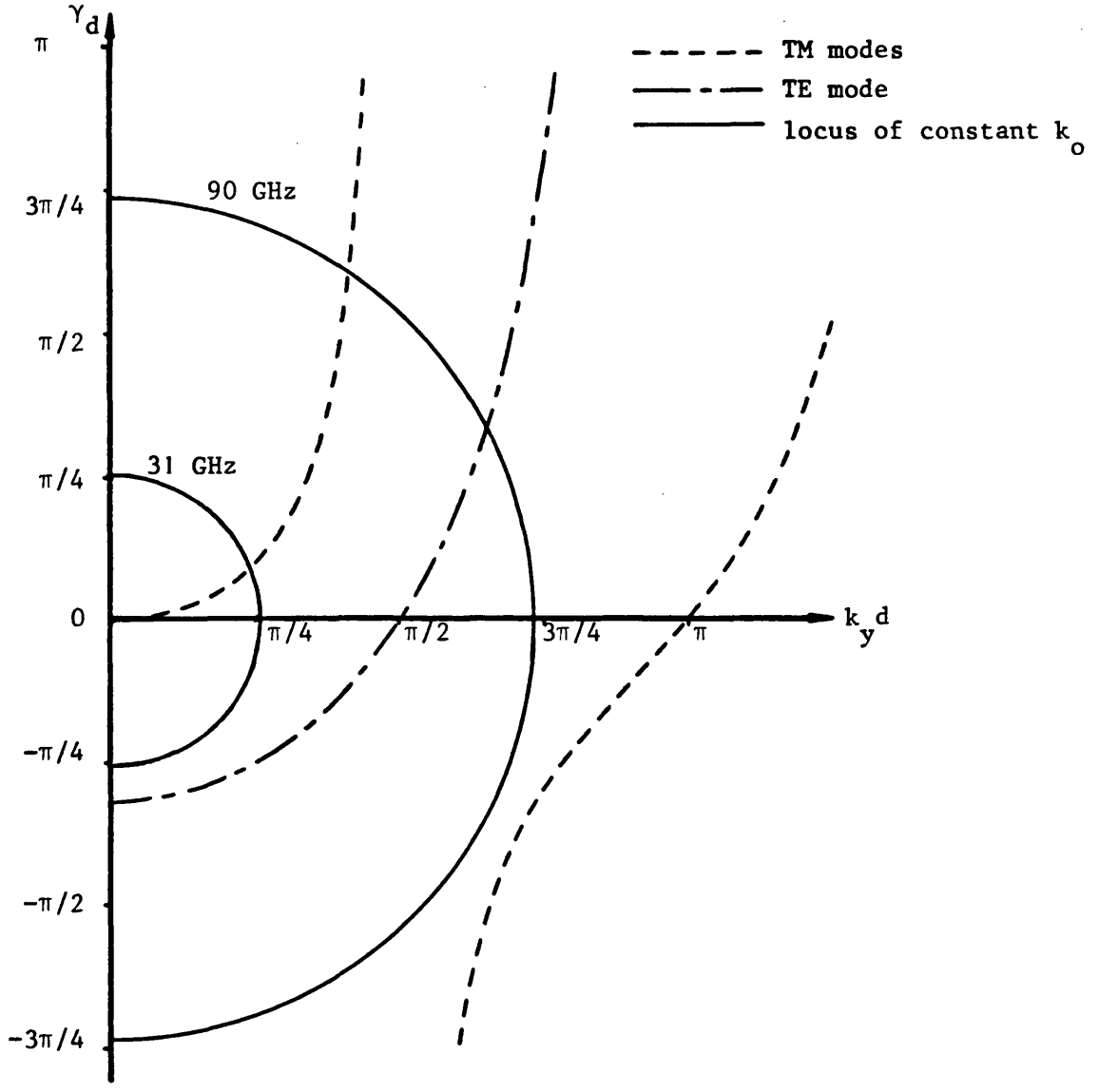

Figure 5.1 Graphical solution for the propagating modes in a 1 mm thick grounded polystyrene slab ($\varepsilon_{rel} = 2.5$)

5.3 Evaluation of the Volume Integral

The integral equation (5.1) may be expanded, by substituting equations (5.14) and (5.10) for the Green's function and the magnetic potential, respectively, to give

$$\psi_{hr}(\underline{x}) = (\varepsilon_r - \varepsilon_a)k_o^2 C_g \exp[-\gamma(y - d)] \iiint_{\text{resonator}} \left\{ H_o^{(2)}(k_\rho|\rho - \rho'|)\exp[-\gamma(y' - d)] \cdot \sum_{n=0}^{N} \frac{P_n}{\eta_n} J_o(\beta_n \rho') \cdot \left\{ \frac{A_o}{\sqrt{h}} + \sqrt{\frac{2}{h}} \sum_{m=1}^{M} \left[A_m \cos\left[\frac{2m\pi}{h}(y' - d)\right] + B_m \sin\left[\frac{2m\pi}{h}(y' - d)\right] \right] \right\} \right\} dV' \qquad (5.16)$$

As it stands, the integration in equation (5.16) is complicated by the argument of the Hankel function containing a modulus. Harrington [2] gives the addition theorem for such a Hankel function as

$$H_o^{(2)}(k_\rho|\rho - \rho'|) = \sum_{t=-\infty}^{\infty} \exp[jt(\theta - \theta')] \begin{cases} H_t^{(2)}(k_\rho \rho')J_t(k_\rho \rho) & \rho < \rho' \\ J_t(k_\rho \rho')H_t^{(2)}(k_\rho \rho) & \rho > \rho' \end{cases} \qquad (5.17)$$

and so equation (5.16) becomes

$$\psi_{hr}(\underline{x}) = (\varepsilon_r - \varepsilon_a)k_o^2 C_g \exp[-\gamma(y - d)] \sum_{t=-\infty}^{\infty} \exp(jt\theta)\, H_t^{(2)}(k_\rho \rho) \cdot \iiint_{\text{resonator}} \exp(-jt\theta')J_t(k_\rho \rho')\exp[-\gamma(y' - d)] \cdot \psi_{hr}(\rho')\psi_{hr}(y')dV' \qquad \rho' < \rho \qquad (5.18a)$$

$$\psi_{hr}(\underline{x}) = (\varepsilon_r - \varepsilon_a)k_o^2 C_g \exp[-\gamma(y - d)] \sum_{t=-\infty}^{\infty} \exp(jt\theta)\, J_t(k_\rho \rho) \cdot \iiint_{\text{resonator}} \exp(-jt\theta')\, H_t^{(2)}(k_\rho \rho') \exp[-\gamma(y' - d)] \cdot \psi_{hr}(\rho')\psi_{hr}(y')dV' \qquad \rho' > \rho \qquad (5.18b)$$

Initially, the use of the addition theorem (5.17) does not appear to give much advantage, for, although the integration is rather less complicated, there is now an infinite summation, and the integral equation has been split into two integral equations under different conditions. However, the volume integral is separable into three integrals over the radial, azimuthal and axial co-ordinates respectively, and it transpires that it is expedient to consider the azimuthal integral first.

It is seen from equations (5.18) that the integral involving θ' is common to both integral equations, and is given by

$$I_\theta = \int_o^{2\pi} \exp(-jt\theta')\, d\theta' \qquad (5.19)$$

This is a straightforward integral, and application of L'Hôpital's rule gives the result

$$I_\theta = \begin{cases} 2\pi & t = 0 \\ 0 & t \neq 0 \end{cases} \qquad (5.20)$$

which removes the infinite summation from equations (5.18).

The analytical evaluation of the radial and axial integrals is rather involved, and the procedure is shown in Appendix G. It is found that the two separate equations (5.18a and b) may be combined together, and the results of the independent radial and axial integrals are given by equations (G.14) and (G.19) respectively, and thus the magnetic scalar potential $\psi_{hr}(\underline{x})$ is

$$\psi_{hr}(\underline{x}) = (\varepsilon_r - \varepsilon_a)k_o^2 C_g \exp[-\gamma(y - d)].2\pi \left\{ \sum_{n=0}^{N} \frac{P_n}{\eta_n(\beta_n^2 - k_\rho^2)} \cdot \right.$$

$$\left. \left[j\frac{2}{\pi} J_o(\beta_n\rho) - (k_\rho R)J_o(\beta_n R)H_1^{(2)}(k_\rho R)J_o(k_\rho\rho) \right] \right\} \cdot$$

$$\sqrt{\frac{2}{h}} [1 - \exp(-\gamma h)] \left\{ \frac{A_o}{\sqrt{2}\gamma} + \sum_{m=1}^{M} \frac{[\gamma A_m + (\frac{2m\pi}{h}) B_m]}{[\gamma^2 + (\frac{2m\pi}{h})^2]} \right\} \quad (5.21)$$

5.4 Construction of the Iterative Expression

In order to solve the resonator problem using the iterative method, it is now necessary to re-express equation (5.21) in terms of the original trial function with new values for the original coefficients P_n, A_m and B_m.

Since the trial function was chosen to consist of series of functions that are orthogonal over the dimensions of the resonator, it is possible to construct the new functions in equation (5.21) out of the original functions by the method of Fourier series.

5.4.1 The radial sum

The radial sum in equation (5.21) is

$$S(\rho) = \sum_{n=0}^{N} \frac{P_n}{\eta_n(\beta_n^2 - k_\rho^2)} [\frac{j2}{\pi} J_o(\beta_n\rho) - (k_\rho R)J_o(\beta_n R) \cdot$$

$$H_1^{(2)}(k_\rho R)J_o(k_\rho\rho)] \quad (5.22)$$

from which it is seen that the difficulty in re-expressing $S(\rho)$ as a new set of $\psi_{hr}(\rho)$, given by equation (5.8), arises from the term $J_o(k_\rho\rho)$. However, since it is an even function, $J_o(k_\rho\rho)$ may be written as

$$J_o(k_\rho\rho) = c_o + \sum_{t=1}^{N} c_t J_o(\beta_t\rho) \quad (5.23)$$

In order to determine the values of the coefficients c_t, the orthogonality property of the series is utilised, so that

$$\int_o^R \rho J_o(k_\rho \rho) J_o(\beta_s \rho) d\rho = c_o \int_o^R \rho J_o(\beta_s \rho) d\rho + \sum_{t=1}^{N} c_t \int_o^R \rho J_o(\beta_t \rho) J_o(\beta_s \rho) d\rho \quad (5.24)$$

where s takes one of the values of $t > 0$.

Using the equations (G.3), (5.2), (5.6) and (5.7), equation (5.24) reduces to

$$c_s \frac{R^2}{2} [J_o(\beta_s R)]^2 = \int_o^R \rho J_o(k_\rho \rho) J_o(\beta_s \rho) \, d\rho \quad (5.25)$$

and evaluation of this integral using equation (5.3) gives

$$c_s = \frac{2k_\rho J_1(k_\rho R)}{[k_\rho^2 - \beta_s^2].R.J_o(\beta_s R)} \quad (5.26)$$

A similar procedure used to evaluate c_o leads to the fact that

$$c_o = \frac{2J_1(k_\rho R)}{(k_\rho R)} \quad (5.27)$$

which is seen to be given by equation (5.26) if $\beta_s = 0$, and thus equation (5.23) becomes

$$J_o(k_\rho \rho) = \sum_{t=0}^{N} \frac{\sqrt{2}\, k_\rho J_1(k_\rho R)}{\eta_t (k_\rho^2 - \beta_t^2)} J_o(\beta_t \rho) \quad (5.28)$$

Substitution of equation (5.28) into equation (5.22) leads to

$$S(\rho) = \sum_{n=0}^{N} \frac{P_n}{\eta_n(\beta_n^2 - k_\rho^2)} \left[\frac{j2}{\pi} J_o(\beta_n \rho) + \sqrt{2}\, (k_\rho^2 R) J_o(\beta_n R) J_1(k_\rho R) H_1^{(2)}(k_\rho R) \sum_{t=0}^{N} \frac{J_o(\beta_t \rho)}{\eta_t(\beta_t^2 - k_\rho^2)} \right] \quad (5.29)$$

Examination of equation (5.29) shows that the radial sum, $S(\rho)$, may be rewritten in the same form as the initial radial trial function $\psi_{hr}(\rho)$, given by equation (5.7), if the terms containing $(\beta_n\rho)$ and $(\beta_t\rho)$ can be added together when the indices are equal. Expanding equation (5.29) gives

$$S(\rho) = \frac{j2}{\pi} \sum_{n=0}^{N} \frac{P_n J_o(\beta_n\rho)}{\eta_n(\beta_n^2 - k_\rho^2)} + 2k_\rho^2 J_1(k_\rho R)H_1^{(2)}(k_\rho R) \cdot \sum_{n=0}^{N} \frac{P_n}{(\beta_n^2 - k_\rho^2)} \sum_{t=0}^{N} \frac{J_o(\beta_t\rho)}{\eta_t(\beta_t^2 - k_\rho^2)} \tag{5.30}$$

and it is evident that the two summations in the second term are independent, and thus equation (5.30) is equivalent to

$$S(\rho) = \sum_{n=0}^{N} \frac{Q_n J_o(\beta_n\rho)}{\eta_n} \tag{5.31}$$

where the new coefficients, Q_n, are given by

$$Q_n = \frac{1}{(\beta_n^2 - k_\rho^2)} \left\{ \frac{j2P_n}{\pi} + 2k_\rho^2 J_1(k_\rho R)H_1^{(2)}(k_\rho R) \sum_{t=0}^{N} \frac{P_t}{(\beta_t^2 - k_\rho^2)} \right\} \tag{5.32}$$

5.4.2 The axial sum

It is seen from equation (5.21) that the result of the integral over the axial source space is invariant with the value of y. Therefore, in order to express the result of the volume integration in terms of the original trial function, it is necessary to expand the exponential for the source co-ordinates in terms of the orthogonal basis functions, so that

$$\exp[-\gamma(y - d)] = a_o + \sum_{s=1}^{M} \left\{ a_s \cos\left[\frac{2s\pi}{h}(y - d)\right] + b_s \sin\left[\frac{2s\pi}{h}(y - d)\right] \right\} \tag{5.33}$$

The procedure for evaluating the coefficients is a straightforward use of the orthogonality properties, and leads to the result

$$\exp[-\gamma(y - d)] = [1 - \exp(-\gamma h)] \left\{ \frac{1}{h\gamma} + \frac{2}{h} \sum_{s=1}^{M} \frac{\left[\gamma \cos[\frac{2s\pi}{h}(y - d)] + (\frac{2s\pi}{h}) \sin [\frac{2s\pi}{h}(y - d)]\right]}{[\gamma^2 + (\frac{2s\pi}{h})^2]} \right\} \tag{5.34}$$

and, consequently, the longitudinal sum, S(y), in equation (5.21) is

$$S(y) = [1 - \exp(-\gamma h)]^2 \sqrt{\frac{2}{h}} \left\{ \frac{A_o}{\sqrt{2}\gamma} + \sum_{m=1}^{M} \frac{(\gamma A_m + (\frac{2m\pi}{h})B_m)}{[\gamma^2 + (\frac{2m\pi}{h})^2]} \right\} \cdot \left\{ \frac{1}{h\gamma} + \frac{2}{h} \sum_{s=1}^{M} \frac{\gamma \cos [\frac{2s\pi}{h}(y - d)] + (\frac{2s\pi}{h}) \sin [\frac{2s\pi}{h}(y - d)]}{[\gamma^2 + (\frac{2s\pi}{h})^2]} \right\} \tag{5.35}$$

Once again, the two summations are independent, and so the longitudinal sum becomes

$$S(y) = \frac{\alpha_o}{\sqrt{h}} + \sqrt{\frac{2}{h}} \sum_{m=1}^{M} \left\{ \alpha_m \cos [\frac{2m\pi}{h}(y - d)] + \beta_m \sin [\frac{2m\pi}{h}(y - d)] \right\} \tag{5.36}$$

where

$$\alpha_o = \frac{\sqrt{2}}{\gamma h} [1 - \exp(-\gamma h)]^2 \sigma_s \tag{5.37a}$$

$$\alpha_m = \frac{2\gamma}{h[\gamma^2 + (\frac{2m\pi}{h})^2]} [1 - \exp(-\gamma h)]^2 \sigma_s \qquad m > 0 \tag{5.37b}$$

and

$$\beta_m = \frac{2(\frac{2m\pi}{h})}{h[\gamma^2 + (\frac{2m\pi}{h})^2]} [1 - \exp(-\gamma h)]^2 \sigma_s \qquad m > 0 \qquad (5.38)$$

where

$$\sigma_s = \frac{A_o}{\sqrt{2}\gamma} + \sum_{s=1}^{M} \frac{[\gamma A_s + (\frac{2s\pi}{h})B_s]}{[\gamma^2 + (\frac{2s\pi}{h})^2]} \qquad (5.39)$$

5.5 Calculation of the Resonant Frequency

The analytical evaluation of the integral equation (5.1) presented in the previous sections, has led to the following expression for the magnetic potential,

$$\psi_{hr}(\underline{x}) = 2\pi C_g(\varepsilon_r - \varepsilon_a)k_o^2 \sum_{n=0}^{N} \frac{Q_n J_o(\beta_n \rho)}{\eta_n} \cdot$$

$$\left\{ \frac{\alpha_o}{\sqrt{h}} + \sqrt{\frac{2}{h}} \sum_{m=1}^{M} \left[\alpha_m \cos[\frac{2m\pi}{h}(y - d)] + \beta_m \sin[\frac{2m\pi}{h}(y - d)] \right] \right\} \qquad (5.40)$$

where the new coefficients Q, α, and β are calculated from the previous $_{co}$(5.37) and (5.38) respectively, and C_g is defined in equation (5.15). ($_5$Ignoring, for a moment, the scale factor $2\pi C_g(\varepsilon_r - \varepsilon_a)k_o^2$, it is apparent

Ignoring, for a moment, the scale factor $2\pi C_g(\varepsilon_r - \varepsilon_a)k_o^2$, it is apparent
from a comparison of equations (5.40) and (5.10) that this new trial function has been obtained in identical form to the original trial function, but with new coefficients, which may be calculated from the simple, linear, numerical relationships of equations (5.32), (5.37) and (5.38). Therefore, it is seen that an iterative relationship has been formed which is ideally suited to numerical solution on a computer.

The method of numerical solution is as follows. Starting with the coefficients P, A, B initialised to unity, successive iteration of the equations (5.32), (5.37) and (5.38) is continued until two consecutive trial functions are found to have a direct linear relationship. For this to be the case, it is evident that both the consecutive radial expansions and the consecutive axial expansions, must each have direct linear relationships, and thus, for all n and m, the successive coefficients must satisfy the equations

$$X_\rho = \frac{Q_n}{P_n} \tag{5.41a}$$

$$X_y = \frac{\alpha_o}{A_o} = \frac{\alpha_m}{A_m} = \frac{\beta_m}{B_m} \tag{5.41b}$$

where X_ρ and X_y are constant values, and so equation (5.40) may be rewritten as

$$\psi_{hr}(\underline{x}) = 2\pi C_g(\varepsilon_r - \varepsilon_a)k_o^2 X_\rho X_y \sum_{n=0}^{N} \frac{P_n J_o(\beta_n \rho)}{\eta_n} \cdot \left\{ \frac{A_o}{\sqrt{h}} + \sqrt{\frac{2}{h}} \sum_{m=1}^{M} \left[A_m \cos\left[\frac{2m\pi}{h}(y - d)\right] + B_m \sin\left[\frac{2m\pi}{h}(y - d)\right] \right] \right\} \tag{5.42}$$

Comparison with equation (5.10) shows that this new trial function is simply a scaled version of the previous trial function, and consideration of equation (5.1), which may be rewritten as

$$\psi_{hr} = \hat{G}.\psi_{hr} \tag{5.43a}$$

where the operator $\hat{G}$ is defined as

$$\hat{G}.f = (\varepsilon_r - \varepsilon_a)k_o^2 \iiint_{\text{resonator}} dV' \; G_a(\underline{x},\underline{x}')f(\underline{x}') \tag{5.43b}$$

for any function, f, shows that the eigenvalue of the integral equation is determined by that value of k_o which sets the scale factor $2\pi C_g(\varepsilon_r - \varepsilon_a)k_o^2 X_\rho X_y$ to unity. Thus, according to the theory given in chapter 4, the iterative method yields the fundamental resonant frequency f_{res}, which is given by the relationship

$$f_{res} = \frac{c}{2\pi}\left[2\pi(\varepsilon_r - \varepsilon_a)C_g X_\rho X_y\right]^{-\frac{1}{2}} \qquad (5.44)$$

where c is the speed of light in vacuo.

In chapter 4, it was mentioned that the eigenvalues of an integral equation are generally complex, and examination of equations (5.15) and (5.32) shows that C_g is imaginary, and that P_n and Q_n must both be complex, and consequently the linear multiplier X_ρ must also be a complex quantity. It is therefore found that the resonant frequency is complex. Considering now the suppressed time dependence, $\exp(j\omega t)$, it is seen that writing the resonant frequency in terms of the complex angular frequency, $\omega_{re} + j\omega_{im}$, leads to the time dependence

$$\psi_{hr}(t) = e^{j\omega_{re}t} \cdot e^{-\omega_{im}t} \qquad (5.45)$$

and it is clear that the real part of the resonant frequency represents the energy stored, while the imaginary part shows that the energy is not stored indefinitely, but dies away exponentially with time.

It is thus seen that the iterative technique described in this chapter produces a value for the fundamental resonant frequency that is in accord both with the mathematical principles, as outlined in chapter 4, and also with the physical behaviour of a dielectric pillbox resonator. However, it is seen from a consideration of the Green's function, $G_a(\underline{x},\underline{x}')$, that the wavenumbers k_y and γ, which are used in the determination of the resonant frequency, are initially obtained

through the choice of an excitation frequency for the dielectric slab waveguide. These values then provide a solution for the fundamental resonant frequency, which is generally found to be different from the slab excitation frequency.

However, the integral equation (5.1) was constructed from the equations (3.39) and (3.40b), namely

$$(\nabla^2 + \varepsilon_a k_o^2)\, \psi_{hr}(\underline{x}) = -(\varepsilon_r - \varepsilon_a) k_o^2\, \psi_{hr}(\underline{x}) \qquad (5.46)$$

$$(\nabla^2 + \varepsilon_a k_o^2)\, G_a(\underline{x},\underline{x}') = -\delta(\underline{x} - \underline{x}') \qquad (5.47)$$

and this clearly shows that the self-consistent solution for the fundamental resonant frequency can only be obtained when the Green's function satisfies equation (5.47) at the resonant frequency. Hence, the true fundamental resonant frequency is provided by the iterative method when the choice of excitation frequency for the dielectric slab leads to an identical value for the resonant frequency.

In order to solve for this fundamental resonant frequency, a FORTRAN program, based upon this iterative technique, was written to run on a PRIME 9950 mainframe computer, and a flowchart of the program operation is given in Figure 5.2. The recursive nature of the program, used to find the desired consistency between the dielectric slab excitation frequency, f_s, and the fundamental resonant frequency, f_{res}, is clearly seen in the flowchart. Furthermore, it is clearly apparent from Figure 5.2, together with consideration of equations (5.32), (5.37) and (5.38), that, although the analytical evaluation of the volume integral, and subsequent expression of the result back in terms of the original trial function, was found to be rather arduous, the final iterative relationships, and the consequent computer program, are extremely simple, and more than compensate for the laborious analysis.

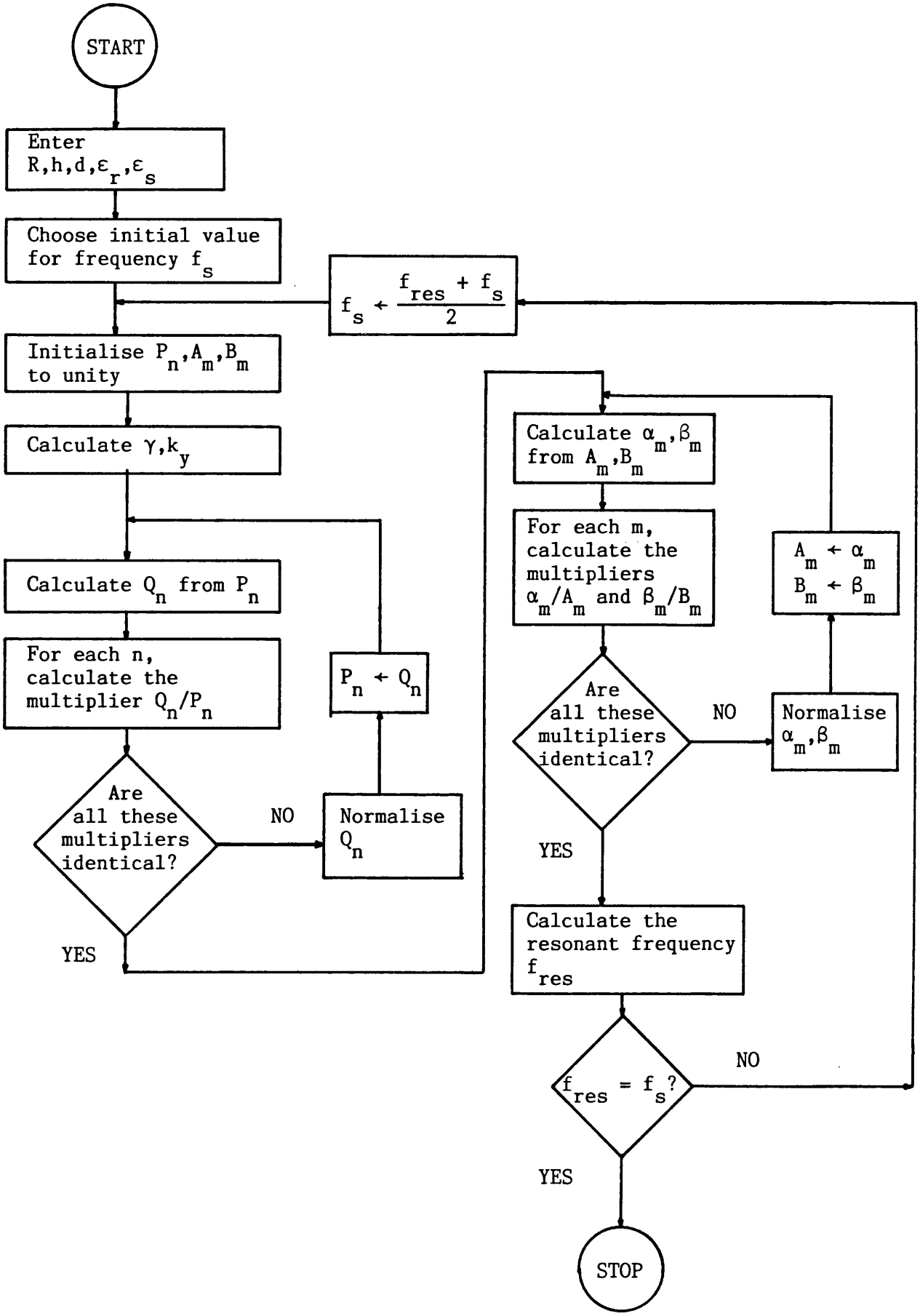

Figure 5.2 Flowchart of the procedure used to calculate the fundamental resonant frequency using the iterative technique

REFERENCES

[1] I.S. Gradshteyn and I.M. Rhyzik, "*Tables of Integrals, Series and Products*". New York: Academic Press, 1965, p.634.

[2] R.F. Harrington, "*Time-Harmonic Electromagnetic Fields*". New York: McGraw-Hill, 1961, p.232.

CHAPTER 6

EVALUATION OF THE ACCURACY OF THE ITERATIVE SOLUTION

In the preceding sections, an iterative technique for calculating the fundamental resonant frequency of the substrate-mounted cylindrical dielectric resonator has been presented, and it is now necessary to analyse the accuracy of this solution. In order to provide a complete evaluation of the iterative technique, it is desirable to compare the theoretical results both with experimental values and also with results produced by an alternative theoretical model.

This chapter briefly describes the work undertaken to obtain some alternative results, based on a previous theoretical model developed by Itoh and Rudokas [1], which are then used to verify that the iterative solution does give results for the fundamental mode. This is followed by a description of the experimental technique employed in order to measure the $TE_{01\delta}$ resonant frequency of cylindrical dielectric resonators, and the chapter concludes with a detailed analysis of the accuracy of the results given by both the iterative solution and the Itoh model.

6.1 The Itoh Approach

Although much attention has been given to the theoretical modelling of the cylindrical pillbox dielectric resonator, the most general case of the substrate-mounted open dielectric resonator has largely been ignored. Until now, only two previous research groups [1,2] have considered the $TE_{01\delta}$ resonance in this situation, and in fact, only Gelin et al. [2] actually presented any theoretical results for the fundamental resonant frequency of this particular type of resonator.

The method developed by this French research team started from the analysis of an abruptly ended dielectric rod, and continued by considering the cylindrical resonator as a length of dielectric rod waveguide sandwiched between two such abrupt interfaces. This procedure led to two coupled integral equations, which, in simplified form, were solved numerically. Although this solution technique proved very costly in terms of computer time, two sets of theoretical results were presented for the substrate-mounted cylindrical resonator and were shown to be in good agreement with experimental values.

The other previous analysis of the substrate-mounted resonator was developed by Itoh and Rudokas [1] in 1977, and was much simpler in concept than the above analysis. The method was based upon the technique, devised by Marcatili [3], for analysing the propagation characteristics of rectangular dielectric waveguide, which was now extended to apply to three-dimensional cylindrical structures. It was argued that certain regions exterior to the dielectric resonator contained little electromagnetic energy, and could therefore be ignored without significantly affecting the computed results. This assumption meant that it was possible to match the electromagnetic fields on the surface of the resonator alone, leading to two coupled eigenvalue equations, which could then be solved to give the resonant frequency.

The nature of this technique necessarily gave rise to approximate solutions, and, as it was constructed in terms of independent TE and TM modes, could only be used in the case of the θ-independent modes. In practice, the two coupled eigenvalue equations turned out to be very complicated, and Itoh and Rudokas only attempted to solve them in the much simplified case of the fundamental mode of the isolated cylindrical pillbox dielectric resonator.

Consequently, in order to provide some theoretical results as a check for the accuracy of the iterative method described in this thesis, it was decided to develop a technique for solving the coupled eigenvalue equations that are generated by Itoh's method for the substrate-mounted dielectric resonator. In chapter 3, it was shown that the integral equation for the $TM_{01\delta}$ mode differed from that of the $TE_{01\delta}$ mode by virtue of a surface integral, which could be ignored in the latter case, but not for the former resonant mode. Therefore, it was decided to solve Itoh's coupled eigenvalue equations for both transverse polarisations, in order to give clear confirmation that the iterative solution gives results for the $TE_{01\delta}$ mode, and not for the $TM_{01\delta}$ mode.

6.1.1 Derivation of the coupled eigenvalue equations according to Itoh's method

A cross-sectional representation of the substrate-mounted dielectric resonator is shown in Figure 6.1, and the numbered regions 1 to 4 are assumed to contain virtually all of the electromagnetic energy. The transverse resonant modes with no azimuthal variation are each seen, from equations (3.34), to consist of three field components, and Itoh's approach matches these components on the resonator boundaries, ignoring regions 5 and 6 (so that no continuity between regions external to the resonator needs to be considered), resulting in a pair of coupled eigenvalue equations.

The Transverse Electric Mode

Consideration of the physical structure of the resonator shown in Figure 6.1 means that judicious choices for the magnetic potential function in each of the four numbered spatial regions are given by,

$$\psi_{h1} = \frac{j\omega\mu_o}{\beta^2} A_1 \sin [k_y(y - y_o)] J_o(\beta\rho) \qquad (6.1a)$$

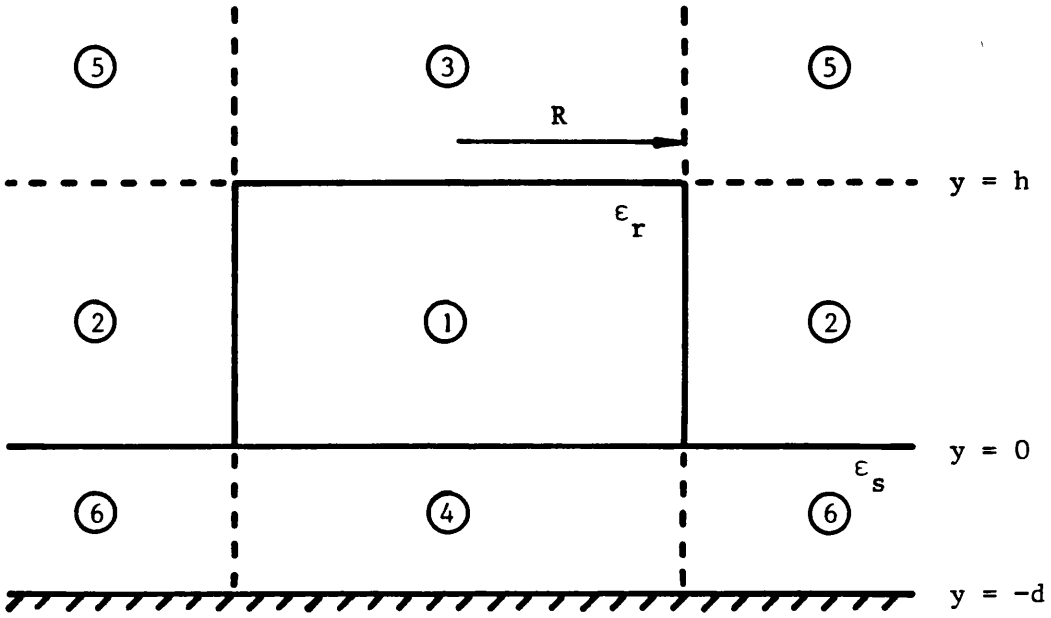

Figure 6.1 Cross-sectional view of the substrate-mounted cylindrical dielectric resonator

$$\psi_{h2} = \frac{j\omega\mu_o}{-k_\rho^2} A_2 \sin [k_y(y - y_o)] K_o(k_\rho\rho) \qquad (6.1b)$$

$$\psi_{h3} = \frac{j\omega\mu_o}{\beta^2} A_3 \exp [-\gamma(y - h)] J_o(\beta\rho) \qquad (6.1c)$$

$$\psi_{h4} = \frac{j\omega\mu_o}{\beta^2} A_4 \sinh [\xi(y + d)] J_o(\beta\rho) \qquad (6.1d)$$

where β and k_ρ are radial wavenumbers, k_y, γ, and ξ are axial wavenumbers, y_o and the coefficients, A, are arbitrary constants, and J_o and K_o are the Bessel function and modified Hankel function, of order zero, respectively.

Applying the relevant boundary conditions gives rise to three eigenvalue equations linking the wavenumbers,

$$\frac{J_o'(\beta R)}{\beta J_o(\beta R)} = - \frac{K_o'(k_\rho R)}{k_\rho K_o(k_\rho R)} \qquad (6.2a)$$

$$k_y \cot (- k_y y_o) = \xi \coth (\xi d) \qquad (6.2b)$$

$$k_y \cot [k_y(h - y_o)] = - \gamma \qquad (6.2c)$$

where the prime denotes differentiation with respect to the argument, and

$$(\varepsilon_r - 1)k_o^2 = \beta^2 + k_\rho^2 \qquad (6.2d)$$

$$\varepsilon_r k_o^2 = \beta^2 + k_y^2 \qquad (6.2e)$$

$$\varepsilon_s k_o^2 = \beta^2 - \xi^2 \qquad (6.2f)$$

$$k_o^2 = \beta^2 - \gamma^2 \qquad (6.2g)$$

and k_y, ξ and γ are positive. Consequently, it is found from equation (6.2b) that $k_y y_o$ must be greater than $\pi/2$ radians, allowing $k_y y_o$ to be replaced by

$$k_y y_o = \frac{\pi}{2} + k_y z_o \qquad (6.3)$$

where z_o is a positive constant yet to be determined, and so equation (6.2b) becomes

$$k_y \tan (k_y z_o) = \xi \coth (\xi d) \qquad (6.4)$$

and elimination of y_o from equation (6.2c) using equations (6.3) and (6.4) yields the general solution,

$$(k_y.h) = \tan^{-1} (\frac{\gamma}{k_y}) + \tan^{-1} [\frac{\xi}{k_y} \coth (\xi d)] + m\pi \qquad (6.5)$$

where m is an integer.

The coupled equations (6.2a) and (6.5), together with the wavenumber relations (6.2d-g), are general equations for any transverse electric mode with no azimuthal variation. Therefore, it is necessary to determine the relations for the fundamental $TE_{01\delta}$ mode, which must have the smallest values possible for both of the wavenumbers β and k_y. Thus, in the axial direction, it is apparent from equation (6.5) that the index m must be zero. In the radial direction, equation (6.2a) has a finite number of roots for any particular value of the free-space wavenumber, k_o, and the lowest root is required for the fundamental resonant mode.

The $TE_{01\delta}$ resonant frequency is therefore found by solving the eigenvalue equations

$$\frac{J_o'(\beta R)}{\beta J_o(\beta R)} = -\frac{K_o'(k_\rho R)}{k_\rho K_o(k_\rho R)} \qquad (6.6a)$$

and

$$(k_y h) = \tan^{-1}\left(\frac{\gamma}{k_y}\right) + \tan^{-1}\left[\frac{\xi}{k_y}\coth(\xi d)\right] \qquad (6.6b)$$

where the wavenumbers are linked by the relations

$$(\varepsilon_r - 1)k_o^2 = \beta^2 + k_\rho^2 \qquad (6.6c)$$

$$\beta^2 = \varepsilon_r k_o^2 - k_y^2 = \varepsilon_s k_o^2 + \xi^2 = k_o^2 + \gamma^2 \qquad (6.6d)$$

The Transverse Magnetic Mode

The coupled eigenvalue equations for the $TM_{01\delta}$ resonant mode may be found by choosing the electric scalar potential in each of the four numbered regions of Figure 6.1 to be

$$\psi_{e1} = \frac{j\omega\varepsilon_o\varepsilon_r}{\beta^2} A_1 \sin[k_y(y - y_o)]\, J_o(\beta\rho) \qquad (6.7a)$$

$$\psi_{e2} = \frac{j\omega\varepsilon_o}{-k_\rho^2} A_2 \sin[k_y(y - y_o)]\, K_o(k_\rho\rho) \qquad (6.7b)$$

$$\psi_{e3} = \frac{j\omega\varepsilon_o}{\beta^2} A_3 \exp[-\gamma(y - h)]\, J_o(\beta\rho) \qquad (6.7c)$$

$$\psi_{e4} = \frac{j\omega\varepsilon_o\varepsilon_s}{\beta^2} A_4 \cosh[\xi(y + d)]\, J_o(\beta\rho) \qquad (6.7d)$$

where the same terminology is used as in the transverse electric case. Elimination of the arbitrary constants through the use of the boundary conditions on the surface of the resonator gives the following coupled eigenvalue equations for the $TM_{01\delta}$ mode,

$$\frac{\varepsilon_r J_o'(\beta R)}{\beta J_o(\beta R)} = -\frac{K_o'(k_\rho R)}{k_\rho K_o(k_\rho R)} \qquad (6.8a)$$

and

$$(k_y h) = \tan^{-1}\left(\frac{\varepsilon_r \gamma}{k_y}\right) + \tan^{-1}\left[\frac{\varepsilon_r}{\varepsilon_s} \cdot \frac{\xi}{k_y} \tanh(\xi d)\right] \qquad (6.8b)$$

where

$$(\varepsilon_r - 1)k_o^2 = \beta^2 + k_\rho^2 \qquad (6.8c)$$

$$\beta^2 = \varepsilon_r k_o^2 - k_y^2 = \varepsilon_s k_o^2 + \xi^2 = k_o^2 + \gamma^2 \qquad (6.8d)$$

6.1.2 Solution of the coupled eigenvalue equations

The process used to solve the coupled eigenvalue equations is substantially the same for both the $TE_{01\delta}$ and $TM_{01\delta}$ modes, and will therefore only be described for the transverse electric case. The analytical solution of the coupled equations (6.6) is very complex due to the transcendental nature of the functions, and it is therefore constructive to consider the nature of the problem using a graphical technique.

It is advantageous to rewrite equations (6.6) such that

$$\alpha = \frac{-J_o'(u)}{uJ_o(u)} \qquad (6.9a)$$

$$\alpha = \frac{K_o'(v)}{vK_o(v)} \qquad (6.9b)$$

$$(\varepsilon_r - 1)(k_o R)^2 = u^2 + v^2 \qquad (6.9c)$$

$$k_y h = \tan^{-1}\left(\frac{\gamma}{k_y}\right) + \tan^{-1}\left[\frac{\xi}{k_y} \coth(\xi d)\right] \qquad (6.10a)$$

$$\beta^2 = \varepsilon_r k_o^2 - k_y^2 = \varepsilon_s k_o^2 + \xi^2 = k_o^2 + \gamma^2 \qquad (6.10b)$$

where βR and $k_\rho R$ have been replaced by the new variables u and v respectively, and α is any arbitrary value. The equations (6.9a) and (6.9b) are shown graphically in Figures 6.2 and 6.3, and it is

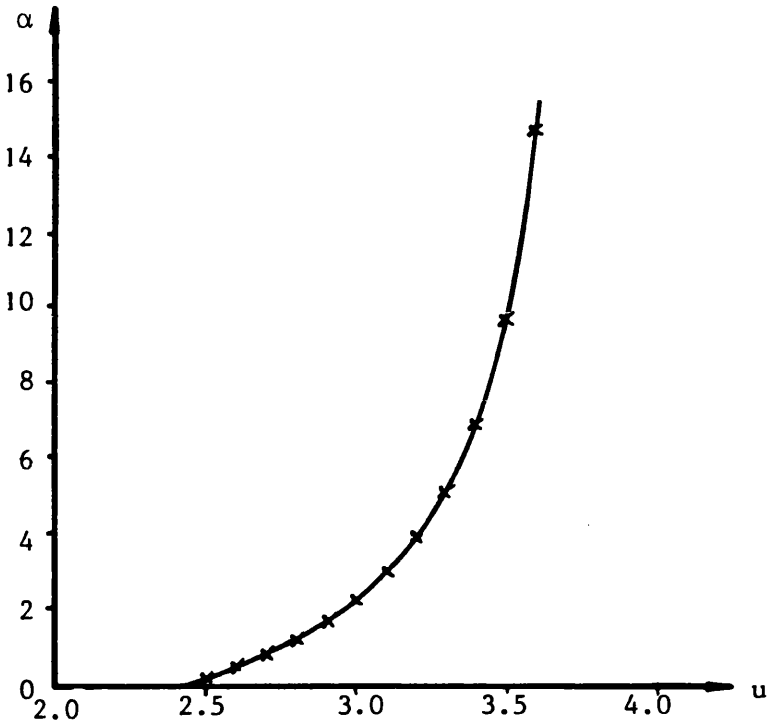

Figure 6.2 Graph of the equation $\alpha = \frac{-J_o'(u)}{uJ_o(u)}$

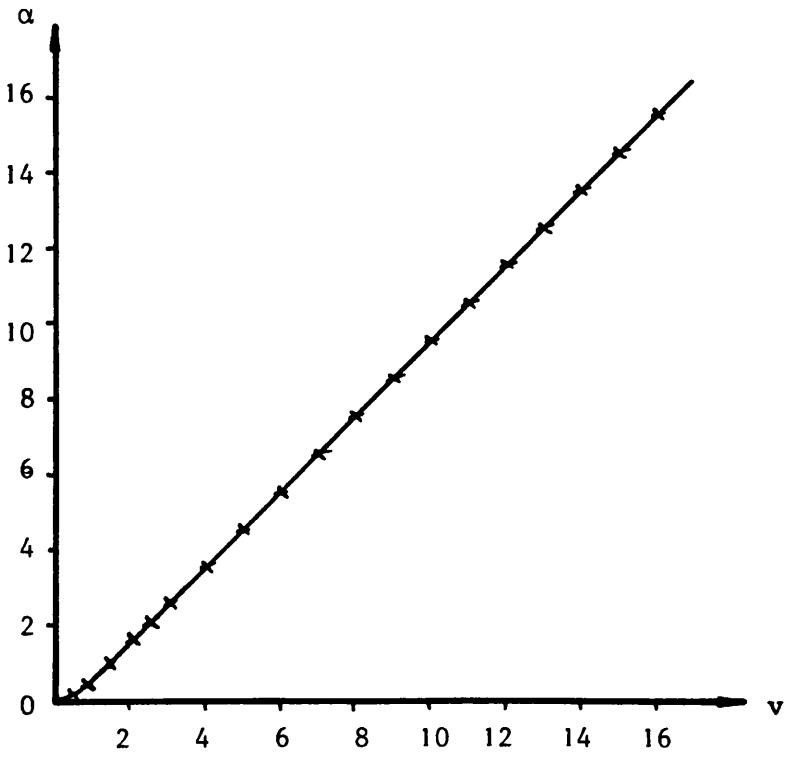

Figure 6.3 Graph of the equation $\alpha = \frac{K_o'(v)}{vK_o(v)}$

immediately apparent that for each value of α there is only one pair of values of u and v. Furthermore, use of equation (6.9c) to calculate values of the free-space wavenumber, k_o, shows that the value of k_o increases monotonically with increasing α, as illustrated by Figure 6.4. Thus, the fundamental $TE_{01\delta}$ resonant frequency may be calculated by finding the lowest value of α that satisfies the equations (6.9) and (6.10).

Examination of the gradients of the two curves in Figures 6.2 and 6.4, together with equation (6.10b), shows that if a value of α is considered where k_o is set to be less than its value at resonance, then both β and k_y must also be less than their resonance values. Moreover, both ξ and γ must be greater than at resonance, and hence it is found that $k_y h$ is less than the right hand side of equation (6.10a). Conversely, if k_o is greater than at resonance, then β and k_y must be greater, and ξ and γ less, than their resonance values, which leads to $k_y h$ being greater than the trigonometric sum of equation (6.10a).

Consequently, the procedure summarised in the flowchart shown in Figure 6.5 was used to write a computer program to solve for the $TE_{01\delta}$ resonant frequency. A similar procedure was implemented to determine the $TM_{01\delta}$ resonant frequency, but with a separate routine for calculating the wavenumbers from the variable α, and also for calculating the variable T, due to the inclusion of the relative permittivities, as shown in equations (6.8).

In order to substantiate the above method for solving the coupled eigenvalue equations, the isolated cylindrical dielectric resonator was analysed for two values of relative permittivity, and the results are given in Figures 6.6 and 6.7. The curves obtained for the $TE_{01\delta}$ mode are in exact agreement with those given by Itoh and Rudokas, and

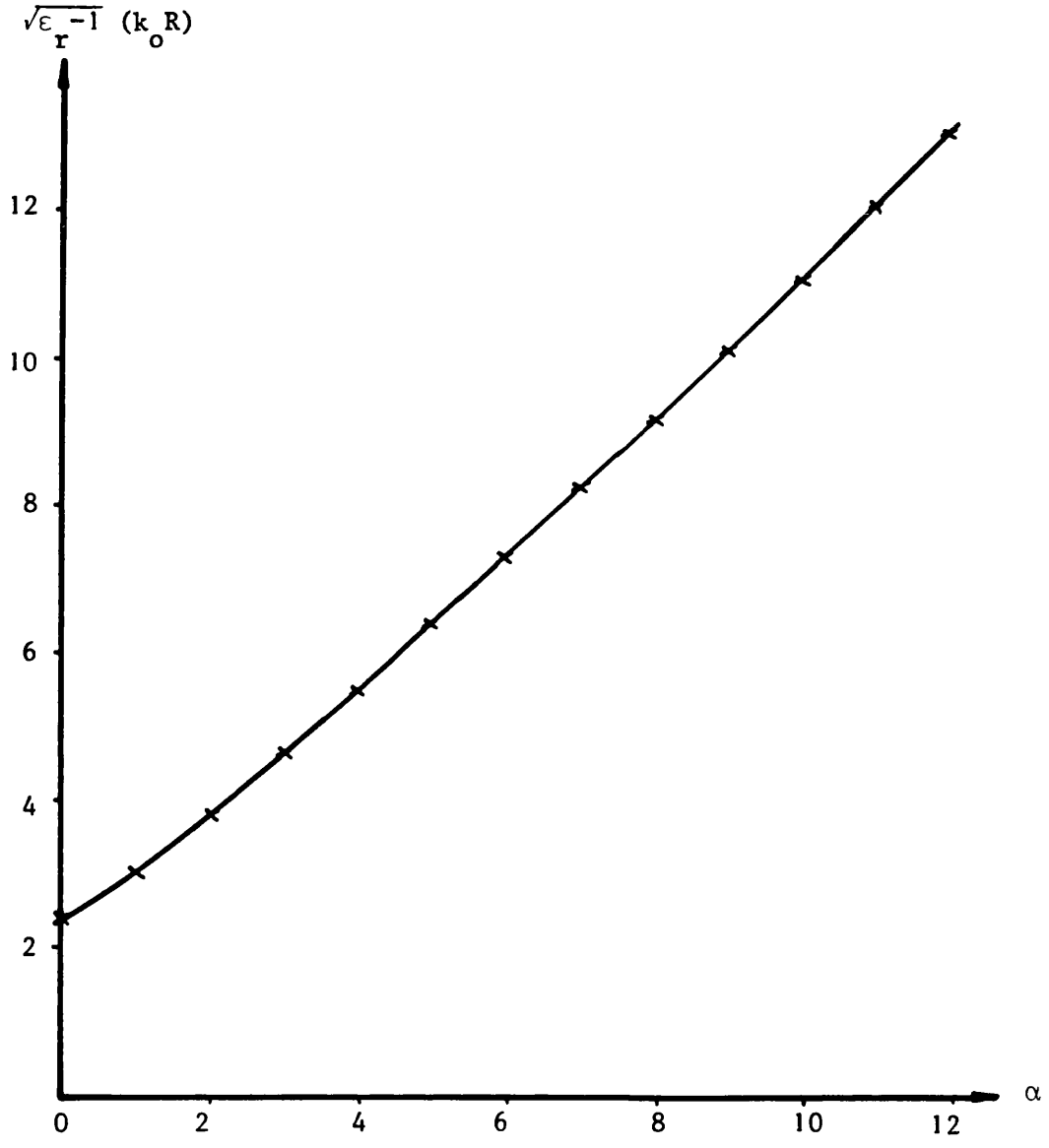

Figure 6.4 Graph showing monotonic relationship between α and k_o

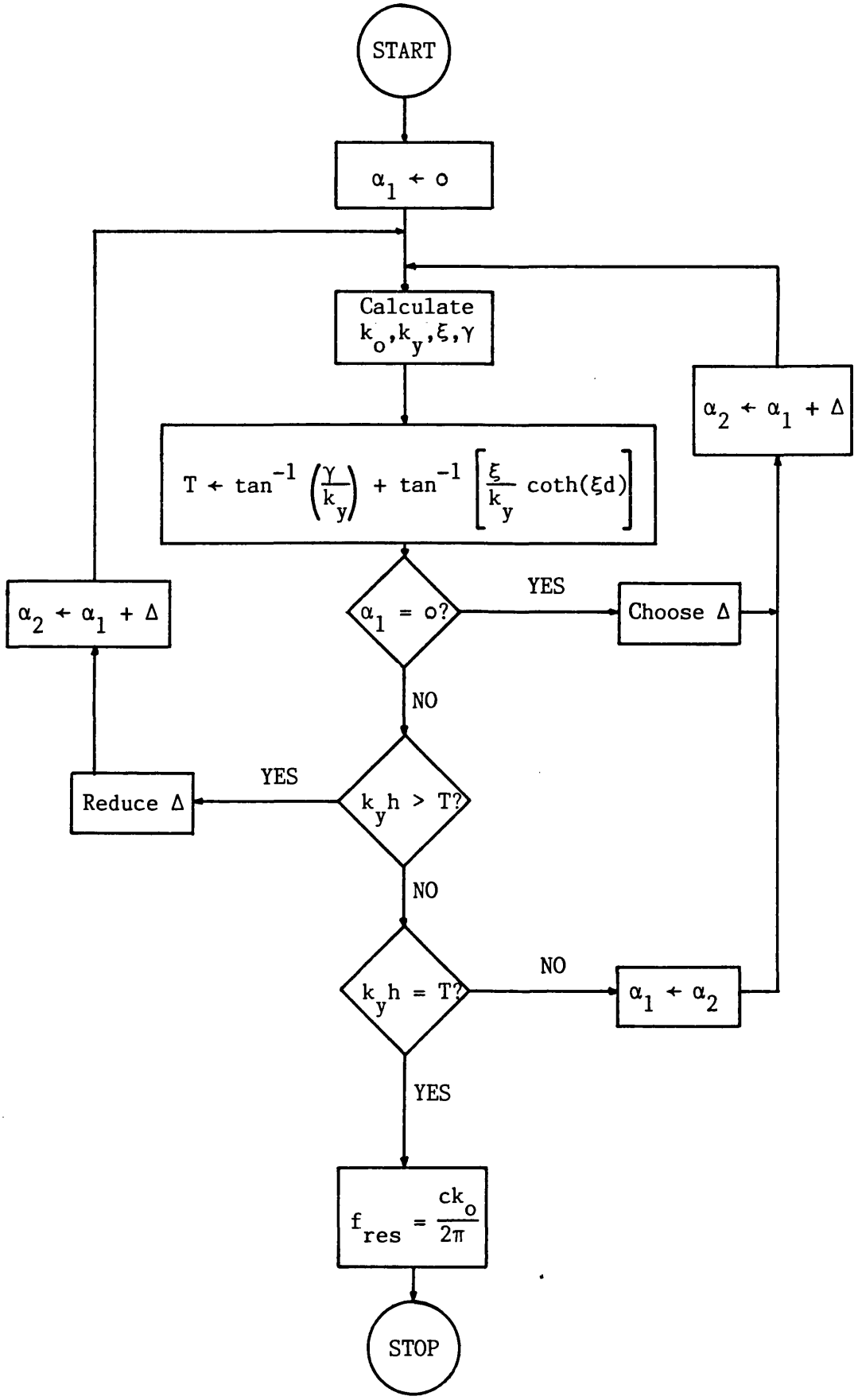

Figure 6.5 Flowchart of the procedure used to calculate the $TE_{01\delta}$ resonant frequency using the Itoh approach

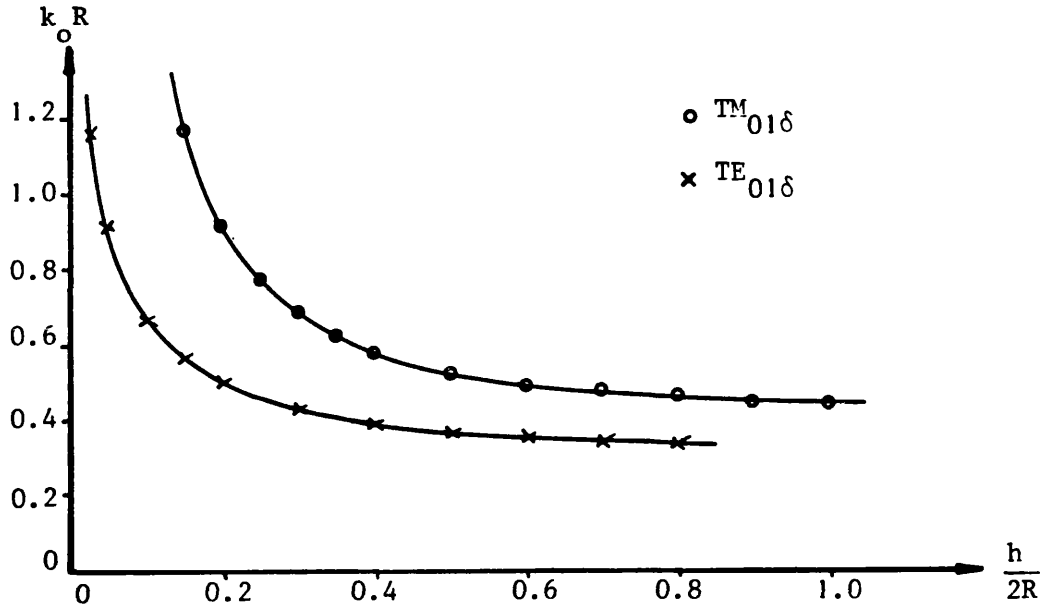

Figure 6.6 $TE_{01\delta}$ and $TM_{01\delta}$ resonant frequencies for an isolated cylindrical resonator, ε_r = 88, obtained using Itoh's models

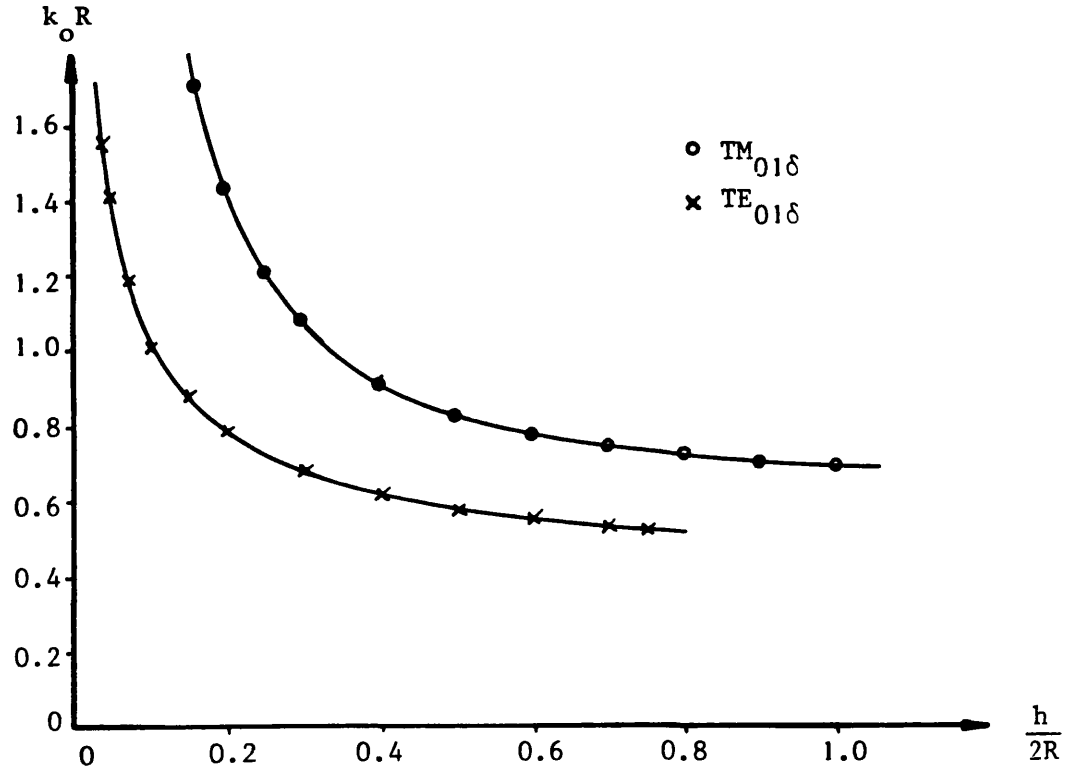

Figure 6.7 $TE_{01\delta}$ and $TM_{01\delta}$ resonant frequencies for an isolated cylindrical resonator, ε_r = 35, obtained using Itoh's models

it is seen that the $TM_{01\delta}$ mode resonates at a higher frequency than the fundamental $TE_{01\delta}$ mode under all conditions, which is the expected result. Therefore, it is seen that the procedure of Figure 6.5 does lead to the correct solution for the coupled eigenvalue equations for the fundamental resonance, and may therefore be used as a comparison for the results obtained from the iterative approach detailed in this thesis.

6.2 Comparison of the Theoretical Results

In the formulation of section 3.3 for the iterative approach, only the resonant modes with no azimuthal field variation can be analysed, and thus the results obtained must belong to one of the independent transverse electric or magnetic modes. Furthermore, it was shown that the integral equation (3.46) is approximately correct for the TE_{omn} modes, whereas the TM_{omn} modes require the full integral equation (3.45) to be solved. Consequently, it is expected that the computer program based on the iterative technique, and summarised in Figure 5.2, should give results for a transverse electric mode, and, due to the nature of the method, it should converge to the solution for the fundamental $TE_{01\delta}$ mode.

Comparisons between the three theoretical models described in this thesis are shown in the graphs of Figures 6.8 and 6.9, where results for the resonant frequencies of two cylindrical dielectric resonators of different dimensions are presented for a wide range of relative permittivities. It is evident from these graphs that the iterative solution is that of the $TE_{01\delta}$ mode, and further confirmation of this is provided by investigating the behaviour of the resonance in the neighbourhood of a metal wall. Yee [4] observed that the resonant frequency of a resonator excited in a transverse electric mode increases

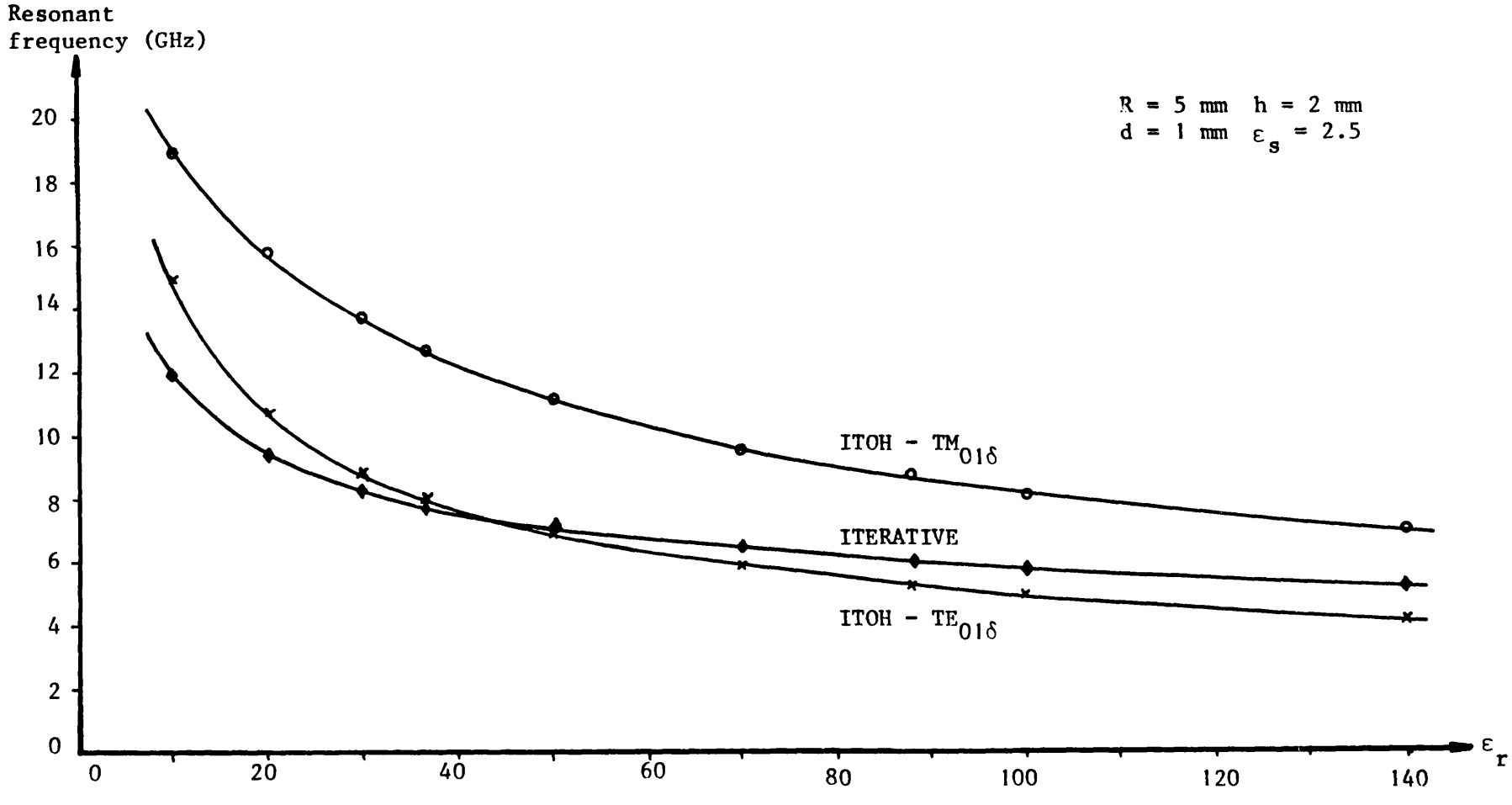

Figure 6.8 Graph comparing the resonant frequency obtained using the iterative method with those results determined from Itoh's $TE_{01\delta}$ and $TM_{01\delta}$ models.

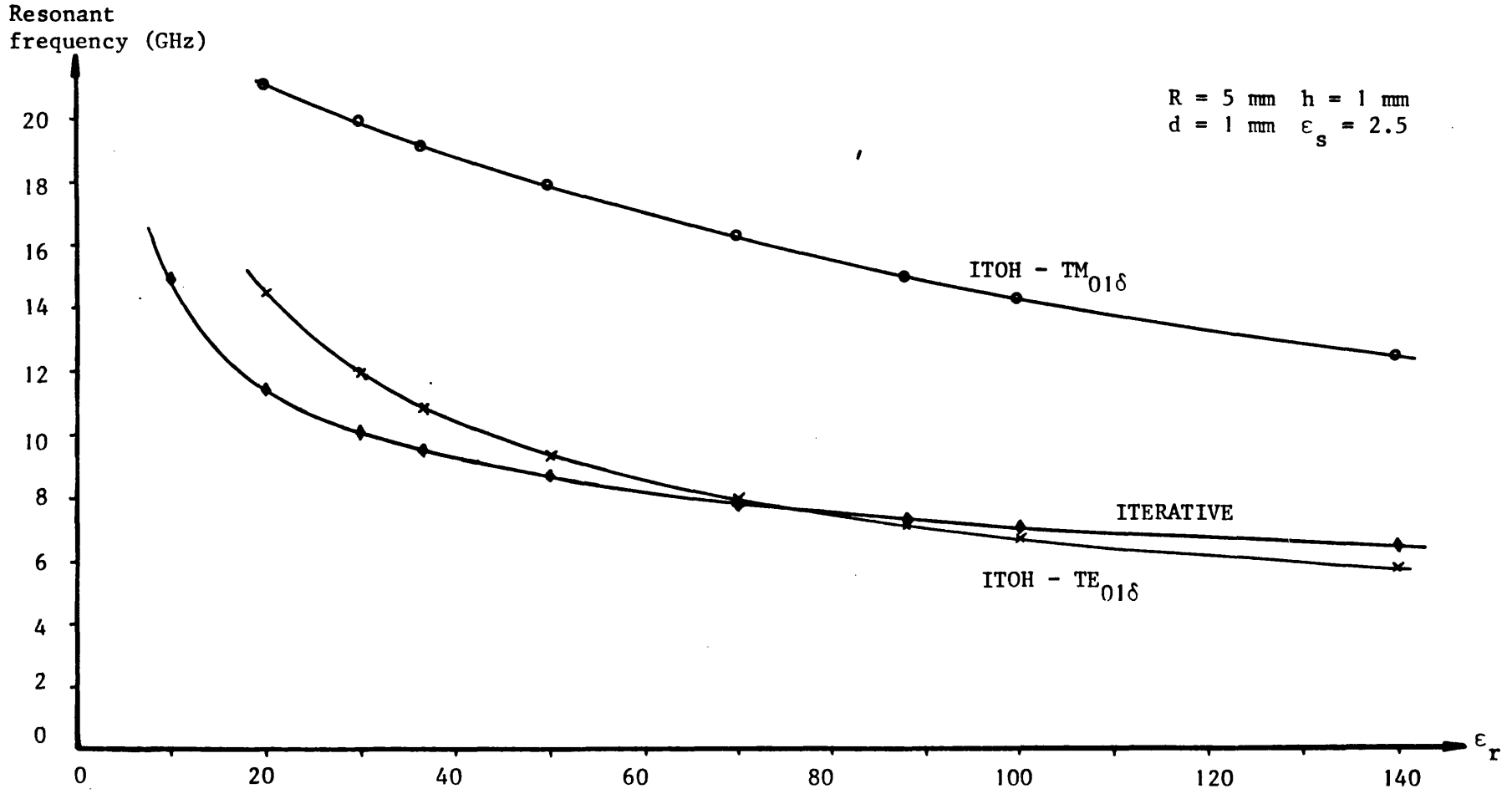

Figure 6.9 Graph comparing the resonant frequency obtained using the iterative method with those results determined from Itoh's $TE_{01\delta}$ and $TM_{01\delta}$ models

as a conducting surface approaches, whereas a decrease in the resonant frequency would result if the same resonator were excited in a transverse magnetic mode. This behaviour is apparent in Figures 6.10 and 6.11, where theoretical $TE_{01\delta}$ and $TM_{01\delta}$ resonant frequency characteristics, computed via the Itoh method, are shown for dielectric substrates of varying height, d. Comparison of these results with those obtained from the iterative technique, as given in Figure 6.12, clearly shows the transverse electric nature of the iterative solution.

6.3 The Experimental Determination of the Fundamental Resonant Frequency

In the previous section, it was shown, from comparison of theoretical results, that the iterative solution provides the resonant frequency of the fundamental resonant mode, and it is now necessary to compare the computed results with experimental values in order to determine the accuracies of the two theoretical models for calculating the $TE_{01\delta}$ resonant frequency. However, the practical method for measuring the fundamental resonance had to be carefully designed in order to ensure that the physical arrangement accurately conformed to the theoretical situation.

6.3.1 The grounded dielectric substrate

In the development of the iterative solution given in chapter 5, the Green's function was determined for a 1 mm thick grounded polystyrene slab excited in its fundamental mode, which is transverse magnetic to the vertical direction. This particular choice of dielectric material for the substrate was made after consideration of the requirements necessary for the experimental measurements. In order to simulate the isolation of the dielectric resonator upon the substrate, a large piece of dielectric material is necessary, and thus, on both economic and practical grounds, polystyrene was chosen, since it is both cheap and widely available.

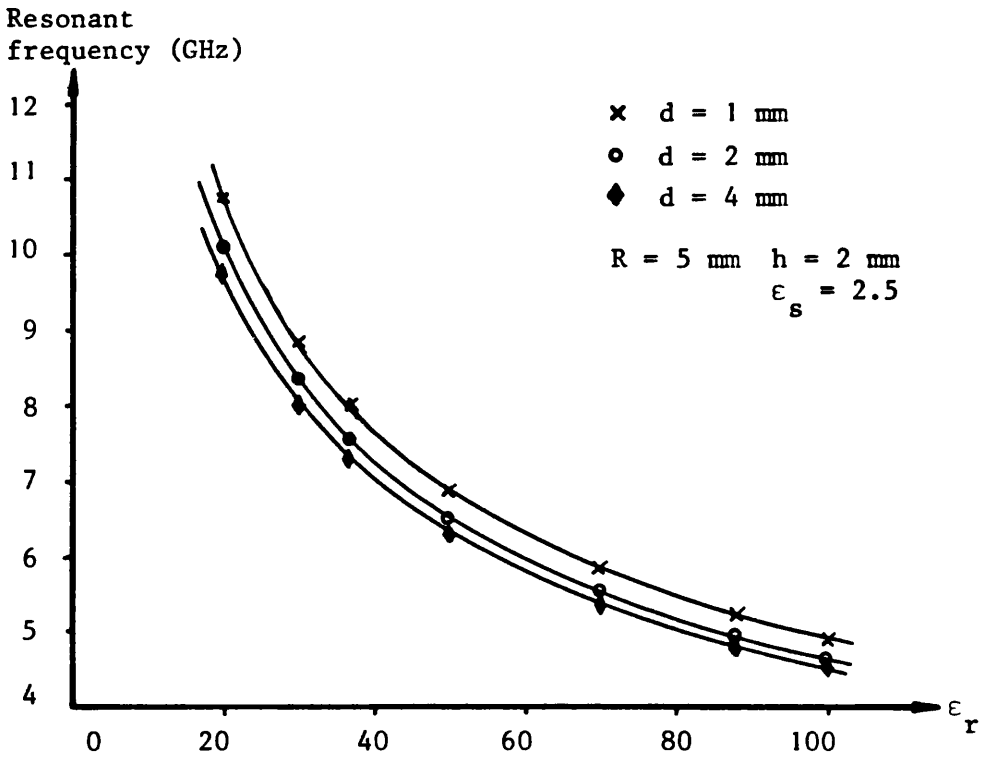

Figure 6.10 Graph showing the variation of the $TE_{01\delta}$ resonant frequency characteristic curves with the height of the dielectric substrate, obtained using Itoh's model

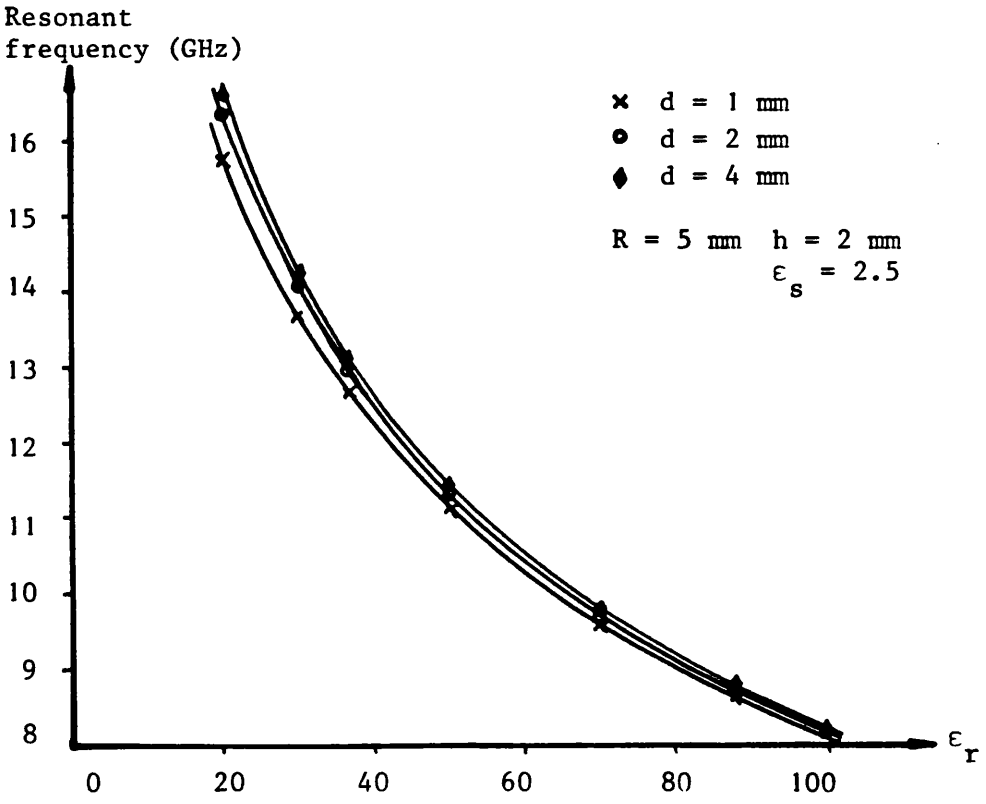

Figure 6.11 Graph showing the variation of the $TM_{01\delta}$ resonant frequency characteristic curves with the height of the dielectric substrate, obtained using Itoh's model

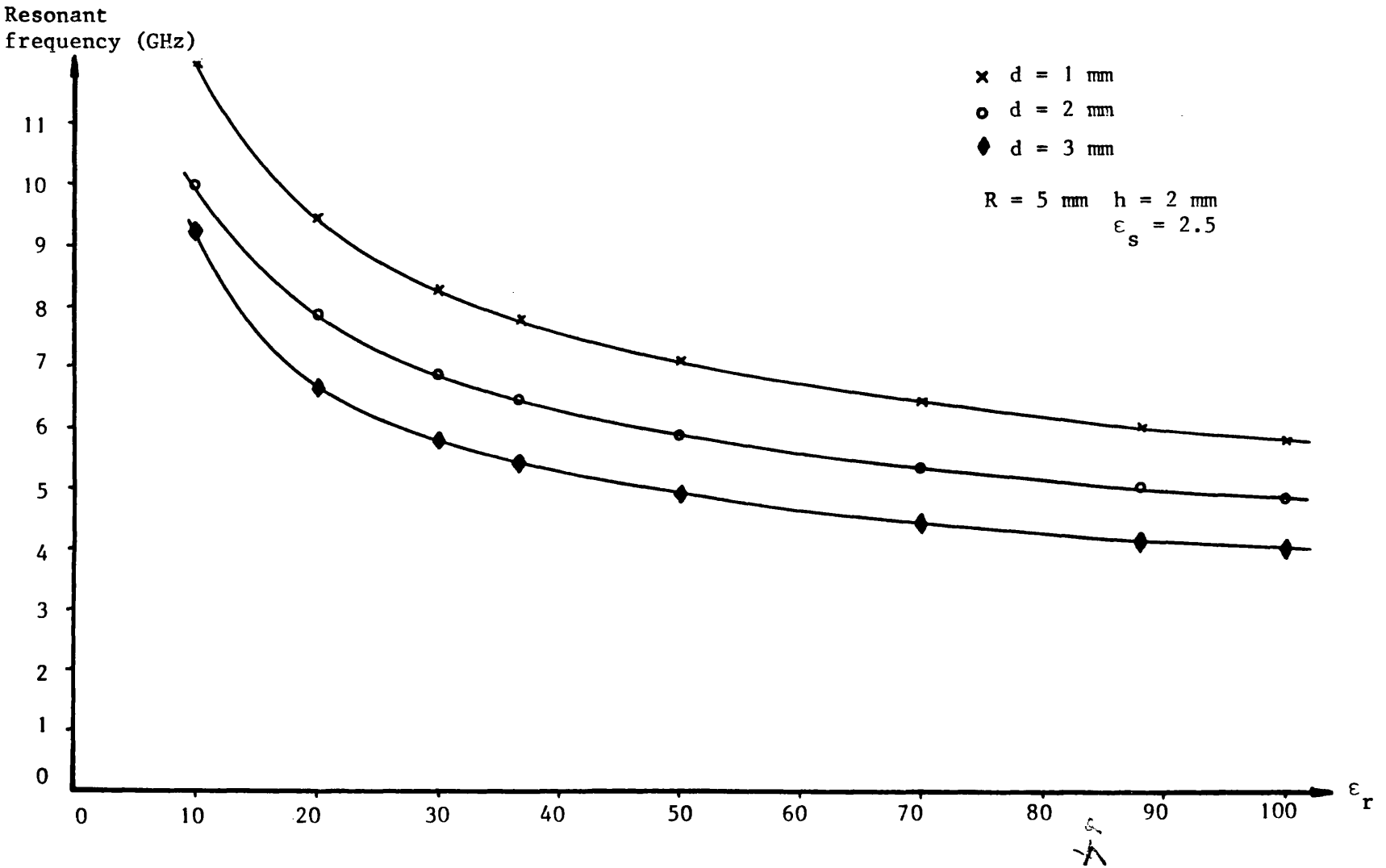

Figure 6.12 Graph showing the variation of the resonant frequency charcteristic curves with the height of the dielectric substrate, for the iterative solution

A sample piece of the polystyrene was used to measure its relative dielectric constant, which was found to be 2.5, and so, as detailed in section 5.2, the thickness of the dielectric substrate was chosen to be one millimetre, so that the dielectric slab waveguide supports only the fundamental TM mode in the frequency range of interest. In order to launch this lowest TM mode on to the dielectric slab waveguide, it was realised that standard waveguide horns, operating in the dominant TE_{01} mode, would excite a surface wave polarised transverse magnetic to the vertical direction. Accordingly, the dielectric slab was manufactured with a taper at each end, so that it could be inserted into the waveguide horns, thus maximising the power coupled into and out of the substrate, and also reducing the effect of the discontinuities at the transitions. Furthermore, in order to remove the unwanted direct air-wave coupling between the waveguide antennas, a microwave absorber was placed above and below the substrate in the horn apertures.

The discontinuities caused by these closed-to-open waveguide transitions, and also other discontinuities due to the open circuited sides of the substrate, needed special consideration since the theoretical analysis was developed for a dielectric resonator placed in isolation on a grounded substrate of infinite extent. Thus any possible reflections had to be minimised, and so the edges of the substrate were lined with Eccosorb, which has an average reflection coefficient of -23 dB at X-band. Moreover, the waveguide to substrate transitions described above needed to be as far removed from the resonator as possible, so that the electromagnetic field at the resonator would be effectively free of any disturbances.

However, it was found in practice that the most efficient method for measuring the fundamental resonant frequency was to examine the effect of the resonator upon the transmitted power characteristic of the grounded slab waveguide, and, unfortunately, the requirement of placing the launching transitions as far as possible from the resonator conflicts with the need for minimum insertion loss, which is necessary for ease and accuracy of measurement. This loss is due to the fact that, once the power is coupled into the substrate, there is no guiding mechanism, and so the power disperses throughout the slab, and only a small proportion takes the direct path into the receiving horn. Furthermore, the efficiency of the waveguide to substrate coupling is poor, and the combination of these two effects leads to an insertion loss of approximately 42 dB/m.

An obvious method of reducing the insertion loss is to introduce some form of guiding structure between the waveguide horns. One such structure is known as dielectric ridge waveguide [5], where the substrate is manufactured with a dielectric ridge running the length of the slab. In order to determine the effectiveness of such a guiding structure, a ridge guide was constructed and found to transmit double the power compared to an ordinary substrate of identical dimensions. However, the ridge introduces extra discontinuities into the resonator problem, and thus a consequent change in the value of the fundamental resonant frequency would be expected. The graphs shown in Figures 6.13 and 6.14 confirm this hypothesis by showing, for two different sizes of resonator and over a wide range of relative permittivities, the discrepancy between the measured values of fundamental resonant frequency obtained using ridge guide and slab waveguide. It is evident that the dielectric ridge affects the value of the fundamental resonant

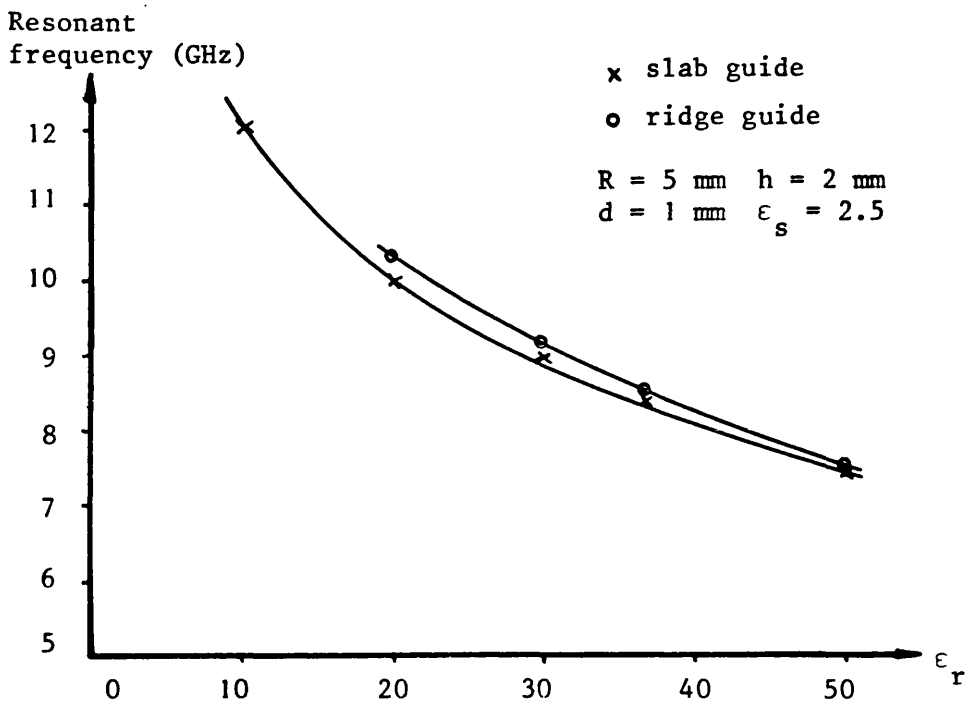

Figure 6.13 Graph showing the effect of the type of substrate upon the measured resonant frequency for resonators of height 2 mm

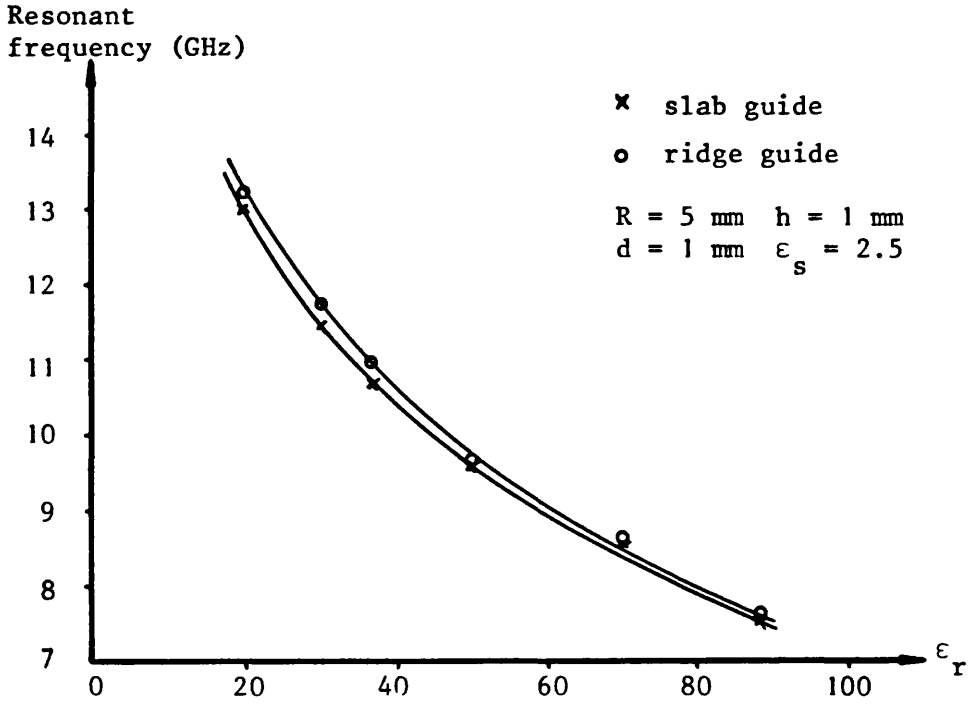

Figure 6.14 Graph showing the effect of the type of substrate upon the measured resonant frequency for resonators of height 1 mm

frequency most for pillboxes made of low permittivity material. The reason for this is that the weak field confinement in such resonators leads to greater coupling of power between the ridge and the resonator, and so the effect is most pronounced, whereas high permittivity resonators are influenced less since they produce tight field confinement. The conclusion drawn from these results was that the ridge guide, or other similar guiding structures, could not be used, since they would lead to false experimental values for the resonant frequency. Therefore, a compromise was reached over the length of the dielectric substrate, so that the discontinuities were having little effect on the resonator, and yet sufficient power was transmitted to enable reliable measurements to be taken.

These measurements were made using a Hewlett-Packard 8510A vector network analyser, shown in Figure 6.15, which can accurately measure signals at a power level of less than -45 dBm, which meant that a substrate of dimensions 0.9 x 0.45 m could be used without rendering the measurements inaccurate. The full experimental arrangement is shown in Figure 6.16, and it is apparent that the discontinuities due to the waveguide to substrate transitions are well-removed from the resonator. In fact, at 6 GHz, the resonator to horn distance was approximately 22 λ_s rising to 45 λ_s at 12 GHz, where λ_s is the wavelength in the dielectric slab waveguide. This confirms that the dielectric resonator was effectively in isolation upon the substrate.

6.3.2 The transmitted power measurement technique

It was mentioned earlier that the determination of the fundamental resonant frequency was performed by examining the effect upon the transmitted power characteristic of the dielectric substrate caused by the introduction of the dielectric resonator. The choice of this

Figure 6.15 Photograph of the Hewlett-Packard 8510A vector network analyser

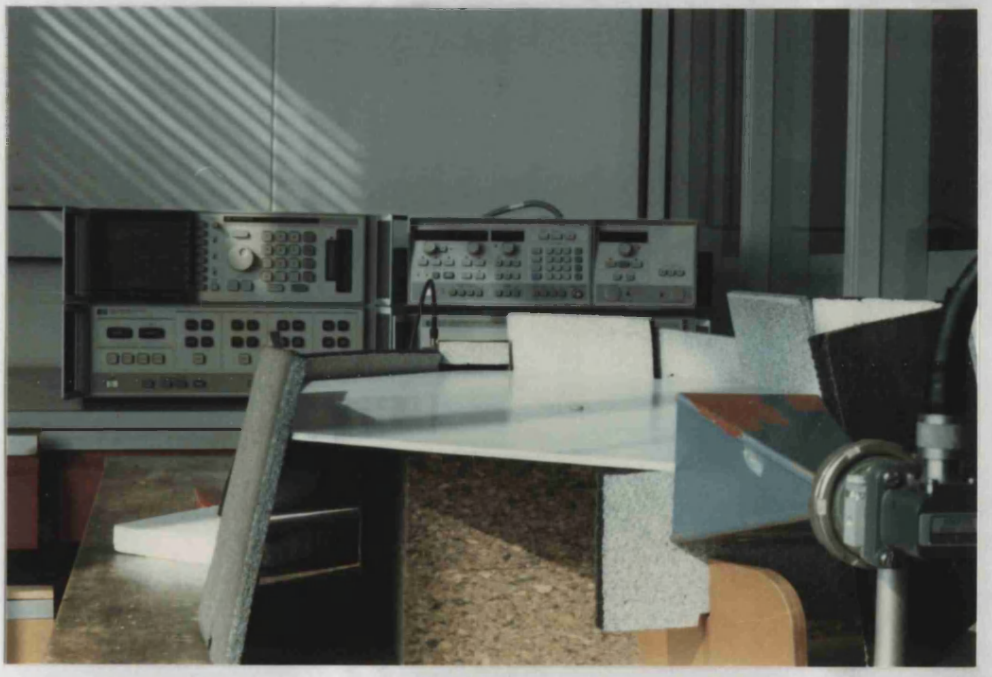

Figure 6.16 The experimental kit used in determining the fundamental resonant frequency of a dielectric resonator

particular technique was determined by two major factors. Firstly, the measurement of transmitted and reflected power was very straightforward, so that techniques based on such measurements were favoured. Secondly, the effect of the dielectic resonator upon the power transmitted through the substrate is well-understood, whereas the behaviour of its reflection coefficient is not at all obvious. Consequently, the only practical technique was the transmitted power method, and the basis of this technique is described below.

The resonant frequencies of a dielectric resonator occur when the electromagnetic field structure within the resonator is such that the energy contained in the field is stored over intervals that are long compared with the period of the incident wave. At such frequencies, this energy storage causes a reduction in the transmitted power, whilst at all other frequencies the introduction of the resonator merely provides a slight additional attenuation in the system. Consequently, comparison of the transmitted power characteristics, measured over an appropriate frequency range, for the dielectric substrate both with and without the dielectric resonator positioned on it, leads to the determination of several resonant frequencies. The problem then becomes one of discovering the lowest resonant frequency.

However, the practical implementation of the transmission method described above was not quite as straightforward as it appears, for there were several major measurement difficulties to be overcome. The first problem was due to the nature of the dielectric substrate itself, which, as is shown in Figure 6.17, does not transmit a constant level of power over a frequency band, but, rather, has a characteristic made up of peaks and troughs. It was found in practice that the resonant dips were less than 0.5 dB deep, and even more shallow for low relative

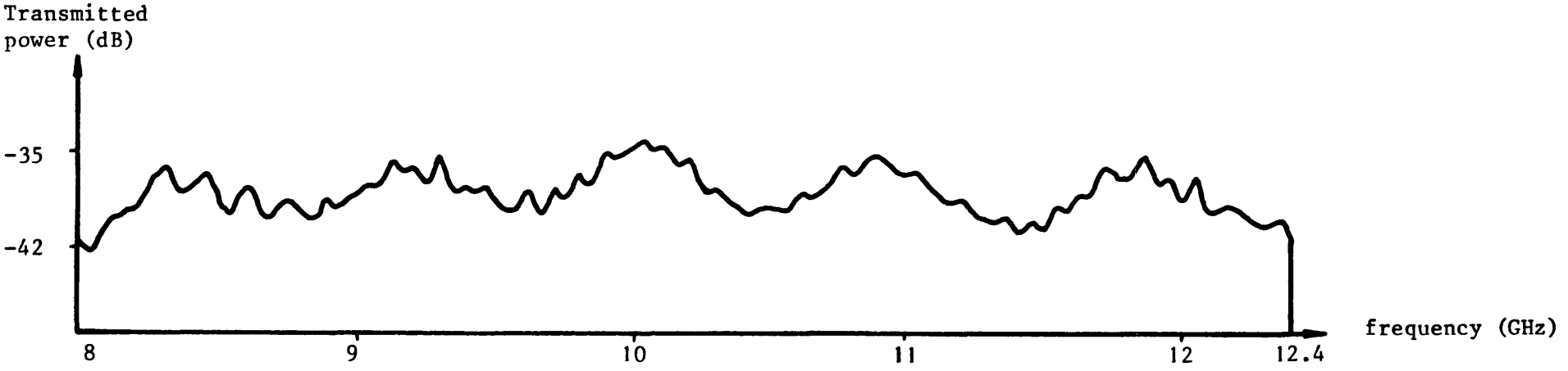

Figure 6.17 Typical transmission characteristic of a 1 mm thick grounded polystyrene slab

permittivity resonators, and thus, even with the sophisticated facilities of the network analyser, great care had to be taken not to miss the lowest resonance.

The general method employed to find the fundamental resonance was to use the memory of the analyser to store the transmission characteristic of the substrate alone, and then introduce the resonator and to display the new characteristic divided by the memory. Consequently, the effect of the resonator was displayed, and the problem reduced to that of discriminating the fundamental resonant frequency from the noise of the system. In order to achieve this, a second, identical resonator was introduced on to the substrate, which had the effect of emphasizing the resonant dips, since now twice as much energy was stored at resonance. However, the second resonator also has the effect of introducing spurious resonances due to inter-resonator coupling, and thus the two resonators were placed as far apart as possible, yet without coming too close to the waveguide horns. To further remove the possibility of taking erroneous results due to the coupling between the resonators, small changes were introduced into the resonator separation, and the consequent effect on the resonant dips observed. If there was no change in an observed resonant frequency, then it was accepted as a true resonant frequency of the cylindrical dielectric resonator. If, however, a resonant dip was seen to alter in frequency, then it was rejected as a false resonance, since the inter-resonator effects are due to the coupling coefficient which depends on the separation of the resonators. This method of altering the resonator position was also used to eliminate any possibility of the pillbox having been placed in such a position that it helped to match in the transition from waveguide to substrate, under which circumstances the fundamental mode might have been rendered invisible.

The only remaining problem was to ensure that the lowest resonant frequency observed was in fact the fundamental resonance. It is known [6] that a cylindrical dielectric resonator has a fundamental $TE_{01\delta}$ resonance followed in quick succession by a series of higher order modes. Therefore, the fundamental resonant frequency may be found by searching for the lowest observable resonant frequency, and then carefully checking the transmission characteristics for further resonances occurring at a lower frequency. If none can be detected in the frequency range 0.6 f_t to f_t, where f_t is the possible fundamental resonant frequency, then the resonant frequency has indeed been found.

In practice, the apparatus available with the Hewlett-Packard vector network analyser was only able to provide measurements in the range 7.0 - 13.0 GHz and, since most of the measured resonances fell in this range, it was necessary to further consider the range from 4.0 - 7.0 GHz. Plessey Materials Ltd. at Towcester kindly offered the use of their test equipment for this purpose, and, according to the above criterion, it was demonstrated that all of the experimental values of fundamental resonant frequency presented below were in fact $TE_{01\delta}$ resonances.

6.4 Comparison of Experimental and Theoretical Results

The fundamental resonant frequencies of fifteen different resonators were measured as described above, and the results obtained are presented graphically, in comparison with theoretical results calculated from both the iterative and Itoh methods, in Figures 6.18 to 6.21. A general inspection of these graphs indicates that the iterative solution gives results that are more accurate over the whole range of values of permittivity, but it is noted that there are two variations that merit detailed attention.

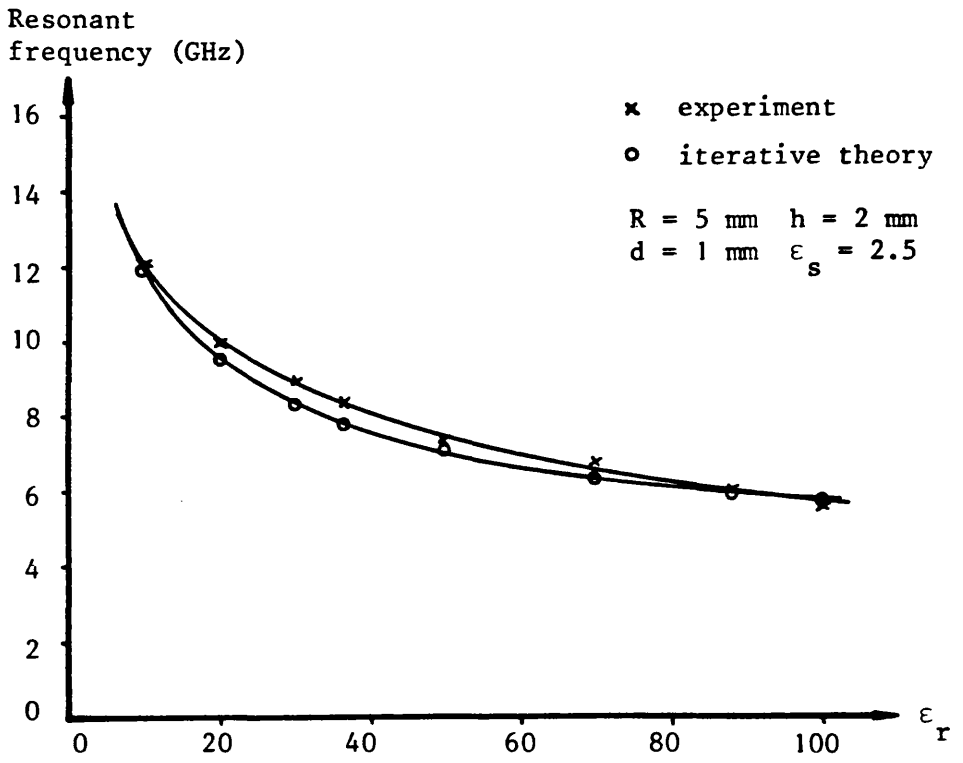

Figure 6.18 Graph of experimental and theoretical results, using the iterative theory, for the $TE_{01\delta}$ mode of a resonator of radius 5 mm and height 2 mm

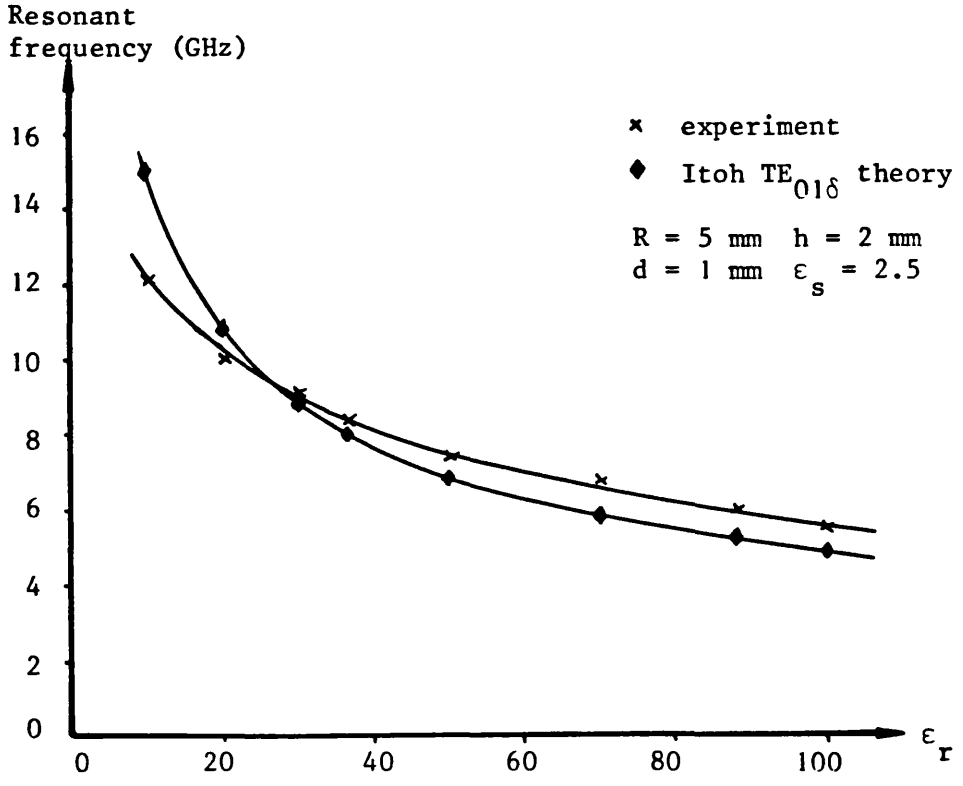

Figure 6.19 Graph of experimental and theoretical results, using Itoh's approach, for the $TE_{01\delta}$ mode of a resonator of radius 5 mm and height 2 mm

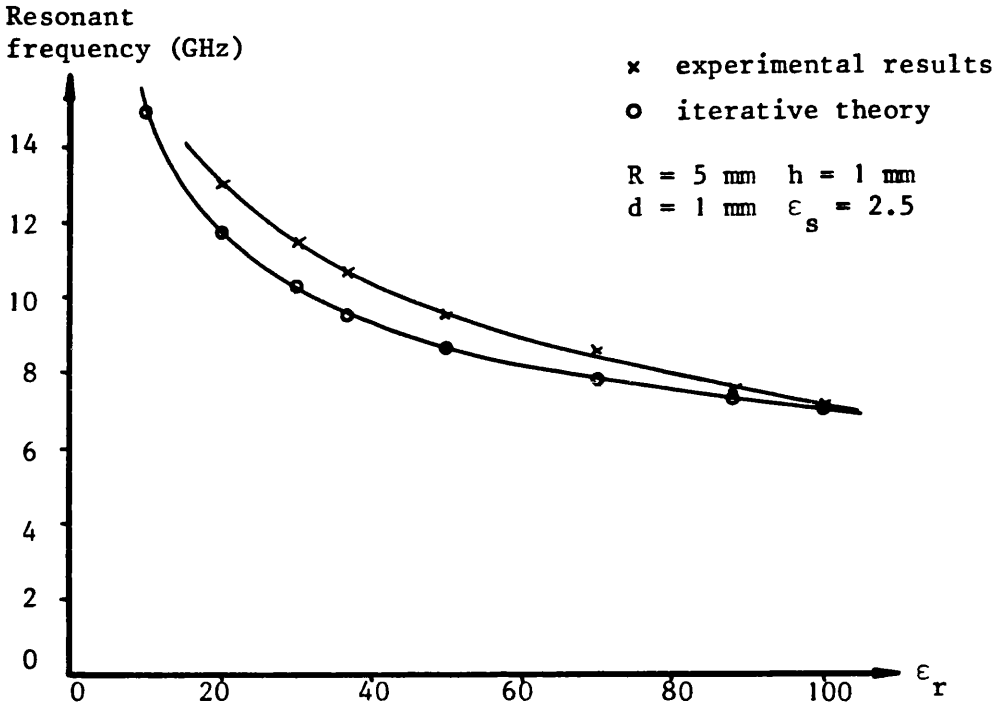

Figure 6.20 Graph of experimental and theoretical results, using the iterative technique, for the $TE_{01\delta}$ mode of a resonator of radius 5 mm and height 1 mm

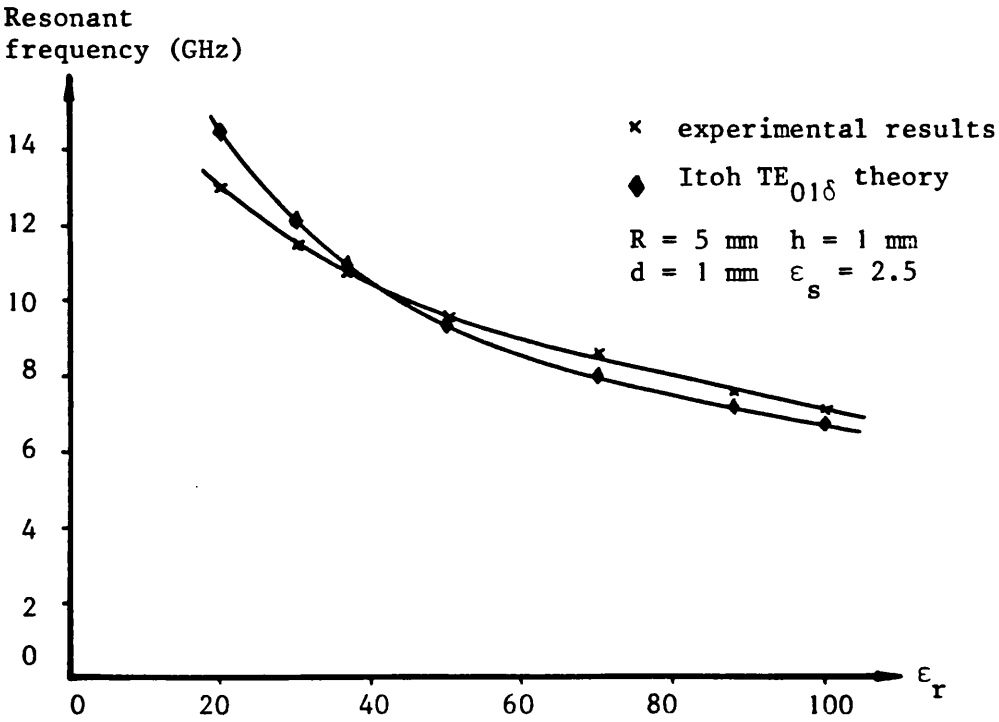

Figure 6.21 Graph of experimental and theoretical results, using Itoh's approach, for the $TE_{01\delta}$ mode of a resonator of radius 5 mm and height 1 mm

6.4.1 The influence of the relative permittivity

It is clearly seen from Figures 6.18 to 6.21 that as the relative permittivity rises, so there is a consequent decrease in the fundamental resonant frequency. This effect may be understood by considering the electrical length of the resonator, which rises as ε_r rises. Consequently, the effective resonant wavelength inside the resonator must also rise, which produces a fall in the resonant frequency.

It is also seen from the Figures 6.18 to 6.21 that the theoretical models reproduce this variation, although it is noted that it is the iterative method which yields results that fit most closely to the shape of the practical curve. The behaviour of the results from the coupled eigenvalue equations derived by Itoh and Rudokas may be explained by realising that the method was based upon the Marcatili approximation, which assumes that certain regions of space immediately exterior to the resonator contain very little electromagnetic energy. It is known that resonators made of high permittivity material exhibit good field confinement, whereas lower values of ε_r do not exert the same influence, and thus it is expected that the high values of ε_r will give results that are in much better agreement with experiment than will low values. Examination of Figures 6.19 and 6.21 shows that this is indeed the case.

It is further seen that the Itoh approach gives results for the resonant frequency that lie either side of the experimental curve, and thus practical design using this theoretical technique is difficult, since the method provides neither an upper or lower bound for the fundamental resonance. However, Figures 6.18 and 6.20 clearly show that the iterative solution provides a lower bound for the fundamental resonance, and, despite neglecting the contributions of both the

continuous part of the Green's function and the surface integral, it is seen that the maximum error between experimental and theoretical results is 10%, whilst for a resonator height of 2 mm, the computed frequencies always lie within 6% of the measured values. This fact suggests that the height of the resonator plays an important part in the accuracy of the iterative technique, and this is now investigated in more detail.

6.4.2 The influence of the resonator height

In order to examine the effect of the height of the resonator upon the accuracy of the theoretical solutions, the fundamental resonant frequencies of three more resonators of different height were measured for $\varepsilon_r = 20$, and the variation of this resonant frequency with height is shown in Figures 6.22 and 6.23. It is immediately apparent that the height makes little difference to the accuracy of the Itoh method, but affects the iterative results dramatically. As the height of the resonator is increased, it is seen that the accuracy improves substantially, as the results in Figures 6.18 and 6.20 indicated might be the case.

The reason for this behaviour is due to the nature of the iterative analysis, which involves the Green's function of the grounded dielectric slab waveguide. As demonstrated in section 3.4, this Green's function consists of both discrete and continuous modes, and it is the relative importance of these two parts of the Green's function that leads to the variation of accuracy due to the resonator height.

The continuous modes are included in the Green's function to take account of the energy that radiates away from the dielectric slab, whilst the discrete modes describe the energy that is carried by the surface waves, which are bound to the dielectric slab. Consequently,

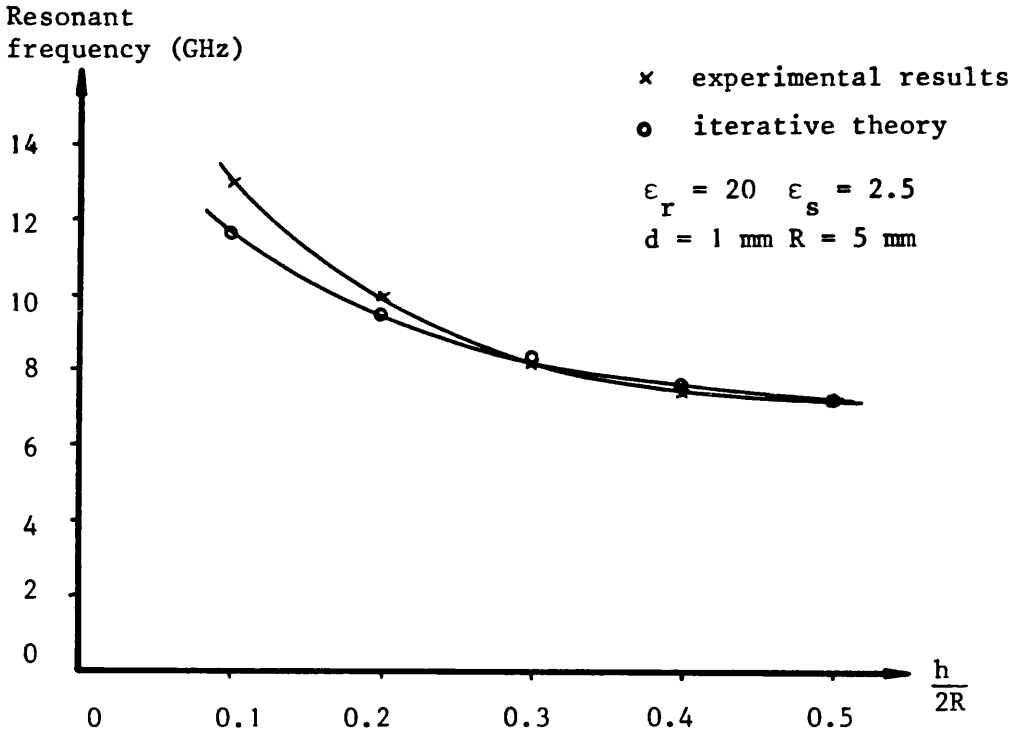

Figure 6.22 Graph of $TE_{01\delta}$ resonant frequency vs resonator height showing the comparison between the iterative theory and experimental results

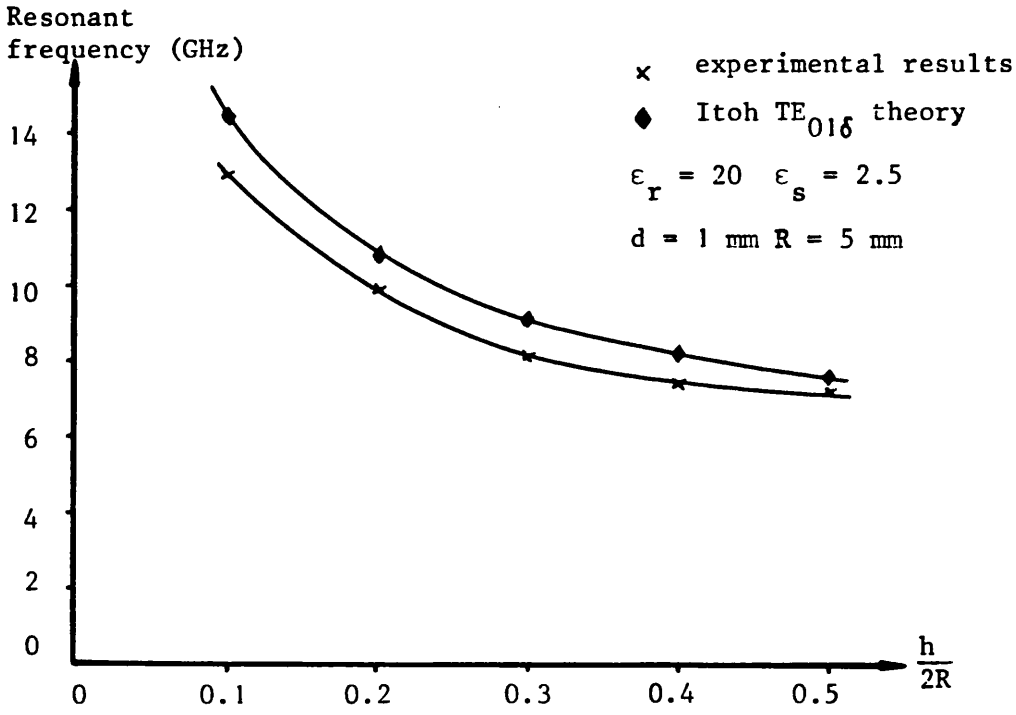

Figure 6.23 Graph of $TE_{01\delta}$ resonant frequency vs resonator height showing the comparison between Itoh's $TE_{01\delta}$ method and experimental results

it is apparent that the relative importance of the discrete and continuous parts of the Green's function to the determination of the fundamental resonant frequency depends upon the relative proportions of stored and radiated energy. It is also clear that a larger resonator will contain more energy than a smaller one, and thus it is seen that the continuous modes become less important as the height of the resonator increases. Therefore, the results given by the iterative solution of chapter 5 would be expected to become more accurate as the height is increased, which is precisely the behaviour seen in Figure 6.22.

6.4.3 Summary of results

It has been demonstrated very clearly, by comparing a wide range of experimental and theoretical results, that, under certain conditions, the iterative solution developed in chapter 5 provides accurate values for the fundamental resonant frequency of the cylindrical pillbox dielectric resonator when placed upon a grounded dielectric substrate. Indeed, it has also been shown that the iterative method yields more accurate and usable solutions than does the approximate technique developed by Itoh and Rudokas.

However, the results given in this chapter for the iterative solution are based upon the simplified Green's function where the continuous modes have been ignored. As indicated in section 6.4.2, it is expected that even more accurate solutions, under all conditions, could be achieved if these continuous modes were included in the Green's function, and so, in the following chapter, the application of the iterative method to the integral over the continuum is now considered.

REFERENCES

[1] T. Itoh and R.S. Rudokas: "New method for computing the resonant frequencies of dielectric resonators", IEEE Trans. Microwave Theory Tech., Vol.MTT-25, pp.52-54, Jan. 1977.

[2] P. Gelin, S. Toutain, P. Kennis and J. Citerne: "Scattering of the TE_{01} and TM_{01} modes on transverse discontinuities in a rod dielectric waveguide - application to the dielectric resonators", IEEE Trans. Microwave Theory Tech., Vol.MTT-29, pp.712-719, July 1981.

[3] E.A.J. Marcatili: "Dielectric rectangular waveguide and directional coupler for integrated optics", Bell Syst. Tech. J., Vol.48, pp.2071-2102, Sept. 1969.

[4] H.Y. Yee: "An investigation of microwave dielectric resonators", Microwave Lab. Rep. 1065, Stanford University, Stanford, CA, July 1963.

[5] S-T. Peng and A.A. Oliner: "Guidance and leakage properties of a class of open dielectric waveguides: part 1 - mathematical formulations", IEEE Trans. Microwave Theory Tech., Vol. MTT-29, pp.843-854, Sept. 1981.

[6] D. Kajfez, A.W. Glisson and J. James: "Computed modal field distributions for isolated dielectric resonators", IEEE Trans. Microwave Theory Tech., Vol.MTT-32, pp.1609-1616, Dec. 1984.

CHAPTER 7

THE INTEGRAL OVER THE CONTINUUM

In chapter 3, the integral equation (3.46),

$$\psi_{hr}(\underline{x}) = (\varepsilon_r - \varepsilon_a)k_o^2 \iiint_{\text{resonator}} G_a(\underline{x},\underline{x}')\psi_{hr}(\underline{x}')dV' \qquad (7.1)$$

was derived, where the Green's function was given by equation (3.56)

$$G_a(\underline{x},\underline{x}') = \frac{1}{4j}\left[\sum_n H_o^{(2)}(k_{\rho n}|\rho - \rho'|)Y_n(y)Y_n(y') + \int_o^\infty H_o^{(2)}(k_{\rho c}|\rho - \rho'|)Y(\chi,y)Y(\chi,y')d\chi\right] \qquad (7.2)$$

and the eigenfunctions $Y_n(y)$ and $Y(\chi,y)$ are as given in Tables D.1 and D.2 of Appendix D. In chapter 5, an iterative method was developed for solving equation (7.1) where the continuous spectrum, which comprises the radiation modes of the dielectric slab, was ignored, since it was shown that the major proportion of the energy coupled into the dielectric resonator is provided by the discrete modes. The results obtained, using this approximation to the true solution, were found to be very accurate, but it was realised that the inclusion of the continuum integral would increase the accuracy of the method still further.

In order to provide a complete theoretical analysis of the substrate-mounted cylindrical dielectric resonator, it is obviously necessary to solve equation (7.1) using the full expression for the Green's function given in equation (7.2). In fact, the process for including the continuum integral into the iterative procedure is relatively straightforward, since equation (7.1) may be rewritten as

$$\psi_{hr}(\underline{x}) = (\varepsilon_r - \varepsilon_a)k_o^2 \left\{ \iiint_{\text{resonator}} G_n(\underline{x},\underline{x}')\psi_{hr}(\underline{x}')dV' \right.$$

$$\left. + \iiint_{\text{resonator}} \left[\int_o^\infty G_c(\underline{x},\underline{x}')d\chi \right] \psi_{hr}(\underline{x}')dV' \right\} \quad (7.3)$$

where $G_n(\underline{x},\underline{x}')$ and $G_c(\underline{x},\underline{x}')$ represent the discrete and continuous parts of the Green's function, $G_a(\underline{x},\underline{x}')$, and thus the iterative procedure may be applied to the two volume integrals of equation (7.3), and the results added together to give the new function $\psi_{hr}(\underline{x})$.

However, although the iterative procedure is well-understood for the discrete situation, the inclusion of the integral over the wave-number χ needs careful consideration. In order to gain some insight into the nature of this new problem, it is prudent to first consider how the iterative technique applies to the radiation integral alone. Consequently, in this chapter, the situation of a cylindrical dielectric pillbox placed directly on a ground plane is considered, since, for this image resonator, the Green's function contains no discrete modes, but purely consists of an integral over the continuum.

7.1 The Integral Equation for the Image Resonator

A diagram of the image resonator is shown in Figure 7.1, and, since it is a structure with cylindrical geometry, the same type of potential functions, $\psi_h(\underline{x})$ and $\psi_e(\underline{x})$, as in chapter 3 may be used to construct the relevant integral equation. Therefore, within the two constituent regions, the following differential scalar potential equations must hold,

$$(\nabla^2 + \varepsilon_r k_o^2)\psi_r(\underline{x}) = 0 \qquad \text{in the resonator} \qquad (7.4a)$$

$$(\nabla^2 + \varepsilon_a k_o^2)\psi_a(\underline{x}) = 0 \qquad \text{in the air} \qquad (7.4b)$$

where $\psi(\underline{x})$ represents both the electric and magnetic potentials.

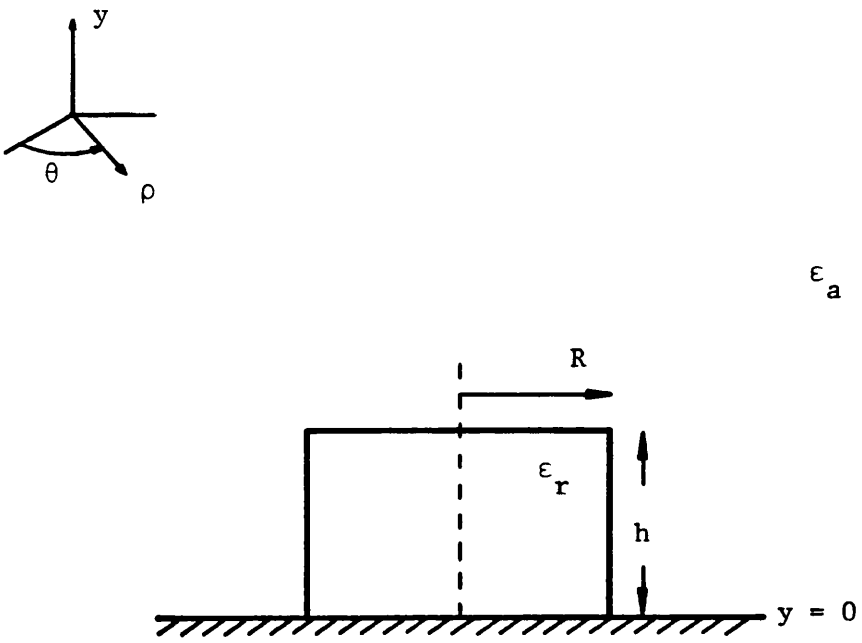

Figure 7.1 Cross-section of the image dielectric resonator, consisting of a cylindrical pillbox mounted on a ground plane

Considering the Green's function of a point source in the air region above a ground plane, which satisfies the relationship

$$(\nabla^2 + \varepsilon_a k_o^2)\, G_i(\underline{x},\underline{x}') = -\delta(\underline{x} - \underline{x}') \qquad (7.5)$$

the equation (7.4a) may be transformed to give the equation

$$\psi_r(\underline{x}) = (\varepsilon_r - \varepsilon_a)k_o^2 \iiint_{\text{resonator}} G_i(\underline{x},\underline{x}')\psi_r(\underline{x}')dV' + \iint_{\substack{\text{resonator}\\ \text{boundary}}} \left[G_i(\underline{x},\underline{x}') \frac{\partial \psi_r(\underline{x}')}{\partial n_r'} - \psi_r(\underline{x}') \frac{\partial G_i(\underline{x},\underline{x}')}{\partial n_r'}\right] dS' \qquad (7.6)$$

As in the case of the substrate-mounted dielectric resonator, this surface integral over the resonator boundary gives the difference between the TE_{omn} and TM_{omn} modes, and, using the technique given in Appendix B, may be shown to give less contribution for the TE_{omn} modes than for the TM_{omn} modes. Furthermore, as shown in chapter 3, the surface integral represents the contribution from external sources induced by the equivalent sources within the resonator, and thus is of less consequence than the volume integral, and may initially be ignored. Thus, the transverse electric modes may be modelled by the reduced integral equation

$$\psi_{hr}(\underline{x}) = (\varepsilon_r - \varepsilon_a)k_o^2 \iiint_{\text{resonator}} G_i(\underline{x},\underline{x}')\psi_{hr}(\underline{x}')dV' \qquad (7.7)$$

7.2 The Green's Function

The Green's function of a point source situated in free-space above a metal ground plane must satisfy equation (7.5), and may be determined by following the procedure given in section 3.4. The difference in the resulting Green's function derives from the nature of the y-directed eigenmodes, which are now found to be purely continuous, and are given by the relations

$$Y_h(\chi,y) = \sqrt{\frac{2}{\pi}} \sin(\chi y) \tag{7.8a}$$

$$Y_e(\chi,y) = \sqrt{\frac{2}{\pi}} \cos(\chi y) \tag{7.8b}$$

so that the delta function $\delta(y - y')$ becomes

$$\delta(y - y') = \int_0^\infty Y(\chi,y)\, Y(\chi,y')\, d\chi \tag{7.9}$$

and the magnetic and electric Green's functions are given, respectively, by

$$G_{ih}(\underline{x},\underline{x}') = \frac{1}{2\pi j} \int_0^\infty H_o^{(2)}(k_\rho|\rho - \rho'|) \sin(\chi y) \sin(\chi y')d\chi \tag{7.10a}$$

$$G_{ie}(\underline{x},\underline{x}') = \frac{1}{2\pi j} \int_0^\infty H_o^{(2)}(k_\rho|\rho - \rho'|)\cos(\chi y)\cos(\chi y')d\chi \tag{7.10b}$$

where the wavenumbers are related by

$$k_\rho^2 = k_o^2 - \chi^2 \tag{7.11}$$

In order to try and evaluate equations (7.10) analytically, the known [1] integral relation

$$\int_0^\infty H_o^{(2)}(\alpha\sqrt{k_o^2 - \chi^2})\cos(\beta\chi)d\chi = \frac{j \exp[-jk_o\sqrt{\alpha^2 + \beta^2}]}{\sqrt{\alpha^2 + \beta^2}}$$

$$\text{where} \quad \begin{cases} \alpha,\beta > 0 \\ -\pi < \arg(\sqrt{k_o^2 - \chi^2}) \leq 0 \end{cases} \tag{7.12}$$

was considered, where the scalar α is $|\rho - \rho'|$ and where β is either $(y - y')$ or $(y + y')$. The condition on the argument of k_ρ is met due to the imposition of the radiation condition, which, as shown in [2],

determines that k_ρ is given by

$$k_\rho = -j|k_\rho| \qquad \chi^2 > k_o^2 \tag{7.13}$$

However, it is also noted that, in order to make the definition of the double-valued wavenumber, k_ρ, unique, a two sheeted complex χ plane is necessary, with branch cuts providing the means of passing from one Riemann sheet to the other. For the case in point, where it is required to integrate over the real χ axis, and k_ρ must be either positive real or negative imaginary, the appropriate branch cuts are shown in Figure 7.2.

Although the integral given in equation (7.12) is applicable to equations (7.10), it was found that further progress using the iterative method of chapter 5 is impossible, since the resulting exponential function cannot be separated into independent radial and axial components. Consequently, it was decided to perform the volume integral before attempting the integral over the continuous spectrum, in order to see whether the resulting radiation integral is any simpler to handle.

7.3 Evaluation of the Volume Integral

With reference to chapter 5, it is clear that the choice of the trial function for the magnetic scalar potential should remain similar, since the problem is still being analysed in cylindrical geometry, and the dielectric resonator will have a similar internal distribution for the scalar potential. The only major difference results from the fact that the resonator base is at $y = 0$, and the potential function must be zero on the metal ground plane. However, the appropriate choice of orthonormal Fourier series in the axial direction will account for these variations, and thus the trial function is chosen to be

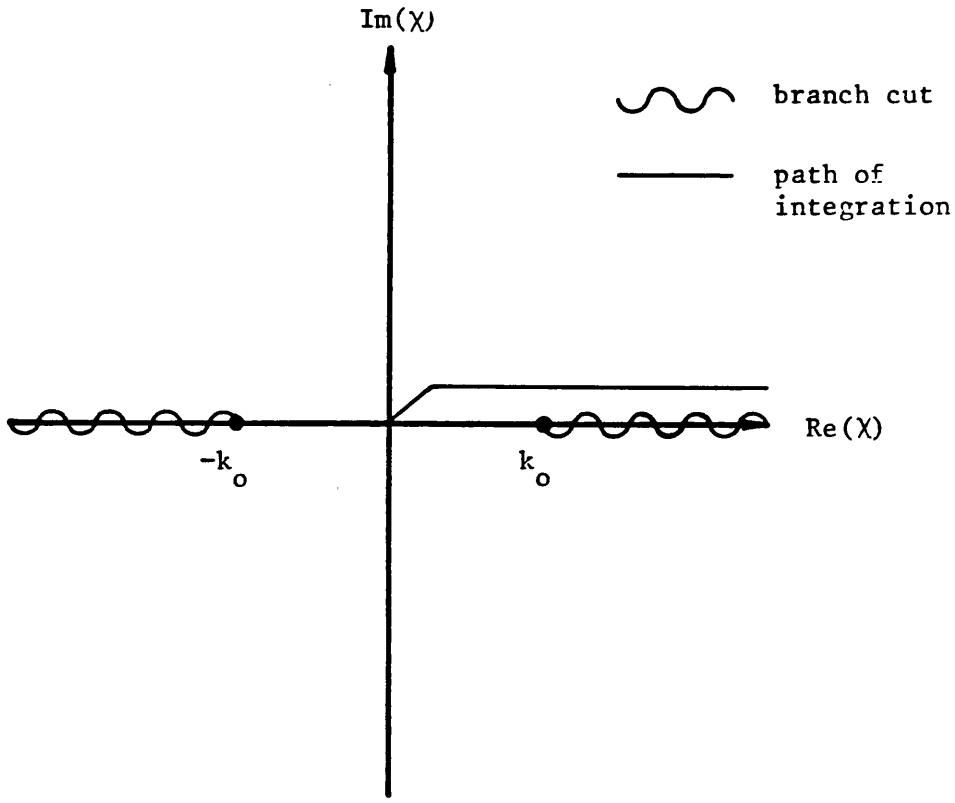

Figure 7.2 The appropriate branch cuts and path of integration for the integrals given in equations (7.10) and (7.11)

$$\psi_{hr}(\underline{x}') = \sum_{n=0}^{N} \frac{P_n J_o(\beta_n \rho')}{\eta_n} \left\{ \frac{A_o}{\sqrt{h}} + \sqrt{\frac{2}{h}} \sum_{m=1}^{M} \left[A_m \cos\left(\frac{2m\pi y'}{h}\right) + B_m \sin\left(\frac{2m\pi y'}{h}\right) \right] \right\} \tag{7.14}$$

It is evident from a comparison of equations (7.10) and (7.14) with equations (5.14) and (5.10), respectively, that the only difference between the volume integral for the discrete case and the volume integral for the radiation modes lies in the axial integration. It is sufficient to initially consider the behaviour of the volume integration using only the magnetic Green's function given by equation (7.10a), for which the axial integral is seen to be

$$I(y) = \sin(\chi y) \int_o^h \sin(\chi y') \left\{ \frac{A_o}{\sqrt{h}} + \sqrt{\frac{2}{h}} \sum_{m=1}^{M} \left[A_m \cos\left(\frac{2m\pi y'}{h}\right) + B_m \sin\left(\frac{2m\pi y'}{h}\right) \right] \right\} dy' \tag{7.15}$$

which results in the expression

$$I(y) = \sin(\chi y) \left\{ \frac{A_o}{\sqrt{h}} \left[\frac{1 - \cos(\chi h)}{\chi} \right] + \sqrt{\frac{2}{h}} \sum_{m=1}^{M} \frac{A_m \chi [1 - \cos(\chi h)] + B_m \frac{2m\pi}{h} \sin(\chi h)}{\left[\chi^2 - \left(\frac{2m\pi}{h}\right)^2\right]} \right\} \tag{7.16}$$

Thus, the result of the volume integration is found to be

$$\psi_{hr}(\underline{x}) = -j(\varepsilon_r - \varepsilon_a) k_o^2 \int_o^{\infty} \left\{ \sum_{n=0}^{N} \frac{P_n}{(\beta_n^2 - k_\rho^2)} \left[\frac{j2}{\pi} \frac{J_o(\beta_n \rho)}{\eta_n} - \sqrt{2}\, k_\rho H_1^{(2)}(k_\rho R) J_o(k_\rho \rho) \right] \cdot \left\{ \frac{A_o}{\sqrt{h}} \frac{[1 - \cos(\chi h)]}{\chi} + \right.$$

$$\sqrt{\frac{2}{h}} \sum_{m=1}^{M} \left\{ \frac{A_m \chi[1 - \cos(\chi h)] + B_m \left(\frac{2m\pi}{h}\right) \sin(\chi h)}{\left[\chi^2 - \left(\frac{2m\pi}{h}\right)^2\right]} \right\} \sin(\chi y) \Bigg\} d\chi \tag{7.17}$$

and re-expressing $J_o(k_\rho \rho)$ in terms of the expansion $J_o(\beta_n \rho)$ gives

$$\psi_{hr}(\underline{x}) = -j(\varepsilon_r - \varepsilon_a)k_o^2 \int_o^\infty \left\{ \sum_{n=0}^{N} \frac{Q_n(\chi) J_o(\beta_n \rho)}{\eta_n} [S_y(\chi)\sin(\chi y)] \right\} d\chi \tag{7.18}$$

where

$$Q_n(\chi) = \frac{1}{[(\beta_n^2 - k_o^2) + \chi^2]} \left\{ \frac{2jP_n}{\pi} + 2(k_o^2 - \chi^2) J_1(\sqrt{k_o^2 - \chi^2}R) \cdot H_1^{(2)}(\sqrt{k_o^2 - \chi^2}R) \sum_{t=0}^{N} \frac{P_t}{[(\beta_t^2 - k_o^2) + \chi^2]} \right\} \tag{7.19}$$

$$S_y(\chi) = \frac{A_o[1 - \cos(\chi h)]}{\sqrt{h}\,\chi} + \sqrt{\frac{2}{h}} \sum_{m=1}^{M} \left\{ \frac{[A_m \chi[1 - \cos(\chi h)] + B_m \left(\frac{2m\pi}{h}\right) \sin(\chi h)]}{\left[\chi^2 - \left(\frac{2m\pi}{h}\right)^2\right]} \right\} \tag{7.20}$$

It is seen from equations (7.18) to (7.20) that there are various separate integrals over the continuous spectrum, which, due to the presence of trigonometric functions, may possibly be performed by the method of residues [3]. In practice, half of these integrals may be performed in this manner, but it turns out that the argument $\sqrt{k_o^2 - \chi^2}$ causes difficulties, since the branch cuts have not been eliminated by the operation of the volume integral.

Although time did not permit the evaluation of the contribution of the integrals involving the Hankel function, those of the integrals shown in equation (7.18) that do not have any branch cuts were performed, and were shown to provide results that could be re-expressed in terms of the original basis functions. Thus, if a method of integration for the remaining integrals were used that preserved the shape of the function being integrated, then the continuous integral may be expressed in terms of the original basis function used for the trial function. Consequently, an iterative relationship could be constructed that is ideally suited to numerical implementation on a computer.

One such integration technique that retains the original shape of the integrand is known as the saddle-point (or steepest-descent) method [4,5], and thus it is expected that use of this technique would enable an iterative relationship to be developed for the image resonator.

Therefore, although the length of time available for this research did not permit the full analysis to be completed, it has been shown that the iterative method, developed to solve the integral equation derived for the magnetic potential function inside the substrate-mounted dielectric resonator, is able to accommodate the continuous modes as well as the discrete modes. Consequently, it is seen that the method described in this thesis is a full theoretical model of the substrate-mounted cylindrical dielectric resonator.

REFERENCES

[1] I.S. Gradshteyn and I.M. Rhyzik, "*Tables of Integrals, Series and Products*". New York: Academic Press, 1965, p.737.

[2] L.B. Felsen and N. Marcuvitz, "*Radiation and Scattering of Waves*". Englewood Cliffs, N.J.: Prentice-Hall, 1973, p.459.

[3] E. Kreyszig, "*Advanced Engineering Mathematics*". New York: Wiley, 1962, pp.700-707.

[4] R.E. Collin, "*Field Theory of Guided Waves*". New York: McGraw-Hill, 1960, pp.495-506.

[5] L.B. Felsen and N. Marcuvitz, "*Radiation and Scattering of Waves*". Englewood Cliffs, N.J.: Prentice-Hall, 1973, Chapter 4.

CHAPTER 8

CONCLUSIONS AND SUGGESTIONS FOR FURTHER WORK

The formulation of a theoretical model for the cylindrical dielectric resonator situated upon a grounded dielectric substrate has been presented in this thesis. The main aim of this research was to develop a model that was able to provide accurate results for the fundamental ($TE_{01\delta}$) resonant frequency, yet, at the same time, it was desired that the solution should be easily implemented on a numerical computer. Having presented an historical review of the previous models developed for the dielectric resonator, the mathematical derivation of an integral equation describing the resonator was given. After discussing several possible solution techniques for this equation, an iterative method was chosen, since it alone offered the characteristics of accuracy and eminent suitability for numerical implementation on a computer. The development of the iterative relationship was then detailed, and the results obtained were compared with both experiment and the extension of a previous theoretical technique, and it was seen that the main aim of the research was satisfied.

However, in the iterative technique described in this thesis, two approximations were necessary to simplify the analysis. In the first case, the integral equation, derived in chapter 3 for the resonator, consisted of a volume integral and an associated surface integral over the resonator. It was shown in Appendix B that this surface integral was present to account for the second-order effects of the equivalent sources outside the resonator, while the principal contribution of these sources was calculated in the volume integral. Furthermore, the difference between the $TE_{01\delta}$ and $TM_{01\delta}$ resonant modes, which

hitherto had been identical, was shown to lie in this surface integral, and, for the $TE_{01\delta}$ mode, it was found that the surface integral would give minimal contribution. Consequently, the theoretical analysis proceeded by considering the volume integration alone.

The second approximation lay in the consideration of the Green's function, which was chosen to be that of the air region above a grounded dielectric slab waveguide. This type of open waveguide supports a finite number of surface waves, and also a continuous spectrum of eigenmodes that represent both radiation from the slab and a continuum of evanescent waves. The surface waves represent most of the energy that is confined to the dielectric slab, and, since the resonator stores electromagnetic energy, it was inferred that the continuous spectrum of eigenmodes could be neglected without significantly reducing the accuracy of the calculated fundamental resonant frequency.

On the basis of these two reasonable approximations, an iterative relationship was developed, through analytical evaluation of the integral, for the case of a dielectric resonator placed on a grounded polystyrene substrate that was 1 mm thick. In order to verify the results obtained using the iterative procedure, a technique was developed to solve the relevant coupled equation set given by Itoh and Rudokas [1]. Comparison between these two methods, and also with experimental results, showed very clearly that the iterative technique produced values of the fundamental resonant frequency that were in close agreement with the true values, and also that it gave a significant improvement over the results obtained from the simple model of Itoh and Rudokas. It was further noted that the iterative method became virtually exact as the height of the resonator increased, because the continuous spectrum has less effect as the resonator

volume increases, since under such conditions more energy is stored within the resonator. Consequently, the two approximations are justified, since the surface integral does have minimal effect upon the accuracy of the solution, while the continuous spectrum of eigen-modes may be ignored with little ill-effect so long as the dimensions of the resonator are such that the proportion of energy storage to energy leakage is high.

However, in order to extend the iterative method to cover all dimensions of resonator, it is obviously necessary to include the continuous modes, and the possibility of this was considered in chapter 7. It was shown that an analytical evaluation of the continuum integral was not possible, but that the saddle-point approximate integration technique would be expected to yield a solution in a form amenable to the iterative technique.

The method presented in this thesis has been shown to provide a good theoretical model of the substrate-mounted cylindrical pillbox dielectric resonator, and furthermore, it has the advantage that, once the iterative procedure has been set up analytically, the actual numerical computation required to calculate the fundamental resonant frequency is very straightforward, and in fact requires less than nine seconds of CPU time on a mainframe computer to converge to the solution.

As a consequence of this research, the following theoretical areas are suggested for further research:

i) The continuum. It has been shown in chapter 7 that this may be included in the iterative expression, and it is obviously advisable to investigate this further in order to extend the applicability of the method.

ii) The surface integral. Although it has been demonstrated that this is of little consequence in determining the fundamental resonant frequency, inclusion of this integral would provide the full theoretical analysis of the dielectric resonator. Moreover, the surface integral is responsible for the difference between the TE and TM resonant modes, and thus this extension to the iterative method would enable the $TM_{01\delta}$ resonant frequency to be calculated.

iii) Higher order resonant modes. It was shown in chapter 4 that the iterative method can be used to calculate the higher resonant frequencies, and this extension to the method would evidently be of value.

iv) Generalisation to thick dielectric substrates. Currently, the iterative method has only been implemented for a mono-mode Green's function suitable for thin dielectric substrates. However, due to the linear nature of the integral operator, the inclusion of further surface waves will present no problems. The method hinges upon evaluating the relevant integrals separately for each surface wave, and then simply adding together the results once they have been re-expressed in terms of the original trial function.

v) The enclosed and isolated dielectric resonators. Since the basic integral equation is taken only over the resonator volume, a judicious choice of the Green's function enables this theoretical method to be applied to other physical situations. The enclosed resonator would require the Green's function valid inside the relevant enclosing structure, while the isolated case would be solved by using

the Green's function valid in free-space. Both of these Green's functions would, of course, need to be expressed in cylindrical co-ordinates.

vi) The Q-factor. Once the complete description of the dielectric resonator has been obtained, the quality factor may be calculated from the real and imaginary components of the resonant frequency, which represent the storage and leakage of energy, respectively, as shown in chapter 5. One result expected to emerge from such a study is that, for a momomode substrate, the Q of the fundamental mode will be high, but, if the substrate is thickened so that the first TE surface wave is also supported, then the Q will drop substantially. The reason for this is that it is seen that the $TE_{01\delta}$ resonant mode is the opposite polarisation to the fundamental slab mode, and thus coupling between the resonator and the substrate is low. However, once the TE surface wave is introduced, the coupling will increase dramatically, and thus the stored energy will easily be transferred from the resonator to the slab and so will be lost, leading to the reduction in the Q-factor.

vii) Coupling coefficient. It was mentioned in chapter 1 that besides the fundamental resonant frequency and the Q-factor, the coupling coefficient was a vital piece of information to microwave designers using dielectric resonators. Thus the development of a theoretical technique giving the coupling between two resonators, and also between a resonator and a guiding mechanism such as microstrip, is important.

REFERENCES

[1] T. Itoh and R.S. Rudokas, "New method for computing the resonant frequencies of dielectric resonators", IEEE Trans. Microwave Theory Tech., Vol.MTT-25, pp.52-54, January 1977.

APPENDIX A

The Vector Operator ∇ in Cylindrical Co-ordinates

The vector operator ∇ is defined in cylindrical co-ordinates r, θ, y as

$$\nabla = \hat{\rho} \frac{\partial}{\partial \rho} + \hat{\theta} \frac{\partial}{\partial \theta} + \hat{y} \frac{\partial}{\partial y} \tag{A.1}$$

where $\hat{\rho}$, $\hat{\theta}$, $\hat{y}$ are unit vectors in the radial, azimuthal, and axial directions, respectively, and may be applied to both scalar and vector functions. The gradient of a scalar, ϕ, is defined to be

$$\nabla\phi = \hat{\rho} \frac{\partial \phi}{\partial \rho} + \hat{\theta} \frac{\partial \phi}{\partial \theta} + \hat{y} \frac{\partial \phi}{\partial y} \tag{A.2}$$

whilst the rate of change of a vector field has two components. The first is known as the divergence of the vector field and is given by

$$\nabla . \underline{A} = \frac{1}{\rho} \frac{\partial}{\partial \rho} (\rho A_1) + \frac{1}{\rho} \frac{\partial A_2}{\partial \theta} + \frac{\partial A_3}{\partial y} \tag{A.3}$$

and the second is the curl (or rotation), given by

$$\nabla x \underline{A} = \hat{\rho}[\frac{1}{\rho} \frac{\partial A_3}{\partial \theta} - \frac{\partial A_2}{\partial y}] + \hat{\theta}[\frac{\partial A_1}{\partial y} - \frac{\partial A_3}{\partial \rho}] + \hat{y} [\frac{1}{\rho} \frac{\partial}{\partial \rho} (\rho A_2) - \frac{1}{\rho} \frac{\partial A_1}{\partial \theta}] \tag{A.4}$$

where the vector field $\underline{A}$ is written as

$$\underline{A} = \hat{\rho} A_1 + \hat{\theta} A_2 + \hat{y} A_3 \tag{A.5}$$

The divergence of the gradient of a scalar function is known as the Laplacian of the scalar and is

$$\nabla . (\nabla \phi) = \nabla^2 \phi = \frac{1}{\rho} \frac{\partial}{\partial \rho} (\rho \frac{\partial \phi}{\partial \rho}) + \frac{1}{\rho^2} \frac{\partial^2 \phi}{\partial \theta^2} + \frac{\partial^2 \phi}{\partial y^2} \tag{A.6}$$

The vector identities involving ∇ are identical for all co-ordinate systems, and some of the important results are given below.

$$\nabla.(\underline{A} + \underline{B}) = \nabla.\underline{A} + \nabla.\underline{B} \qquad (A.7)$$

$$\nabla x(\underline{A} + \underline{B}) = \nabla x\underline{A} + \nabla x\underline{B} \qquad (A.8)$$

$$\nabla(\phi\psi) = \phi\nabla\psi + \psi\nabla\phi \qquad (A.9)$$

$$\nabla x\nabla x\underline{A} = \nabla(\nabla.\underline{A}) - \nabla^2 A \qquad (A.10)$$

$$\nabla x(\nabla\phi) = 0 \qquad (A.11)$$

$$\nabla.(\nabla \times \underline{A}) = 0 \qquad (A.12)$$

$$\nabla x(\psi\underline{A}) = \psi\nabla \times \underline{A} - \underline{A} \times \nabla\psi \qquad (A.13)$$

APPENDIX B

Consideration of the Surface Integral over the Resonator Volume

In Section 3.3, the method of Green's functions was used to transform the differential equation for the scalar potential, ψ_r, within the resonator, into the integral equation (3.45),

$$\psi_r(\underline{x}) = (\varepsilon_r - \varepsilon_a)k_o^2 \iiint_{\text{resonator}} G_a(\underline{x},\underline{x}')\psi_r(\underline{x}')dV' + \iint_{\substack{\text{resonator}\\ \text{boundary}}} [G_a(\underline{x},\underline{x}') \frac{\partial \psi_r(\underline{x}')}{\partial n_r'} - \psi_r(\underline{x}') \frac{\partial G_a(\underline{x},\underline{x}')}{\partial n_r'}]dS' \quad (B.1)$$

Using the same method, integral equations for the scalar potentials in the slab and air regions may also be derived as

$$\iint_{\substack{\text{slab}\\ \text{boundary}}} [G_s(\underline{x},\underline{x}') \frac{\partial \psi_s(\underline{x}')}{\partial n_s'} - \psi_s(\underline{x}') \frac{\partial G_s(\underline{x},\underline{x}')}{\partial n_s'}] \, dS' = \iiint_{\text{slab}} \psi_s(\underline{x}')\delta(\underline{x} - \underline{x}')dV' \quad (B.2)$$

$$\iint_{\substack{\text{air}\\ \text{boundary}}} [G_a(\underline{x},\underline{x}') \frac{\partial \psi_a(\underline{x}')}{\partial n_a'} - \psi_a(\underline{x}') \frac{\partial G_a(\underline{x},\underline{x}')}{\partial n_a'}] \, dS' = \iiint_{\text{air}} \psi_a(\underline{x}')\delta(\underline{x} - \underline{x}')dV' \quad (B.3)$$

where n_s' and n_a' are the outward normals to the surfaces bounding the slab and air regions, respectively, as shown in two-dimensions in Figure B.1, where the dashed hemispherical boundary represents $x' \to \infty$.

Examination of this diagram shows clearly that the boundaries of both the resonator, and the dielectric slab at $y' = d$, are shared surface areas. Moreover, on these interfaces the outward normals to

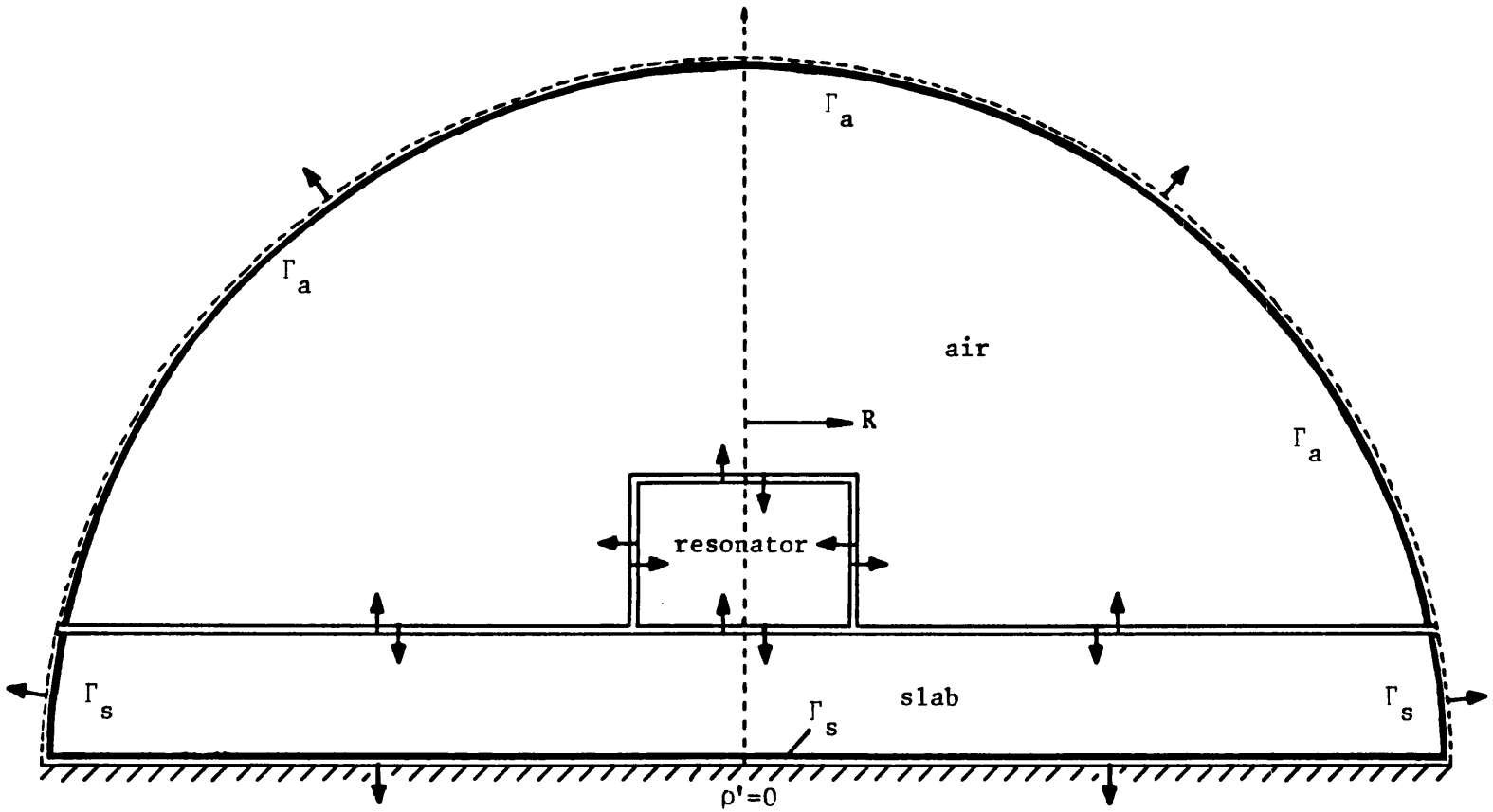

Figure B.1 Two-dimensional diagram of the substrate-mounted cylindrical dielectric resonator showing both the boundaries pertinent to the surface integrals, and the orientation of the outward normals

the adjacent regions are in opposite directions. Consequently, on the surfaces where both the potential functions, and the Green's functions, in the two adjacent regions are continuous, both in value and normal derivative, then addition of equations (B.1), (B.2) and (B.3) causes these surface integrals to vanish.

In this thesis, the magnetic and electric potentials are considered separately, and in Appendix C the possible discontinuity of these potentials on dielectric interfaces is investigated. One of the first conclusions drawn is that the boundary conditions on the cylindrical surface of the resonator cannot be satisfied by either the electric, or the magnetic, potential alone, unless that potential is θ-independent. Therefore, the analysis proceeds by considering the independent TE_{omn} and TM_{omn} modes, and it is found that the electric and magnetic potentials for these modes satisfy the boundary conditions in different manners. This results in the fact that the magnetic potential is continuous, both in value and normal derivative, on all the horizontal interfaces, but on the cylindrical surface of the resonator, although continuous in normal derivative, it has a discontinuity in value, as given by equation (C.25),

$$\psi_{ha} = \left(\frac{k_{\rho r}}{k_{\rho a}}\right)^2 \psi_{hr} \qquad (B.4)$$

where k_ρ is the radial wavenumber. However, the situation for the electric potential is more involved, and on the horizontal interfaces it is discontinuous, in the manner given by equation (C.26),

$$\frac{\partial \psi_{e1}}{\partial y} = \frac{\varepsilon_1}{\varepsilon_2} \frac{\partial \psi_{e2}}{\partial y} \qquad (B.5)$$

whilst on the cylindrical surface the potentials are discontinuous in the manner given in equation (C.27)

$$\psi_{ea} = \frac{\varepsilon_a}{\varepsilon_r} \left(\frac{k_{\rho r}}{k_{\rho a}}\right)^2 \psi_{er} \tag{B.6}$$

The application of these discontinuity relations, together with the fact that the source is completely contained within the resonator volume, leads to two different integral equations for the scalar potentials. In order to derive the following equations, it was assumed that the slab was excited into monomode operation, such that the Green's function satisfied the TM boundary conditions. This condition is valid for the analysis presented in the thesis, and is not an unreasonable assumption, for a grounded polystyrene slab waveguide 1 mm thick is monomode in operation up to 36 GHz.

The magnetic scalar potential, which gives the TE_{omn} modes, must satisfy the equation

$$\begin{aligned}
\psi_{hr} = {} & (\varepsilon_r - \varepsilon_a)k_o^2 \iiint_{\text{resonator}} G_a \psi_{hr} dV' \\
& + \frac{(k_{\rho r}^2 - k_{\rho a}^2)}{k_{\rho a}^2} \int_o^{2\pi} \int_d^{d+h} \psi_{hr} \frac{\partial G_a}{\partial \rho'} \, dy' d\theta' \\
& \qquad \rho' = R \\
& - \frac{(\varepsilon_s - \varepsilon_a)}{\varepsilon_a} \left\{ \int_o^{2\pi} \int_o^{R} \psi_{hr} \frac{\partial G_a}{\partial y'} \rho' d\rho' d\theta' \right. \\
& \qquad y' = d \\
& \left. + \int_o^{2\pi} \int_R^{\infty} \psi_{ha} \frac{\partial G_a}{\partial y'} \rho' d\rho' d\theta' \right\} \\
& \qquad y' = d \\
& + \iint_{\Gamma_s} \left[G_s \frac{\partial \psi_{hs}}{\partial n_s'} - \psi_{hs} \frac{\partial G_s}{\partial n_s'} \right] dS' \\
& + \iint_{\Gamma_a} \left[G_a \frac{\partial \psi_{ha}}{\partial n_a'} - \psi_{ha} \frac{\partial G_a}{\partial n_a'} \right] dS'
\end{aligned} \tag{B.7}$$

while the electric potential, which gives the TM_{omn} modes, must satisfy the equation

$$\psi_{er} = (\varepsilon_r - \varepsilon_a)k_o^2 \iiint_{\text{resonator}} G_a \psi_{er} dV'$$

$$+ \frac{(\varepsilon_a k_{\rho r}^2 - \varepsilon_r k_{\rho a}^2)}{\varepsilon_r k_{\rho a}^2} \int_o^{2\pi} \int_d^{d+h} \psi_{er} \frac{\partial G_a}{\partial \rho'} \, dy' d\theta' \Big|_{\rho'=R}$$

$$+ \frac{(\varepsilon_r - \varepsilon_a)}{\varepsilon_r} \int_o^{2\pi} \int_o^{R} G_a \frac{\partial \psi_{er}}{\partial y'} \rho' d\rho' d\theta' \Big|_{y'=d+h}$$

$$+ \frac{(\varepsilon_s - \varepsilon_r)}{\varepsilon_r} \int_o^{2\pi} \int_o^{R} G_a \frac{\partial \psi_{er}}{\partial y'} \rho' d\rho' d\theta' \Big|_{y'=d}$$

$$- \frac{(\varepsilon_s - \varepsilon_a)}{\varepsilon_a} \int_o^{2\pi} \int_o^{R} \psi_{er} \frac{\partial G_a}{\partial y'} \rho' d\rho' d\theta' \Big|_{y'=d}$$

$$+ \frac{(\varepsilon_s - \varepsilon_a)}{\varepsilon_a} \int_o^{2\pi} \int_R^{\infty} \left[G_a \frac{\partial \psi_{ea}}{\partial y'} - \psi_{ea} \frac{\partial G_a}{\partial y'}\right] \rho' d\rho' d\theta' \Big|_{y'=d}$$

$$+ \iint_{\Gamma_s} \left[G_s \frac{\partial \psi_{es}}{\partial n_s'} - \psi_{es} \frac{\partial G_s}{\partial n_s'}\right] dS'$$

$$+ \iint_{\Gamma_a} \left[G_a \frac{\partial \psi_{ea}}{\partial n_a'} - \psi_{ea} \frac{\partial G_a}{\partial n_a'}\right] dS' \qquad \text{(B.8)}$$

where the arguments of the functions are obvious, and the surfaces Γ_s and Γ_a are as defined in Figure B1.

Further simplification of equations (B.7) and (B.8) is afforded by examining the surface integrals along the boundaries Γ_s and Γ_a. The choice of the Green's function of the slab waveguide is such that

$$\lim_{\underline{x}'\to\infty}\left\{G(\underline{x},\underline{x}')\right\} = 0 \tag{B.9}$$

where this limit is approached faster than x^{-1} tends to zero, and

$$\lim_{\underline{x}'\to\infty}\left\{\frac{\partial G(\underline{x},\underline{x}')}{\partial n'}\right\} = 0 \tag{B.10}$$

so that the surface integral, as $\underline{x}' \to \infty$, gives no contribution. Furthermore, on the metal ground plane, the boundary conditions (3.37) must be satisfied, and so the equations (B.7) and (B.8) become

$$\begin{aligned}
\psi_{hr} = {} & (\varepsilon_r - \varepsilon_a)k_o^2 \iiint_{\text{resonator}} G_a \psi_{hr}\, dV' \\
& + \frac{(k_{\rho r}^2 - k_{\rho a}^2)}{k_{\rho a}^2} \int_o^{2\pi}\int_d^{d+h}_{\rho'=R} \psi_{hr}\frac{\partial G_a}{\partial \rho'}\, dy'd\theta' \\
& - \frac{(\varepsilon_s - \varepsilon_a)}{\varepsilon_a}\left\{\int_o^{2\pi}\int_o^{R}_{y'=d} \psi_{hr}\frac{\partial G_a}{\partial y'}\rho' d\rho' d\theta'\right. \\
& \left. + \int_o^{2\pi}\int_R^{\infty}_{y'=d} \psi_{ha}\frac{\partial G_a}{\partial y'}\rho' d\rho' d\theta'\right\} \\
& + \int_o^{2\pi}\int_o^{\infty}_{y'=0} G_s \frac{\partial \psi_{hs}}{\partial y'}\rho' d\rho' d\theta'
\end{aligned} \tag{B.11}$$

$$\begin{aligned}
\psi_{er} = {} & (\varepsilon_r - \varepsilon_a)k_o^2 \iiint_{\text{resonator}} G_a \psi_{er}\, dV' \\
& + \frac{(\varepsilon_a k_{\rho r}^2 - \varepsilon_r k_{\rho a}^2)}{\varepsilon_r k_{\rho a}^2} \int_o^{2\pi}\int_d^{d+h}_{\rho'=R} \psi_{er}\frac{\partial G_a}{\partial \rho'}\, dy'd\theta' \\
& + \frac{(\varepsilon_r - \varepsilon_a)}{\varepsilon_r} \int_o^{2\pi}\int_o^{R}_{y'=d+h} G_a \frac{\partial \psi_{er}}{\partial y'}\rho' d\rho' d\theta'
\end{aligned}$$

$$+\frac{(\varepsilon_s-\varepsilon_r)}{\varepsilon_r}\int_0^{2\pi}\int_0^{R} G_a\,\frac{\partial\psi_{er}}{\partial y'}\,\rho'd\rho'd\theta' \qquad y'=d$$

$$-\frac{(\varepsilon_s-\varepsilon_a)}{\varepsilon_a}\int_0^{2\pi}\int_0^{R} \psi_{er}\,\frac{\partial G_a}{\partial y'}\,\rho'd\rho'd\theta' \qquad y'=d$$

$$+\frac{(\varepsilon_s-\varepsilon_a)}{\varepsilon_a}\int_0^{2\pi}\int_R^{\infty} \left[G_a\,\frac{\partial\psi_{ea}}{\partial y'}-\psi_{ea}\,\frac{\partial G_a}{\partial y'}\right]\rho'd\rho'd\theta' \qquad y'=d \qquad \text{(B.12)}$$

The resulting difference in the two integral equations (B.11) and (B.12) is not really a surprise, since it was pointed out in section 3.2 that the independent TE_{omn} and TM_{omn} resonant modes must have different resonant frequencies. It is clear from these equations that it is the surface integrals which produce the different results for the resonant frequencies of the two transverse families of modes, and thus it is useful to seek a physical interpretation for the surface integral, in order to discover its relationship to the volume integral.

Stratton [1] has analysed the various terms arising from the use of Green's second identity, as performed in Chapter 3 of this thesis. Considering equation (B.1), he has demonstrated that the volume integral represents the contribution from sources within the resonator volume, while the surface integral may be considered to account for all the sources exterior to the resonator. It is now necessary, therefore, to investigate the causes of these sources in order to understand the relationship between the volume and the surface integrals in equation (B.1).

The Green's function solution to the differential scalar potential equation is a reciprocal procedure. The determination of the potential function at a point $\underline{x}'$ within the resonator is accomplished by placing

a unit source at that point and examining its effect upon the dielectric slab waveguide. The distribution of such sources within the resonator is then found that gives the appropriate scalar potential for the dielectric slab waveguide. Consequently, by reciprocity, the scalar potential distribution within the resonator has been obtained when the dielectric slab is supporting a transmitted mode excited by some external source.

Thus, the sources within the resonator volume are accounted for by the unit sources used in the Green's function approach. However, the nature of the external sources is still unclear. Considering, for a moment, the presence of sources within a dielectric volume, it is known that, on the surface of this volume, layers of charge are induced due to polarisation caused by the internal sources. Thus, the surface integral of equation (B.1) is calculating the effect, upon the potential within the resonator, from the external surface charges induced by the internal equivalent sources.

This fact is clearly shown in equations (B.11) and (B.12), where the surface integral over the resonator boundary has been expanded, and it is seen that contributions only arise from the dielectric boundaries. It is further apparent that the transverse electric modes, which are represented by the magnetic potential of equation (B.11), are affected by these surface charges to a much lesser extent than are the transverse magnetic modes, whose electric potential satisfies equation (B.12), where contributions are received from every dielectric interface.

Consequently, it is reasonable to suppose that, for the TE polarisation, solving the reduced integral equation,

$$\psi_{hr}(\underline{x}) = (\varepsilon_r - \varepsilon_a)k_o^2 \iiint_{\text{resonator}} G_a(\underline{x},\underline{x}')\psi_{hr}(\underline{x}')dV' \qquad (B.13)$$

where the surface integral has been ignored, will lead to close approximations to the TE_{omn} resonances. This is further justified by the fact that the surface charges are caused by the equivalent sources, and hence the effect of the surface integral in equation (B.1) will be second order with respect to the contribution of the volume integral.

REFERENCES

[1] J.A. Stratton, "*Electromagnetic Theory*". New York: McGraw-Hill, 1941, pp.192-193.

APPENDIX C

Discontinuity of the Potential Functions at Dielectric Interfaces

The two scalar potential functions, ψ_h and ψ_e, are independent, and they excite TE and TM modes with respect to the y-direction respectively. Within a uniform region of space, the electromagnetic fields are continuous, and thus the potential functions are continuous. However, at an interface between two uniform regions of differing dielectric constant, the following boundary conditions must be satisfied,

$$\underline{n} \times \underline{E}_1 = \underline{n} \times \underline{E}_2 \tag{C.1a}$$

$$\underline{n} \cdot (\varepsilon_1 \underline{E}_1) = \underline{n} \cdot (\varepsilon_2 \underline{E}_2) \tag{C.1b}$$

$$\underline{n} \times \underline{H}_1 = \underline{n} \times \underline{H}_2 \tag{C.1c}$$

$$\underline{n} \cdot \underline{H}_1 = \underline{n} \cdot \underline{H}_2 \tag{C.1d}$$

where the subscripts 1 and 2 represent the two adjacent regions, and $\underline{n}$ is the normal to the interface. It is clearly seen that equation (C.1b) shows that the normal electric field is discontinuous across the interface due to the difference in relative dielectric constant, and it is now necessary to discover the effect this has upon the scalar potential functions.

C.1 The magnetic scalar potential

The electromagnetic field components produced by the magnetic scalar potential are given by equations (3.21) and (3.22),

$$E_\rho = \frac{1}{\rho} \frac{\partial \psi_h}{\partial \theta} \tag{C.2a}$$

$$E_\theta = - \frac{\partial \psi_h}{\partial \rho} \tag{C.2b}$$

$$E_y = 0 \tag{C.2c}$$

$$H_\rho = \frac{-1}{j\omega\mu_o} \frac{\partial^2\psi_h}{\partial\rho\partial y} \qquad (C.2d)$$

$$H_\theta = \frac{-1}{j\omega\mu_o} \frac{1}{\rho} \frac{\partial^2\psi_h}{\partial\theta\partial y} \qquad (C.2e)$$

$$H_y = \frac{-1}{j\omega\mu_o} \left[\frac{\partial^2\psi_h}{\partial y^2} + \varepsilon_{rel} k_o^2 \psi_h \right] \qquad (C.2f)$$

The substrate-mounted cylindrical dielectric resonator, as shown in Figure C.1 , has two types of dielectric interface. The first is transverse to the y-direction, at y = d and at y = d + h, and it is seen from Appendix D that the magnetic potential function, and its normal derivative, are always continuous across such an interface. The second type of interface is on the cylindrical surface of the resonator. It is well-known [1],[2], from the analysis of a cylindrical dielectric rod waveguide, that the boundary conditions on such an interface can only be satisfied by pure TE or TM modes if the field is independent of the angular co-ordinate θ. All modes with an angular dependence are formed from a combination of a TE and a TM mode and are classified as hybrid EH or HE modes, depending on whether the TM or TE mode predominates, respectively.

Since the solution of the resonator problem is formulated in terms of independent transverse modes, in order to solve for the $TE_{01\delta}$ resonance, it is only the circularly symmetrical modes with

$$\frac{\partial}{\partial\theta} = 0 \qquad (C.3)$$

that will be considered henceforward. For such a TE mode, the field equations (C.2) reduce to

$$E_\rho = E_y = H_\theta = 0 \qquad (C.4a)$$

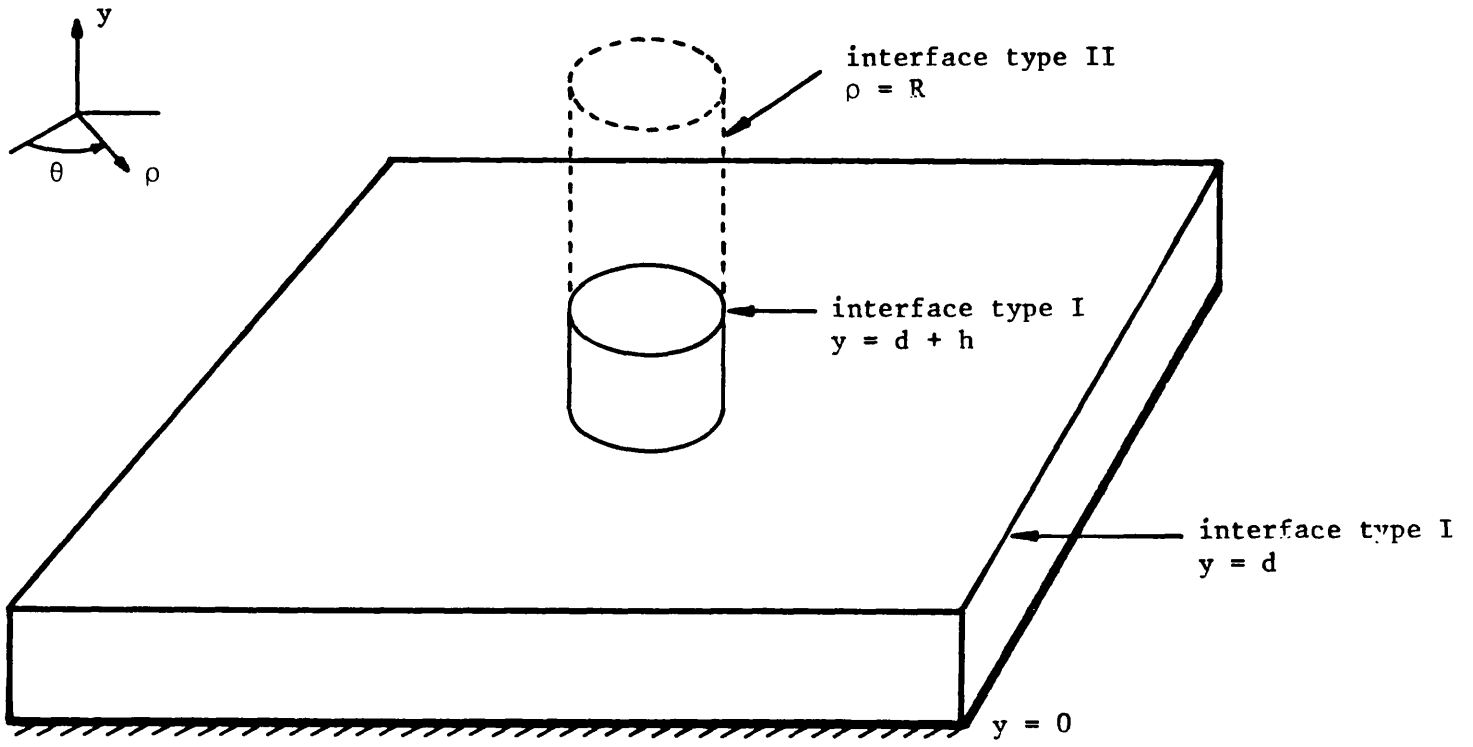

Figure C.1 The substrate-mounted cylindrical dielectric resonator showing the two different types of dielectric interface

$$E_\theta = -\frac{\partial \psi_h}{\partial \rho} \qquad \text{(C.4b)}$$

$$H_\rho = \frac{-1}{j\omega\mu_o} \frac{\partial^2 \psi_h}{\partial \rho \partial y} \qquad \text{(C.4)}$$

$$H_y = \frac{-1}{j\omega\mu_o} \left[\frac{\partial^2 \psi_h}{\partial y^2} + \varepsilon_{rel} k_o^2 \psi_h \right] \qquad \text{(C.4d)}$$

where ψ_h must satisfy the scalar differential equation (3.35)

$$\nabla^2 \psi_h + \varepsilon_{rel} k_o^2 \psi_h = 0 \qquad \text{(C.4e)}$$

The analysis proceeds by assuming a separable solution for ψ_h, of the form

$$\psi_{hb} = A_b B_{ob}(k_{\rho b}\rho)\, \Psi_b(y) \qquad \text{(C.5)}$$

where $B_o(x)$ is a linear combination of cylindrical Bessel functions of order zero and argument x, and $\Psi_b(y)$ is the solution to the equation

$$\left(\frac{\partial^2}{\partial y^2} + k_{yb}^2\right) \Psi_b(y) = 0 \qquad \text{(C.6)}$$

where the subscript b takes the value r or a depending upon whether the resonator or air region, respectively, is being considered. The radial and axial wavenumbers are related through the equation

$$k_{\rho b}^2 = \varepsilon_b k_o^2 - k_{yb}^2 \qquad \text{(C.7)}$$

and the boundary conditions (C.1) lead to the relationships

$$A_r k_{\rho r} B'_{or}(k_{\rho r}R)\Psi_r(y) = A_a k_{\rho a} B'_{oa}(k_{\rho a}R)\Psi_a(y) \qquad \text{(C.8a)}$$

$$A_r k_{\rho r} B'_{or}(k_{\rho r}R) \frac{\partial \Psi_r(y)}{\partial y} = A_a k_{\rho a} B'_{oa}(k_{\rho a}R) \frac{\partial \Psi_a(y)}{\partial y} \qquad \text{(C.8b)}$$

$$A_r B_{or}(k_{\rho r}R) k_{\rho r}^2 \Psi_r(y) = A_a B_{oa}(k_{\rho a}R) k_{\rho a}^2 \Psi_a(y) \qquad \text{(C.8c)}$$

where the prime indicates differentiation with respect to the argument. In order to satisfy these relations (C.8) for all y on $\rho = R$, it is evident that the eigenmode $\Psi(y)$ must be identical in both the resonator and air regions, and thus $k_{yr} = k_{ya}$, so that equations (C.8) reduce to

$$A_r k_{\rho r} B'_{or}(k_{\rho r}R) = A_a k_{\rho a} B'_{oa}(k_{\rho a}R) \tag{C.9a}$$

$$A_r k^2_{\rho r} B_{or}(k_{\rho r}R) = A_a k^2_{\rho a} B_{oa}(k_{\rho a}R) \tag{C.9b}$$

Consequently, the constants A_r and A_a are related by

$$A_a = A_r \left(\frac{k_{\rho r}}{k_{\rho a}}\right)^2 \frac{B_{or}(k_{\rho r}R)}{B_{oa}(k_{\rho a}R)} \tag{C.10}$$

and the radial wavenumbers can be obtained by solving the coupled equations

$$\frac{B'_{or}(k_{\rho r}R)}{k_{\rho r}B_{or}(k_{\rho r}R)} = \frac{B'_{oa}(k_{\rho a}R)}{k_{\rho a}B_{oa}(k_{\rho a}R)} \tag{C.11a}$$

$$k^2_{\rho r} - k^2_{\rho a} = (\varepsilon_r - \varepsilon_a)k_o^2 \tag{C.11b}$$

Therefore, the magnetic potential may be written as

$$\psi_{hr} = A_r B_{or}(k_{\rho r}\rho)\Psi(y) \qquad \rho \leq R \tag{C.12a}$$

$$\psi_{ha} = A_r \left(\frac{k_{\rho r}}{k_{\rho a}}\right)^2 \frac{B_{or}(k_{\rho r}R)}{B_{oa}(k_{\rho a}R)} \cdot B_{oa}(k_{\rho a}\rho)\Psi(y) \qquad \rho \geq R \tag{C.12b}$$

At $\rho = R$, it is seen that

$$\psi_{hr} = A_r B_{or}(k_{\rho r}R)\Psi(y) \tag{C.13a}$$

$$\psi_{ha} = A_r \left(\frac{k_{\rho r}}{k_{\rho a}}\right)^2 B_{or}(k_{\rho r}R)\Psi(y) \tag{C.13b}$$

and thus the magnetic potential function is discontinuous, at $\rho = R$, as

$$\psi_{ha} = \left(\frac{k_{\rho r}}{k_{\rho a}}\right)^2 \psi_{hr} \qquad (C.14)$$

However, differentiation of equations (C.12) with respect to the radial direction, together with the use of equation (C.11a), shows that the normal derivative of ψ_h on the cylindrical surface is continuous.

C.2 The electric scalar potential

It is shown in Appendix D that, on the dielectric interfaces transverse to the y-direction, the electric scalar potential, ψ_e, is continuous, whereas its normal derivative is found to be discontinuous as

$$\frac{\partial \psi_{e1}}{\partial y} = \frac{\varepsilon_1}{\varepsilon_2} \frac{\partial \psi_{e2}}{\partial y} \qquad (C.15)$$

where the subscripts 1 and 2 differentiate between the two adjacent regions.

Considering now the second type of dielectric interface at $\rho = R$, the field components for the TM_{omn} modes are obtained from equations (3.32) and (3.33), and are

$$E_\rho = \frac{1}{j\omega\varepsilon} \frac{\partial^2 \psi_e}{\partial \rho \partial y} \qquad (C.16a)$$

$$E_y = \frac{1}{j\omega\varepsilon} \left[\frac{\partial^2 \psi_e}{\partial y^2} + \varepsilon_{rel} k_o^2 \psi_e \right] \qquad (C.16b)$$

$$H_\theta = - \frac{\partial \psi_e}{\partial \rho} \qquad (C.16c)$$

$$E_\theta = H_\rho = H_y = 0 \qquad (C.16d)$$

and assuming a separable solution, that satisfies the scalar differential equation (3.35), of the form

$$\psi_{eb} = C_b B_{ob}(k_{\rho b}\rho)\Psi_b(y) \tag{C.17}$$

the boundary conditions (C.1) lead to the relations

$$C_r k_{\rho r} B'_{or}(k_{\rho r}R) \frac{\partial \Psi_r(y)}{\partial y} = C_a k_{\rho a} B'_{oa}(k_{\rho a}R) \frac{\partial \Psi_a(y)}{\partial y} \tag{C.18a}$$

$$\frac{C_r}{\varepsilon_r} B_{or}(k_{\rho r}R)k^2_{\rho r}\Psi_r(y) = \frac{C_a}{\varepsilon_a} B_{oa}(k_{\rho a}R)k^2_{\rho a}\Psi_a(y) \tag{C.18b}$$

$$C_r k_{\rho r} B'_{or}(k_{\rho r}R)\Psi_r(y) = C_a k_{\rho a} B'_{oa}(k_{\rho a}R)\Psi_a(y) \tag{C.18c}$$

Continuity of these relations for all y on $\rho = R$ means that the y-directed eigenmode must be identical in both the resonator and air regions, and so equations (C.18) become

$$C_r k_{\rho r} B'_{or}(k_{\rho r}R) = C_a k_{\rho a} B'_{oa}(k_{\rho a}R) \tag{C.19a}$$

$$\frac{C_r}{\varepsilon_r} k^2_{\rho r} B_{or}(k_{\rho r}R) = \frac{C_a}{\varepsilon_a} k^2_{\rho a} B_{oa}(k_{\rho a}R) \tag{C.19b}$$

and thus

$$C_a = C_r\left(\frac{\varepsilon_a}{\varepsilon_r}\right)\left(\frac{k_{\rho r}}{k_{\rho a}}\right)^2 \frac{B_{or}(k_{\rho r}R)}{B_{oa}(k_{\rho a}R)} \tag{C.20}$$

and the radial wavenumbers may be obtained by solving the coupled equations

$$\frac{\varepsilon_r B'_{or}(k_{\rho r}R)}{k_{\rho r} B_{or}(k_{\rho r}R)} = \frac{\varepsilon_a B'_{oa}(k_{\rho a}R)}{k_{\rho a} B_{oa}(k_{\rho a}R)} \tag{C.21a}$$

$$k^2_{\rho r} - k^2_{\rho a} = (\varepsilon_r - \varepsilon_a)k^2_o \tag{C.21b}$$

Therefore, the electric potential may be written as

$$\psi_{er} = C_r B_{or}(k_{\rho r}\rho)\Psi(y) \qquad \rho \leq R \qquad \text{(C.22a)}$$

$$\psi_{ea} = C_r \left(\frac{\varepsilon_a}{\varepsilon_r}\right)\left(\frac{k_{\rho r}}{k_{\rho a}}\right)^2 \frac{B_{or}(k_{\rho r}R)}{B_{oa}(k_{\rho a}R)} B_{oa}(k_{\rho a}\rho)\Psi(y) \qquad \rho \geq R \qquad \text{(C.22b)}$$

At $\rho = R$, it seen that

$$\psi_{er} = C_r B_{or}(k_{\rho r}R)\Psi(y) \qquad \text{(C.23a)}$$

$$\psi_{ea} = C_r \left(\frac{\varepsilon_a}{\varepsilon_r}\right)\left(\frac{k_{\rho r}}{k_{\rho a}}\right)^2 B_{or}(k_{\rho r}R)\Psi(y) \qquad \text{(C.23b)}$$

and thus the electric potential function is discontinuous, at $\rho = R$, as

$$\psi_{ea} = \frac{\varepsilon_a}{\varepsilon_r}\left(\frac{k_{\rho r}}{k_{\rho a}}\right)^2 \psi_{er} \qquad \text{(C.24)}$$

However, differentiation of equations (C.22) with respect to the radial direction, together with the use of equation (C.21a), shows that the normal derivative of ψ_e at the cylindrical surface is continuous.

C.3 Summary of results

It has been shown that, for independent TE and TM modes in the cylindrical dielectric resonator, the fields must be rotationally symmetric, and thus the θ-variation must be zero.

Within the situation of the substrate-mounted cylindrical pillbox dielectric resonator, the magnetic scalar potential ψ_h, which produces the TE_{omn} modes, has been shown to have a discontinuity, at $\rho = R$, of the form

$$\psi_{ha} = \left(\frac{k_{\rho r}}{k_{\rho a}}\right)^2 \psi_{hr} \qquad \text{(C.25)}$$

while the normal derivative remains continuous. At all other points within the structure, ψ_h, and its normal derivative, are continuous.

The electric scalar potential ψ_e, which produces the TM_{omn} modes has been shown to have discontinuities in its normal derivative, at the interfaces y = d and y = d + h, of the form

$$\frac{\partial \psi_{e1}}{\partial y} = \frac{\varepsilon_1}{\varepsilon_2} \frac{\partial \psi_{e2}}{\partial y} \tag{C.26}$$

and at the interface $\rho = R$, the potential function is discontinuous as

$$\psi_{ea} = \frac{\varepsilon_a}{\varepsilon_r} \left(\frac{k_{\rho r}}{k_{\rho a}} \right)^2 \psi_{er} \tag{C.27}$$

At all other points within the structure, ψ_e and its normal derivative are continuous.

REFERENCES

[1] R.E. Collin, "*Field Theory of Guided Waves*". New York: McGraw-Hill, 1960, pp.480-483.

[2] R.F. Harrington, "*Time-Harmonic Electromagnetic Fields*". New York: McGraw-Hill, 1961, pp.219-222.

APPENDIX D

The Derivation of the y-directed Orthonormal Eigenmodes of a Dielectric Slab Waveguide

In section 3.4, it is shown that the required Green's functions for the grounded dielectric slab waveguide can be determined by combining the appropriate two-dimensional Green's function with the y-directed orthonormal eigenmodes of the slab waveguide. In order to determine these eigenmodes, it is necessary to consider the situation in terms of y-directed potential functions, Φ_s and Φ_a in the slab and air regions respectively. TE and TM fields are therefore determined by magnetic and electric scalar potentials that must satisfy

$$\nabla^2\Phi_s + \varepsilon_s k_o^2 \Phi_s = 0 \qquad \text{in the slab} \qquad \text{(D.1)}$$

$$\nabla^2\Phi_a + \varepsilon_a k_o^2 \Phi_a = 0 \qquad \text{in the air} \qquad \text{(D.2)}$$

where Φ represents either the magnetic or electric scalar potential.

Expanding the Laplacian, ∇^2, in cylindrical co-ordinates, and assuming a separable solution of the form

$$\Phi_b(\underline{x}) = R_b(\rho)L_b(\theta)\Psi_b(y) \qquad \text{(D.3)}$$

where b takes either the value s or a depending upon the region under consideration, gives

$$\frac{R_b''}{R_b} + \frac{1}{\rho}\frac{R_b'}{R_b} + \frac{1}{\rho^2}\frac{L_b''}{L_b} + \frac{\Psi_b''}{\Psi_b} + \varepsilon_b k_o^2 = 0 \qquad \text{(D.4)}$$

where the prime indicates differentiation with respect to the argument.

In order that equation (D.4) is satisfied for all positions (ρ,θ,y) it is found that the fourth term must be independent of position, and so

$$\frac{\Psi_b''}{\Psi_b} = -k_{yb}^2 \tag{D.5}$$

and equation (D.4) becomes

$$\rho^2 \frac{R_b''}{R_b} + \rho \frac{R_b'}{R_b} + \frac{L_b''}{L_b} + \rho^2(\varepsilon_b k_o^2 - k_{yb}^2) = 0 \tag{D.6}$$

In a similar fashion, it is found that

$$\frac{L_b''}{L_b} = -q_b^2 \tag{D.7}$$

and equation (D.6) becomes the Bessel differential equation of order q,

$$\rho^2 R_b'' + \rho R_b' + (\rho^2 k_{\rho b}^2 - q_b^2) R_b = 0 \tag{D.8}$$

where

$$k_{\rho b}^2 = \varepsilon_b k_o^2 - k_{yb}^2 \tag{D.9}$$

On the dielectric boundaries, the electromagnetic fields must satisfy the following conditions:

At y = 0

$$\hat{y} \times \underline{E}_s = 0 \tag{D.10a}$$

$$\hat{y} \cdot \underline{H}_s = 0 \tag{D.10b}$$

At y = d

$$\hat{y} \times \underline{E}_s = \hat{y} \times \underline{E}_a \tag{D.11a}$$

$$\hat{y} \cdot (\varepsilon_s \underline{E}_s) = \hat{y} \cdot (\varepsilon_a \underline{E}_a) \tag{D.11b}$$

$$\hat{y} \times \underline{H}_s = \hat{y} \times \underline{H}_a \tag{D.11c}$$

$$\hat{y} \cdot \underline{H}_s = \hat{y} \cdot \underline{H}_a \tag{D.11d}$$

where $\hat{y}$ is a unit vector in the y-direction. Applying these boundary conditions determines that the radial and circumferential components of the scalar potentials are identical in the two regions, and are given by

$$R(\rho) = \Lambda B_q(k_\rho \rho) \tag{D.12}$$

$$L(\theta) = T \cos(q\theta) + \Delta \sin(q\theta) \tag{D.13}$$

where $B_n(x)$ represents a linear combination of cylindrical Bessel functions of order n and argument x, and Λ, T, and Δ are constants.

The solution for the y-directed component of the scalar potentials is not quite as straightforward, since the magnetic and electric potentials satisfy the boundary conditions in different manners. In addition there are two distinct types of solutions that satisfy the requirements imposed by equations (D.1) to (D.11).

The first type of wave that propagates through the dielectric slab is known as a surface wave, and has the restriction that its energy in the air region must decay exponentially away from the dieletric interface. For such waves, it is found that only certain pairs of values of the y-directed wavenumbers satisfy the boundary conditions. Consequently, the first type of solution, known also as the bound modes, consists of a discrete set of y-directed eigenmodes.

However, if the condition of exponential energy decay outside the dielectric substrate is not applied, but instead the energy is allowed to radiate subject to the condition that it is finite at infinity, then it is found that all real values of the y-directed wavenumber in the air region will satisfy the boundary conditions. In order to satisfy the above energy restriction, these radiation modes must be written as an integral over the continuous spectrum of the wavenumber χ, and thus the general form of the y-directed component of the potential function is

$$\Psi(y) = \sum_n Y_n(y) + \int_0^\infty Y(\chi, y) d\chi \tag{D.14}$$

The particular functions $Y_n(y)$ and $Y(\chi,y)$ have to be determined for the magnetic and electric potentials.

D.1 The magnetic potential

The bound modes require that the discrete y-directed wavenumber in the air region is imaginary, and, since the magnetic potential produces a TE field, according to equations (3.21) and (3.22), application of the boundary conditions (D.10) leads to the discrete modes being

$$Y_{hs}(y) = B_n \sin(k_{yn}y) \tag{D.15a}$$

$$Y_{ha}(y) = \alpha_n \exp(-\gamma_n y) \tag{D.15b}$$

where k_{yn} and γ_n are the y-directed wavenumbers in the slab and air regions respectively. The remaining boundary conditions (D.11) produce the relations

$$B_n \sin(k_{yn}d) = \alpha_n \exp(-\gamma_n d) \tag{D.16a}$$

$$k_{yn}B_n \cos(k_{yn}d) = -\gamma_n\alpha_n \exp(-\gamma_n d) \tag{D.16b}$$

$$(\varepsilon_s k_o^2 - k_{yn}^2)B_n \sin(k_{yn}d) = (\varepsilon_a k_o^2 + \gamma_n^2)\alpha_n \exp(-\gamma_n d) \tag{D.16c}$$

from which it is found that

$$\alpha_n = B_n \sin(k_{yn}d) \exp(\gamma_n d) \tag{D.17}$$

and the wavenumbers k_{yn} and γ_n are linked through the transcendental equation

$$k_{yn} \cot(k_{yn}d) = -\gamma_n \tag{D.18a}$$

and also satisfy

$$k_{yn}^2 + \gamma_n^2 = (\varepsilon_s - \varepsilon_a)k_o^2 \tag{D.18b}$$

Therefore equations (D.15) become

$$Y_{hs} = B_n \sin (k_{yn} y) \qquad \text{(D.19a)}$$

$$Y_{ha} = B_n \sin (k_{yn} d) \exp [- \gamma_n (y - d)] \qquad \text{(D.19b)}$$

The radiation modes have solutions outside and inside the substrate that may be written

$$Y_{hs}(\chi, y) = A_{hc} \cos (\sigma y) + B_{hc} \sin (\sigma y) \qquad \text{(D.20a)}$$

$$Y_{ha}(\chi, y) = \alpha_{hc} \cos (\chi y) + \beta_{hc} \sin (\chi y) \qquad \text{(D.20b)}$$

where the subscript c indicates that the continuous spectrum is being considered, and σ and χ are the y-directed continuum wavenumbers in the slab and air regions respectively.

On the ground plane, the boundary conditions (D.10) require that A_{hc} be zero, and the boundary conditions at y = d give

$$B_{hc} \sin (\sigma d) = \alpha_{hc} \cos (\chi d) + \beta_{hc} \sin (\chi d) \qquad \text{(D.21a)}$$

$$\sigma B_{hc} \cos (\sigma d) = \chi \beta_{hc} \cos (\chi d) - \chi \alpha_{hc} \sin (\chi d) \qquad \text{(D.21b)}$$

$$\sigma^2 - \chi^2 = (\varepsilon_s - \varepsilon_a) k_o^2 \qquad \text{(D.21c)}$$

Hence

$$\alpha_{hc} = B_{hc} \left[\sin (\sigma d) \cos (\chi d) - \frac{\sigma}{\chi} \cos (\sigma d) \sin (\chi d)\right] \qquad \text{(D.22a)}$$

$$\beta_{hc} = B_{hc} \left[\sin (\sigma d) \sin (\chi d) + \frac{\sigma}{\chi} \cos (\sigma d) \cos (\chi d)\right] \qquad \text{(D.22b)}$$

and the equations (D.20) become

$$Y_{hs}(\chi, y) = B_{hc} \sin (\sigma y) \qquad \text{(D.23a)}$$

$$Y_{ha}(\chi, y) = B_{hc} \left\{\sin (\sigma d) \cos[\chi(y - d)] + \frac{\sigma}{\chi} \cos(\sigma d) \sin[\chi(y - d)]\right\} \qquad \text{(D.23b)}$$

Examination of equations (D.23) and (D.19) together with equation (D.18a), reveals that the boundary conditions for the TE field have produced a magnetic potential function that is continuous both in value and in derivative across the dielectric interface at y = d.

In order to complete the derivation of the y-directed component of the magnetic potential function, it is necessary to determine the value of the coefficients B_n and B_{hc} by normalising $\Psi(y)$ over the range of y. The relevant orthogonality relations are given in Appendix E, and it is seen that for the TE mode it is necessary to set

$$\int_o^\infty Y_{hn}^2(y)dy = 1 \qquad (D.24a)$$

and

$$\int_o^\infty Y_h(X,y)Y_h(X',y)dy = \delta(X - X') \qquad (D.24b)$$

Substitution of equations (D.19) into equation (D.24a) leads to

$$B_n^2 \int_o^d \sin^2(k_{yn}y)dy + B_n^2 \sin^2(k_{yn}d) \int_d^\infty \exp[-2\gamma_n(y - d)]dy = 1 \qquad (D.25)$$

which reduces, through use of equation (D.18a), to give

$$B_n = \left[\frac{2}{d + 1/\gamma_n}\right]^{\frac{1}{2}} \qquad (D.26)$$

The evaluation of the normalisation detailed in equation (D.24b) is more complex, but, according to the procedure detailed by Shevchenko [1], this operation is equivalent to setting

$$\alpha_{hc}^2 + \beta_{hc}^2 = \frac{2}{\pi} \qquad (D.27)$$

from which it is found that

$$B_{hc} = \left[\frac{2}{\pi[\sin^2(\sigma d) + \left(\frac{\sigma}{\chi}\right)^2 \cos^2(\sigma d)]} \right]^{\frac{1}{2}} \qquad (D.28)$$

D.2 The electric potential

The electric scalar potential produces a field that is transverse magnetic to the y-direction according to the equations (3.32) and (3.33). Consequently, application of the boundary conditions (D.10) leads to the discrete modes being

$$Y_{es}(y) = A_n \cos(k_{yn} y) \qquad (D.29a)$$

$$Y_{ea}(y) = \beta_n \exp(-\gamma_n y) \qquad (D.29b)$$

where k_{yn} and γ_n are the y-directed wavenumbers in the slab and air regions respectively. The remaining boundary conditions (D.11) give

$$A_n \cos(k_{yn} d) = \beta_n \exp(-\gamma_n d) \qquad (D.30a)$$

$$\frac{k_{yn}}{\varepsilon_s} A_n \sin(k_{yn} d) = \frac{\gamma_n}{\varepsilon_a} \beta_n \exp(-\gamma_n d) \qquad (D.30b)$$

$$(\varepsilon_s k_o^2 - k_{yn}^2) A_n \cos(k_{yn} d) = (\varepsilon_a k_o^2 + \gamma_n^2)\beta_n \exp(-\gamma_n d) \qquad (D.30c)$$

and thus

$$\beta_n = A_n \cos(k_{yn} d) \exp(\gamma_n d) \qquad (D.31)$$

and the wavenumbers k_{yn} and γ_n are linked through the transcendental equation

$$k_{yn} \tan(k_{yn} d) = \frac{\varepsilon_s}{\varepsilon_a} \gamma_n \qquad (D.32a)$$

and also satisfy

$$k_{yn}^2 + \gamma_n^2 = (\varepsilon_s - \varepsilon_a) k_o^2 \qquad (D.32b)$$

Therefore equations (D.29) become

$$Y_{es}(y) = A_n \cos(k_{yn} y) \tag{D.33a}$$

$$Y_{ea}(y) = A_n \cos(k_{yn} d) \exp[-\gamma_n (y - d)] \tag{D.33b}$$

The TM radiation modes may be written as

$$Y_{es}(\chi, y) = A_{ec} \cos(\sigma y) + B_{ec} \sin(\sigma y) \tag{D.34a}$$

$$Y_{ea}(\chi, y) = \alpha_{ec} \cos(\chi y) + \beta_{ec} \sin(\chi y) \tag{D.34b}$$

and the boundary conditions (D.10) and (D.11) give

$$A_{ec} \cos(\sigma d) = \alpha_{ec} \cos(\chi d) + \beta_{ec} \sin(\chi d) \tag{D.35a}$$

$$-\frac{\sigma}{\varepsilon_s} A_{ec} \sin(\sigma d) = \frac{\chi}{\varepsilon_a} \{\beta_{ec} \cos(\chi d) - \alpha_{ec} \sin(\chi d)\} \tag{D.35b}$$

$$\sigma^2 - \chi^2 = (\varepsilon_s - \varepsilon_a) k_o^2 \tag{D.35c}$$

Hence,

$$\alpha_{ec} = A_{ec} [\cos(\sigma d) \cos(\chi d) + (\frac{\varepsilon_a}{\varepsilon_s})(\frac{\sigma}{\chi}) \sin(\sigma d) \sin(\chi d)] \tag{D.36a}$$

$$\beta_{ec} = A_{ec} [\cos(\sigma d) \sin(\chi d) - (\frac{\varepsilon_a}{\varepsilon_s})(\frac{\sigma}{\chi}) \sin(\sigma d) \cos(\chi d)] \tag{D.36b}$$

and the equations (D.34) become

$$Y_{es}(\chi, y) = A_{ec} \cos(\sigma y) \tag{D.37a}$$

$$Y_{ea}(\chi, y) = A_{ec} \{\cos(\sigma d) \cos[\chi(y - d)] - (\frac{\varepsilon_a}{\varepsilon_s})(\frac{\sigma}{\chi}) \sin(\sigma d) \sin[\chi(y - d)]\} \tag{D.37b}$$

Examination of equations (D.37), and (D.33) together with equation (D.32a), shows that the boundary conditions for the TM field have produced an electric scalar potential that is continuous across the interface at y = d, but that the normal derivative is discontinuous as

$$\frac{d\Psi_{ea}}{dy} = \frac{\varepsilon_a}{\varepsilon_s} \frac{d\Psi_{es}}{dy} \qquad (D.38)$$

The reason for this is that the y-directed electric potential is seen, from equation (3.32), to be proportional to the normal electric flux density which is continuous across the dielectric interface at y = d. However, the electric flux density tangential to the interface is proportional to the derivative of the y-directed electric potential, thus determining the discontinuity relation (D.38) through the boundary condition (D.11a).

In order to complete the derivation of the y-directed component of the electric potential function, it is necessary to determine the value of the coefficients A_n and A_{ec} by normalisation over the range of y. It is seen from Appendix E that for the TM mode it is necessary to set

$$\int_o^\infty \frac{1}{\varepsilon_{rel}} Y_{en}^2(y)\, dy = 1 \qquad (D.39a)$$

and

$$\int_o^\infty \frac{1}{\varepsilon_{rel}} Y_e(X,y) Y_e(X',y) dy = \delta(X - X') \qquad (D.39b)$$

and, consequently, the coefficients are given by

$$A_n = \left[\frac{2}{\left(\frac{d}{\varepsilon_s}\right) + \left(\frac{\varepsilon_a}{\gamma_n}\right)\left[\frac{\gamma_n^2 + k_{yn}^2}{(\varepsilon_s\gamma_n)^2 + (\varepsilon_a k_{yn})^2}\right]} \right]^{\frac{1}{2}} \qquad (D.40)$$

$$A_{ec} = \left[\frac{2}{\pi\left[\cos^2(\sigma d) + \left(\frac{\varepsilon_a}{\varepsilon_s}\right)^2 \left(\frac{\sigma}{\chi}\right)^2 \sin^2(\sigma d)\right]} \right]^{\frac{1}{2}} \qquad (D.41)$$

The complete solutions for the orthonormal eigenmodes for the TM and TE y-directed scalar potentials are presented in Tables (D.1) and (D.2), where

$$\Psi(y) = \sum_{n} Y_n(y) + \int_{o}^{\infty} Y(X,y)\, dX \qquad (D.42)$$

	DISCRETE	CONTINUUM
$0 \leq y \leq d$	$Y_n(y) = A_n \cos(k_{yn} y)$	$Y(\chi, y) = A_c \cos(\sigma y)$
$y \geq d$	$Y_n(y) = A_n \cos(k_{yn} d) \exp[-\gamma_n (y - d)]$	$Y(\chi, y) = A_c \left\{ \cos(\sigma d)\cos[\chi(y - d)] - \frac{\varepsilon_a}{\varepsilon_s} \frac{\sigma}{\chi} \sin(\sigma d)\sin[\chi(y - d)] \right\}$
	$A_n = \left[\frac{2}{\left(\frac{d}{\varepsilon_s}\right) + \left(\frac{\varepsilon_a}{\gamma_n}\right) \left[\frac{\gamma_n^2 + k_{yn}^2}{\varepsilon_s^2 \gamma_n^2 + \varepsilon_a^2 k_{yn}^2} \right]} \right]^{\frac{1}{2}}$	$A_c = \left[\frac{(2/\pi)}{\cos^2(\sigma d) + \left(\frac{\varepsilon_a}{\varepsilon_s}\right)^2 \left(\frac{\sigma}{\chi}\right)^2 \sin^2(\sigma d)} \right]^{\frac{1}{2}}$
	$k_{yn} \tan(k_{yn} d) = \left(\frac{\varepsilon_s}{\varepsilon_a}\right) \gamma_n$ $k_{yn}^2 + \gamma_n^2 = (\varepsilon_s - \varepsilon_a) k_o^2$	$\sigma^2 - \chi^2 = (\varepsilon_s - \varepsilon_a) k_o^2$

Table D.1 The TM y-directed eigenmodes of a grounded dielectric slab waveguide

	DISCRETE	CONTINUUM
$0 \leq y \leq d$	$Y_n(y) = B_n \sin(k_{yn} y)$	$Y(\chi, y) = B_c \sin(\sigma y)$
$y \geq d$	$Y_n(y) = B_n \sin(k_{yn} d)\exp[-\gamma_n(y - d)]$	$Y(\chi, y) = B_c \left\{ \sin(\sigma d)\cos[\chi(y - d)] + \frac{\sigma}{\chi} \cos(\sigma d)\sin[\chi(y - d)] \right\}$
	$B_n = \left[\frac{2}{d + \frac{1}{\gamma_n}} \right]^{\frac{1}{2}}$	$B_c = \left[\frac{(2/\pi)}{\sin^2(\sigma d) + (\frac{\sigma}{\chi})^2 \cos^2(\sigma d)} \right]^{\frac{1}{2}}$
	$k_{yn} \cot(k_{yn} d) = -\gamma_n$	$\sigma^2 - \chi^2 = (\varepsilon_s - \varepsilon_a)k_o^2$
	$k_{yn}^2 + \gamma_n^2 = (\varepsilon_s - \varepsilon_a)k_o^2$	

Table D.2 The TE y-directed eigenmodes of a grounded dielectric slab waveguide

REFERENCES

[1] V.V. Shevchenko, "*Continuous Transitions in Open Waveguides*". Boulder, Colorado: The Golem Press, 1971, pp.138-142.

APPENDIX E

The Orthogonality Relations for the y-directed Eigenmodes of the Grounded Dielectric Slab

In order to derive the orthogonality relations, it is necessary to examine the derivation of the scalar potential function differential equation in an inhomogeneous region. The situation under consideration is that of a grounded dielectric slab waveguide, and it is evident that the relative dielectric constant is inhomogeneous across the substrate-air interface. Thus, the relative permittivity is not constant, but varies with the vertical direction, y, and so Maxwell's equations become

$$\nabla \times \underline{E} = - j\omega\mu_o \underline{H} \tag{E.1a}$$

$$\nabla \times \underline{H} = j\omega\varepsilon_o \varepsilon(y)\, \underline{E} \tag{E.1b}$$

$$\nabla . (\varepsilon(y)\underline{E}) = 0 \tag{E.1c}$$

$$\nabla . \underline{H} = 0 \tag{E.1d}$$

The analysis of the TE mode proceeds exactly as in section 3.1.3 with ε_{rel} replaced by $\varepsilon(y)$, and the magnetic scalar potential differential equation is found to be

$$\nabla^2 \psi_h + \varepsilon(y) k_o^2 \psi_h = 0 \tag{E.2}$$

which, using the method of separation of variables, gives for the y-directed eigenfunction, $Y_h(y)$,

$$\frac{\partial^2}{\partial y^2} Y_h(y) + k_y^2 Y_h(y) = 0 \tag{E.3}$$

The analysis of the TM modes is, however, more complicated. Initially the procedure is the same as in section 3.1.4, and choosing

an electric vector potential, $\underline{\Pi}e$, such that

$$\underline{H} = \nabla \times \underline{\Pi}e \tag{E.4}$$

gives the electric field as

$$\underline{E} = -j\omega\mu_o \underline{\Pi}e + \nabla\phi \tag{E.5}$$

where ϕ is an arbitrary scalar. Substitution of equations (E.4) and (E.5) into equation (E.1b) leads to the relation

$$\nabla(\nabla.\underline{\Pi}e) - \nabla^2\underline{\Pi}e = \varepsilon(y)k_o^2\underline{\Pi}e + j\omega\varepsilon_o\varepsilon(y)\nabla\phi \tag{E.6}$$

which is rewritten, using the relationship (A.9), as

$$\nabla(\nabla.\underline{\Pi}e) - \nabla^2\underline{\Pi}e - \varepsilon(y)k_o^2\underline{\Pi}e = j\omega\varepsilon_o(\nabla(\varepsilon(y)\phi) - \phi\nabla\varepsilon(y)) \tag{E.7}$$

The divergence of the electric vector potential is now defined to be

$$\nabla.\underline{\Pi}e = j\omega\varepsilon_o\varepsilon(y)\phi \tag{E.8}$$

and equation (E.7) reduces to

$$\nabla^2\psi_e - \frac{1}{\varepsilon(y)}\frac{\partial\varepsilon(y)}{\partial y}\frac{\partial\psi_e}{\partial y} + \varepsilon(y)k_o^2\psi_e = 0 \tag{E.9}$$

which, upon separation of variables, leads to the relation

$$\frac{\partial}{\partial y}\left(\frac{1}{\varepsilon(y)}\frac{\partial Y_e(y)}{\partial y}\right) + \frac{1}{\varepsilon(y)}k_y^2 Y_e(y) = 0 \tag{E.10}$$

for the y-directed eigenfunction, $Y_e(y)$.

A very important form of second-order differential equation is known as the Sturm-Liouville equation,

$$[\frac{\partial}{\partial y}(p(y)\frac{\partial}{\partial y}) - q(y) + \lambda_m w(y)]\, f_m(y) = 0 \tag{E.11}$$

and it is clear that equations (E.3) and (E.10) are of this kind, where

$$p(y) = w(y) = \begin{cases} 1 & \text{TE modes} \\ 1/\varepsilon(y) & \text{TM modes} \end{cases} \qquad \text{(E.12)}$$

and

$$q(y) = 0 \qquad \text{(E.13)}$$

The general orthogonality relationship for both of the discrete transverse modes is determined by considering the equation

$$\left[\frac{\partial}{\partial y}\left(p(y)\,\frac{\partial}{\partial y}\right) + k_{yn}^2 w(y)\right] Y_n(y) = 0 \qquad \text{(E.14)}$$

where $Y_n(y)$ represents the y-directed eigenmode corresponding to the eigenvalue k_{yn}, and $Y_n(y)$ must satisfy the appropriate boundary conditions for the grounded dielectric slab waveguide.

A second eigenmode, $Y_m(y)$, must satisfy

$$\left[\frac{\partial}{\partial y}\left(p(y)\,\frac{\partial}{\partial y}\right) + k_{ym}^2 w(y)\right] Y_m(y) = 0 \qquad \text{(E.15)}$$

and thus, multiplying equation (E.14) by $Y_m(y)$ and equation (E.15) by $Y_n(y)$, subtracting one from the other, and integrating over the y-domain, gives

$$\int_o^\infty \left[Y_m \frac{\partial}{\partial y}\left(p(y)\,\frac{\partial Y_n}{\partial y}\right) - Y_n \frac{\partial}{\partial y}\left(p(y)\,\frac{\partial Y_m}{\partial y}\right)\right] dy + \left[k_{yn}^2 - k_{ym}^2\right] \int_o^\infty w(y) Y_n Y_m dy = 0 \qquad \text{(E.16)}$$

which after a simple integration by parts yields

$$\left[k_{yn}^2 - k_{ym}^2\right] \int_o^\infty w(y) Y_n Y_m dy = \left[p(y)\left(Y_n \frac{\partial Y_m}{\partial y} - Y_m \frac{\partial Y_n}{\partial y}\right)\right]_o^\infty \qquad \text{(E.17)}$$

The relevant boundary conditions ensure that the right hand side of equation (E.17) is identically zero, and thus the orthogonality relation for normalised y-directed eigenmodes, for both TE and TM modes, is

$$\int_0^\infty w(y)Y_n(y)Y_m(y)dy = \delta_{mn} \qquad \text{(E.18)}$$

where

$$\delta_{nm} = \begin{cases} 1 & n = m \\ 0 & n \neq m \end{cases} \qquad \text{(E.19)}$$

and w(y) is given by equation (E.12).

The equivalent procedure used to determine the orthogonality relationship for the continuum modes is complicated due to the property that these modes are not zero at an infinite distance from the slab. However, Shevchenko [1] has shown that the orthogonality for the normalised continuum modes also takes place with regard to the weight function, and is given by

$$\int_0^\infty w(y)\ Y(\chi,y)\ Y(\chi',y)\ dy = \delta(\chi - \chi') \qquad \text{(E.20)}$$

where χ and χ' are radiation wavenumbers.

Furthermore, Shevchenko has shown that the discrete and continuous parts of the eigenmodes are orthogonal, so that

$$\int_0^\infty w(y)\ Y_n(y)\ .\ Y(\chi,y)\ dy = 0 \qquad \text{(E.21)}$$

REFERENCES

[1] V.V. Shevchenko, "*Continuous Transitions in Open Waveguides*". Boulder, Colorado: The Golem Press, 1971, pp.138-141.

APPENDIX F

The Completeness Relationship

The orthonormal set of y-directed eigenmodes given in Appendix D may be used to construct a permissible function, $\Phi(y)$, such that

$$\Phi(y) = \sum_n \phi_n Y_n(y) + \int_o^\infty \phi(\chi) Y(\chi,y) d\chi \qquad (F.1)$$

The orthogonality relations, given in Appendix E, may be used to determine the values of the coefficients ϕ_n and $\phi(\chi)$, which are found to be

$$\phi_n = \int_o^\infty w(y)\ \Phi(y)\ Y_n(y) dy \qquad (F.2)$$

$$\phi(\chi) = \int_o^\infty w(y)\ \Phi(y)\ Y(\chi,y)\ dy \qquad (F.3)$$

where $w(y)$ is given by $w(y) = \begin{cases} 1 & \text{TE modes} \\ 1/\varepsilon_{rel} & \text{TM modes} \end{cases}$ (F.4)

If the function $\Phi(y)$ is chosen to be the Dirac delta function, $\delta(y - y')$, then the coefficients become

$$\phi_n = w(y')\ Y_n(y') \qquad (F.5)$$

$$\phi(\chi) = w(y')\ Y(\chi,y') \qquad (F.6)$$

and thus, from equation (F.1), the completeness relation is found to be

$$\delta(y - y') = w(y') \left\{ \sum_n Y_n(y) Y_n(y') + \int_o^\infty Y(\chi,y) Y(\chi,y') d\chi \right\} \qquad (F.7)$$

APPENDIX G

The Analytical Evaluation of the Radial and Axial Integrals

In section 5.3, the integral over the resonator volume was found to be given by equations (5.18), which upon application of the result of the azimuthal integral given in equation (5.20), become

$$\psi_{hr}(\underline{x}) = (\varepsilon_r - \varepsilon_a)k_o^2 C_g \exp[-\gamma(y - d)] \cdot \{H_o^{(2)}(k_\rho \rho) \int_o^R \rho' J_o(k_\rho \rho')\psi_{hr}(\rho')d\rho'\} \cdot \left[\int_d^{d+h} \exp[-\gamma(y' - d)]\psi_{hr}(y')dy'\right] \quad \rho' < \rho \tag{G.1a}$$

$$\psi_{hr}(\underline{x}) = (\varepsilon_r - \varepsilon_a)k_o^2 C_g \exp[-\gamma(y - d)] \cdot \{J_o(k_\rho \rho) \int_o^R \rho' H_o^{(2)}(k_\rho \rho')\psi_{hr}(\rho')d\rho'\} \cdot \left[\int_d^{d+h} \exp[-\gamma(y' - d)]\psi_{hr}(y')dy'\right] \quad \rho' > \rho \tag{G.1b}$$

where $\psi_{hr}(\rho')$ and $\psi_{hr}(y')$ are given by equations (5.8) and (5.9) respectively.

G.1 The radial integral

It may be seen from equations (G.1) that the radial integral is performed over the source space, and thus the value of ρ may be considered constant. Furthermore, ρ must lie within the resonator volume, and so the two radial integrals in equations (G.1) may be combined to give

$$I_{rad} = \frac{\sqrt{2}P_o}{R}\left[H_o^{(2)}(k_\rho\rho)\int_o^\rho \rho' J_o(k_\rho\rho')d\rho' + J_o(k_\rho\rho)\int_\rho^R \rho' H_o^{(2)}(k_\rho\rho')d\rho'\right] + \sum_{n=1}^{N}\frac{P_n}{\eta_n}\left[H_o^{(2)}(k_\rho\rho)\int_o^\rho \rho' J_o(k_\rho\rho')J_o(\beta_n\rho')d\rho' + J_o(k_\rho\rho)\int_\rho^R \rho' H_o^{(2)}(k_\rho\rho')J_o(\beta_n\rho')d\rho'\right] \quad (G.2)$$

Using equations (5.3), (5.7), and the result

$$\int_a^b x\, Z_o(\alpha x)dx = \frac{1}{\alpha}[bZ_1(\alpha b) - aZ_1(\alpha a)] \quad (G.3)$$

where $Z_o(x)$ is an arbitrary Bessel function, equation (G.2) becomes

$$I_{rad} = \frac{\sqrt{2}P_o}{k_\rho R}\{H_o^{(2)}(k_\rho\rho)\rho J_1(k_\rho\rho) + J_o(k_\rho\rho)[RH_1^{(2)}(k_\rho R) - \rho H_1^{(2)}(k_\rho\rho)]\} + \sum_{n=1}^{N}\frac{P_n}{\eta_n}\{H_o^{(2)}(k_\rho\rho)I_{\rho 1} + J_o(k_\rho\rho)I_{\rho 2}\} \quad (G.4)$$

where

$$I_{\rho 1} = \frac{(\beta_n\rho)J_o(k_\rho\rho)J_{-1}(\beta_n\rho) - (k_\rho\rho)J_{-1}(k_\rho\rho)J_o(\beta_n\rho)}{(k_\rho^2 - \beta_n^2)} \quad (G.5)$$

and

$$I_{\rho 2} = \frac{(k_\rho\rho)H_{-1}^{(2)}(k_\rho\rho)J_o(\beta_n\rho) - (\beta_n\rho)H_o^{(2)}(k_\rho\rho)J_{-1}(\beta_n\rho) - (k_\rho R)H_{-1}^{(2)}(k_\rho R)J_o(\beta_n R)}{(k_\rho^2 - \beta_n^2)} \quad (G.6)$$

Now, for integer values of p,

$$Z_{-p}(x) = (-1)^p Z_p(x) \quad (G.7)$$

and so equation (G.4) becomes

$$I_{rad} = \frac{\sqrt{2}P_o}{R} \cdot \frac{1}{k_\rho} \cdot \{RH_1^{(2)}(k_\rho R)J_o(k_\rho \rho) + \rho S_w\}$$

$$+ \sum_{n=1}^{N} \frac{P_n}{\eta_n(k_\rho^2 - \beta_n^2)} \{(k_\rho \rho)S_w J_o(\beta_n \rho)$$

$$+ (k_\rho R)H_1^{(2)}(k_\rho R)J_o(\beta_n R)J_o(k_\rho \rho)\} \qquad (G.8)$$

where

$$S_w = H_o^{(2)}(k_\rho \rho)J_1(k_\rho \rho) - H_1^{(2)}(k_\rho \rho)J_o(k_\rho \rho) \qquad (G.9)$$

The Hankel function, $H_p^{(2)}(z)$, is defined as

$$H_p^{(2)}(z) = J_p(z) - jN_p(z) \qquad (G.10)$$

where $N_p(z)$ is the cylindrical Bessel function of the second kind of order p and argument z, and thus equation (G.9) may be expanded to give

$$S_w = -j\{N_o(k_\rho \rho)J_1(k_\rho \rho) - N_1(k_\rho \rho)J_o(k_\rho \rho)\} \qquad (G.11)$$

and the term in the braces is the Wronskian,

$$W\{J_n(z), N_n(z)\} = N_n(z)J_{n+1}(z) - N_{n+1}(z)J_n(z) = \frac{2}{\pi z} \qquad (G.12)$$

and so the radial integral becomes

$$I_{rad} = \frac{\sqrt{2}P_o}{R} \cdot \left(\frac{-1}{k_\rho^2}\right) \cdot \left[\frac{j2}{\pi} - (k_\rho R)H_1^{(2)}(k_\rho R)J_o(k_\rho \rho)\right]$$

$$+ \sum_{n=1}^{N} \frac{P_n}{\eta_n(\beta_n^2 - k_\rho^2)} \left\{ \frac{j2}{\pi} J_o(\beta_n \rho) \right.$$

$$\left. - (k_\rho R)H_1^{(2)}(k_\rho R)J_o(\beta_n R)J_o(k_\rho \rho) \right\} \qquad (G.13)$$

and, recalling that $\beta_o = 0$, it is clear that equation (G.13) is identical to

$$I_{rad} = \sum_{n=0}^{N} \frac{P_n}{\eta_n(\beta_n^2 - k_\rho^2)} \cdot \left\{ \frac{j2}{\pi} J_o(\beta_n\rho) - (k_\rho R)H_1^{(2)}(k_\rho R)J_o(\beta_n R)J_o(k_\rho\rho) \right\} \quad (G.14)$$

G.2 The axial integral

It is evident from the above result that the equations (G.1) may be combined to give

$$\psi_{hr}(\underline{x}) = (\varepsilon_r - \varepsilon_a)k_o^2 C_g \exp[-\gamma(y - d)]\, I_{rad} \cdot \int_o^{d+h} \exp[-\gamma(y' - d)]\psi_{hr}(y')dy' \quad (G.15)$$

The axial integral is given by

$$I_y = \frac{A_o}{\sqrt{h}} \int_d^{d+h} \exp[-\gamma(y' - d)]dy' + \sqrt{\frac{2}{h}} \sum_{m=1}^{M} \{A_m \int_d^{d+h} \exp[-\gamma(y' - d)] \cos[\frac{2m\pi}{h}(y' - d)]dy' + B_m \int_d^{d+h} \exp[-\gamma(y' - d)] \sin[\frac{2m\pi}{h}(y' - d)]dy'\} \quad (G.16)$$

and the latter integrals in equation (G.16) are standard indefinite integrals with the solutions

$$\int \exp(-ax)\cos(bx)dx = -\frac{\exp(-ax)}{(a^2 + b^2)} [a\cos(bx) - b\sin(bx)] \quad (G.17)$$

$$\int \exp(-ax)\sin(bx)dx = -\frac{\exp(-ax)}{(a^2 + b^2)} [a\sin(bx) + b\cos(bx)] \quad (G.18)$$

and equation (G.16) therefore reduces to

$$I_y = [1 - \exp(-\gamma h)]\sqrt{\frac{2}{h}} \left\{ \frac{A_o}{\sqrt{2}\gamma} + \sum_{m=1}^{M} \frac{[\gamma A_m + (\frac{2m\pi}{h})B_m]}{[\gamma^2 + (\frac{2m\pi}{h})^2]} \right\} \quad (G.19)$$